

## INFORMATION TO USERS

This manuscript has been reproduced from the microfilm master. UMI films the text directly from the original or copy submitted. Thus, some thesis and dissertation copies are in typewriter face, while others may be from any type of computer printer.

**The quality of this reproduction is dependent upon the quality of the copy submitted.** Broken or indistinct print, colored or poor quality illustrations and photographs, print bleedthrough, substandard margins, and improper alignment can adversely affect reproduction.

In the unlikely event that the author did not send UMI a complete manuscript and there are missing pages, these will be noted. Also, if unauthorized copyright material had to be removed, a note will indicate the deletion.

Oversize materials (e.g., maps, drawings, charts) are reproduced by sectioning the original, beginning at the upper left-hand corner and continuing from left to right in equal sections with small overlaps. Each original is also photographed in one exposure and is included in reduced form at the back of the book.

Photographs included in the original manuscript have been reproduced xerographically in this copy. Higher quality 6" x 9" black and white photographic prints are available for any photographs or illustrations appearing in this copy for an additional charge. Contact UMI directly to order.

**UMI<sup>®</sup>**

Bell & Howell Information and Learning  
300 North Zeeb Road, Ann Arbor, MI 48106-1346 USA  
800-521-0600



**The University of Alberta**

**EQUILIBRIA AND KINETICS OF ORGANIC MODIFIER SORPTION  
AND SWELLING BY AMBERLITE XAD-2**

By

Clara Hernandez



A thesis

submitted to the Faculty of Graduate studies and Research in partial fulfillment of the  
requirements for the degree of  
DOCTOR OF PHILOSOPHY

Department of Chemistry

Edmonton, Alberta

Spring, 1999



National Library  
of Canada

Acquisitions and  
Bibliographic Services

395 Wellington Street  
Ottawa ON K1A 0N4  
Canada

Bibliothèque nationale  
du Canada

Acquisitions et  
services bibliographiques

395, rue Wellington  
Ottawa ON K1A 0N4  
Canada

*Your file Votre référence*

*Our file Notre référence*

The author has granted a non-exclusive licence allowing the National Library of Canada to reproduce, loan, distribute or sell copies of this thesis in microform, paper or electronic formats.

The author retains ownership of the copyright in this thesis. Neither the thesis nor substantial extracts from it may be printed or otherwise reproduced without the author's permission.

L'auteur a accordé une licence non exclusive permettant à la Bibliothèque nationale du Canada de reproduire, prêter, distribuer ou vendre des copies de cette thèse sous la forme de microfiche/film, de reproduction sur papier ou sur format électronique.

L'auteur conserve la propriété du droit d'auteur qui protège cette thèse. Ni la thèse ni des extraits substantiels de celle-ci ne doivent être imprimés ou autrement reproduits sans son autorisation.

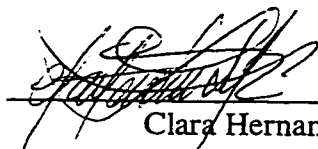
0-612-39539-1

**The University of Alberta  
Library Release form**

**Name of Author:** Clara Hernandez  
**Title of Thesis:** Equilibria and Kinetics of Organic Modifier  
Sorption and Swelling by Amberlite XAD-2.  
**Degree:** Doctor of Philosophy  
**Year this Degree Granted:** 1999

Permission is hereby granted to the University of Alberta Library to reproduce single copies of this thesis and to lend or sell such copies for private, scholarly or scientific research purposes only.

The author reserves all other publication and other rights in association with the copyright of the thesis, and except as herein before provided, neither the thesis or any substantial portion thereof may be printed or otherwise reproduced in any material form whatever without the author's prior written permission.

  
Clara Hernandez

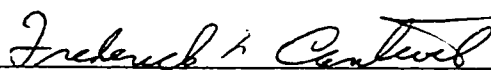
Ave. Romulo Gallegos, Edif.  
Interlands, 5C, El Marques, Caracas  
1070, Venezuela.

Date: April 20<sup>th</sup>, 1999

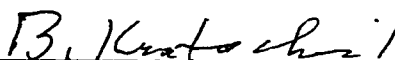
**The University of Alberta**

**Faculty of Graduate Studies and Research**

The undersigned certify that they have read, and recommend to the Faculty of Graduate studies and Research for acceptance, a thesis entitled EQUILIBRIA AND KINETICS OF ORGANIC MODIFIERS SORPTION AND SWELLING BY AMBERLITE XAD-2 submitted by CLARA HERNANDEZ in partial fulfillment of the requirements for the degree of DOCTOR OF PHILOSOPHY.



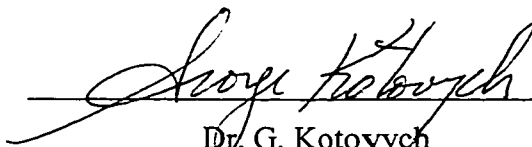
Dr. F. F. Cantwell



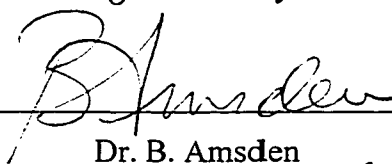
Dr. B. Kratochvil



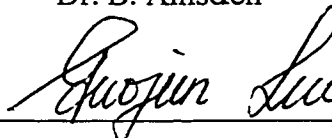
Dr. L. Li



Dr. G. Kotovych



Dr. B. Amsden



Dr. G. Liu

(External Examiner)

April 19<sup>th</sup>, 1999

*...To my family, for always being there for me...*

*Rafael  
Clarel  
Rafael Jr.  
and my grandparents*

*God bless you all.*

*...and to you too B.D.E...I will never forget you.*

## Abstract

Aromatic compounds show tailed and broad peaks when eluted from PSDVB packings due to the microporosity in the matrix. In this work, swelling and sorption studies were performed on XAD-2, commercially available PSDVB copolymer, in binary aqueous solutions. The solvents used are classified as: a good (tetrahydrofuran, THF), an intermediate (acetonitrile, AN), and a poor (methanol, MeOH) solvent, based on the difference in solubility parameter between the solvent and the PSDVB matrix.

The sorption isotherms of the organic solvent component of these three systems were measured. The quantity of organic modifier sorbed onto the XAD-2 resin was calculated from a mass balance on the organic modifier in the supernatant. Swelling of the resin, in similar solutions, was obtained by microscopic measurements of XAD-2 particle diameters before and after swelling. Fractional swelling is presented as a function of the organic modifier concentration and/or activity in the solution. Composite plots of the fractional swelling versus concentration of organic modifier in the solid phase, at different liquid equilibrium concentration (activity) values, were obtained.

Both sorption and swelling kinetics were also measured. For the swelling kinetic measurements, a special flow cell was designed to hold a single particle of XAD-2. Sorption kinetics was followed in the bath equilibration mode.

Equilibrium studies show that the solvent effect decreases in the order THF>AN>MeOH. THF was the most sorbed and caused the most swelling. MeOH had the least effect on both sorption and swelling. The swelling rate of XAD-2 is fast in the



three solvents whilst the sorption rate is relatively slower. The polymer matrix is composed of a network of interconnected macro-, meso- and micropores going from a collapsed (dry) gel moderately cross-linked region able to swell in good solvents to a rigid highly cross-linked permanent micropore region able to uptake good solvents without swelling. Depending on the solvent solubility parameter, the collapsed structure will swell as the solvent diffuses into this region from an open permanent macroporous structure where only adsorption, without swelling, is present.

## **Acknowledgements**

I would like to thank my supervisor, Dr. Fred Cantwell, for his guidance and patience during all the stages of my research. I would also thank Ing. Rene Rojas from PDVSA-INTEVEP for running the TGA measurements and my research partner, Dr. Barb Ells, for her opportune comments and invaluable help. Many thanks to Rafael Golding for his useful ideas and the machine shop and glass shop staff in the Department of Chemistry for making the different versions of the observation cell used in this research. My gratitude to Carmen Murgich and Marisol Brito from PDVSA-INTEVEP for their infinite patience and unconditional help.

Finally, I give my sincere thanks to PDVSA-INTEVEP (Venezuelan oil research company) for giving me the scholarship that allowed me to come to the University of Alberta and to the Department of Chemistry at the University of Alberta for financial assistance.

## Table of Contents

	Page
<b>Chapter 1    Introduction</b>	<b>1</b>
1.1    High-Performance Liquid Chromatography as a Separation Technique	1
1.2    Retention and Equilibrium	3
1.3    Bandbroadening, Efficiency, and Resolution in HPLC	5
1.3.1    Efficiency and Resolution	6
1.3.2    Bandbroadening in Liquid Chromatography	9
1.3.3    Tailing	15
1.4    Reversed Phase Liquid Chromatography	18
1.4.1    Mobile Phases for Reversed Phase Liquid Chromatography	19
1.4.2    Stationary Phases for Reversed Phase Liquid Chromatography	19
1.4.2.1    Silica Based Stationary Phases	20
1.4.2.2    Polystyrene-divinylbenzene co-polymer (PSDVB) stationary Phases	21
1.5    Excessive Bandbroadening on PSDVB	24
1.6    Overview of the Present Work	26
 <b>Chaper 2    Experimental Section</b>	 <b>29</b>
2.1    Introduction	29
2.2    Sorbent. Amberlite XAD-2	29

2.3	Reagents and Solvents	33
2.4	Water Uptake Measurements Using Thermal Gravimetric Analysis	34
2.4.1	Apparatus for Thermal Gravimetric Analysis	34
2.4.2	Sample Preparation	36
2.4.3	TGA Measurements	36
2.5	Uptake of Organic Modifiers	37
2.5.1	The Gas Chromatograph Apparatus	37
2.5.2	Chromatographic Conditions for multicomponent samples	37
2.5.3	Thermostated Bath	39
2.5.4	Equilibrium Time Required in Sorption Experiments	39
2.5.5	Sorption Isotherm Experiments	39
2.5.6	Sorption Rate Experiments	42
2.6	Swelling Studies on Amberlite XAD-2	43
2.6.1	Apparatus for Swelling Measurements	43
2.6.1.1	Multiple Particle Measurements	43
2.6.1.2	Single Particle Measurements	45
2.6.2	Procedures for Swelling Measurements	47
2.6.2.1	Equilibrium Swelling Measurements on XAD-2	47
2.6.2.2	Swelling rate measurements on XAD-2	48
2.6.2.3	Microscopic Measurements of Glass Beads in Solvents	49

<b>Chapter 3</b>	<b>Equilibrium Sorption Isotherms of Organic Modifiers and Swelling of Amberlite XAD-2</b>	<b>50</b>
3.1	Introduction	50
3.2	Theory	51
3.2.1	Distribution Coefficient Measurements	51
3.2.2	Equilibrium Sorption Isotherms	54
3.2.3	Polymer Swelling	57
3.2.3.1	The PSDVB Structure	57
3.2.3.2	Methods to Determine Polymer Swelling	63
3.2.4	Activity Considerations for High Concentration Solutions	68
3.3	Results and Discussion	73
3.3.1	Water Uptake on XAD-2	73
3.3.2	Sorption Isotherms on XAD-2 Using Aqueous Phase Concentrations	80
3.3.3	Sorption Isotherms on XAD-2 Using Aqueous Phase Activities	84
3.3.4	Swelling of XAD-2 in Different Organic/Aqueous Solutions	95
3.3.5	Relationship Between Swelling and Sorption	100
3.3.5.1	Composite Plot of Sorption and Swelling at Equilibrium	101
3.3.5.2	Structural Interpretation of PSDVB	107
3.3.6	Effect of the Solvent Present in the Mobile Phase on Efficiency and Peak Symmetry	114
3.3.7	Conclusion	115

<b>Chapter 4</b>	<b>Sorption Rate of Some Organic Modifiers From Binary Solution and the Rate of Swelling of Amberlite XAD-2</b>	<b>116</b>
4.1	Introduction	116
4.2	Theory	118
4.2.1	Kinetic Processes in Porous Materials	118
4.2.1.1	Sorption and Diffusion into Porous Materials	119
4.2.1.2	Swelling Kinetics of Polymeric Materials	122
4.2.2	Rate Controlling Processes	123
4.2.2.1	Case I	123
4.2.2.2	Case II	127
4.2.3	Sorption and Swelling Rate Measurements	129
4.2.3.1	Finite Bath Method	130
4.2.3.2	Shallow Bed Method	131
4.2.4	Effect of the Mobile Phase on the Sorption Kinetics of Organic Solutes in HPLC	132
4.3	Results and Discussion	133
4.3.1	Rate of Sorption of Different OM <sub>s</sub> from Aqueous Solutions by XAD-2	133
4.3.2	Rate of Swelling of XAD-2 in Different Aqueous Solutions of OM <sub>s</sub>	145
4.3.3	Rate of Sorption Versus Rate of Swelling	170
4.3.4	Proposed Mechanism for Solvent Sorption and Swelling by XAD-2	178

<b>Chapter 5</b>	<b>Conclusions and Future Work</b>	<b>179</b>
5.1	Conclusions and Significance for Chromatography	179
5.2	Recommended Future Work	181
	<b>Bibliography</b>	<b>183</b>
	<b>Appendix A. Procedure to Pack a GC Column</b>	<b>195</b>
	<b>Appendix B. Calculation of Distribution Coefficients in the Batch Method</b>	<b>197</b>
	<b>Appendix C. Tables for Figures in Chapters 3 and 4</b>	<b>200</b>
	<b>Appendix D. Differential Scanning Calorimetry (DSC)</b>	<b>235</b>

## List of Tables

<b>TABLE</b>	<b>Page</b>
2.1 Physical properties of the Amberlite XAD-2 resin	32
2.2 GC Conditions for standards and samples used	38
3.1 Parameters for THF/water, AN/water, and MeOH/water for the calculation of activity coefficients using Margules and NRTL equations	71
3.2 Physical properties of OM used to calculate sorbed volumes	91
3.3 Exponential term from equation 3.20 and $p/p_s$ for THF, AN, and MeOH at 25°C as a function of pore radius.	94
3.4 Characteristics of the fractional swelling–sorption curves	106
4.1 Activity of the initial and equilibrium solutions used to determine sorption rate of OMs on XAD-2 by using Margules and NRTL equations	138
4.2 Fitting parameters of the triexponential equations for the OMs	143
4.3 Fitting parameters for the swelling kinetics of XAD-2 using THF	152
4.4 Fitting parameters for the swelling kinetics of XAD-2 using AN	159
4.5 Fitting parameters for the swelling kinetics of XAD-2 using MeOH	166
4.6 Initial and equilibrium concentrations of OM in the liquid phase in the sorption and swelling experiments at similar concentrations	174



## List of Figures

Figure	Page
2.1 Schematic of the general synthesis of Polystyrene-divinylbenzene copolymers	31
2.2 TG50 Thermobalance for TGA Measurements	35
2.3 Sorption flask for bath equilibration method	41
2.4 Continuous flow cell for swelling measurements of multiple particles	44
2.5 Continuous flow cell for measurements of a single particle	46
3.1 Sorption isotherm for a solute i	52
3.2 Representation of the most common isotherms and their corresponding chromatographic elution peaks	55
3.3 Pictorial representation of the PSDVB structure	58
3.4 Diagram of terminology describing the different regions In the PSDVB beads based on figure 3.3	59
3.5a Activity coefficients, $\gamma_i$ , calculated by using the Margules (MeOH) and NRTL (THF and AN) equations, versus mole fraction, $x_i$ , for THF, AN, and MeOH in aqueous solutions	72
3.5b Activities, $a_i$ , calculated by using the Margules (MeOH) and NRTL (THF and AN) equations, versus mole fraction, $x_i$ , for THF, AN, and MeOH in aqueous solutions	72
3.6 Thermal study of “dry XAD-2”. Temperature range: 35-240°C	74
3.7 Thermal study of “dry XAD-2”. Temperature range: 35-290°C	75
3.8 Thermal study of “humid XAD-2”. Temperature range 39-290°C	77
3.9 Thermal study of “humid XAD-2”. Temperature range 32-290°C	78

3.10	Thermal study of “water sprinkled XAD-2”. Temperature range 32-290°C	79
3.11	Sorption isotherms for THF, AN, and MeOH on XAD-2 from aqueous solutions (concentration of OM)	81
3.12	Sorption isotherms for THF, AN, and MeOH on XAD-2 from aqueous solutions (activity of OM)	85
3.13	Sorption isotherms for THF on XAD-2 (activity of THF)	88
3.14	Sorption isotherms for AN on XAD-2 (activity of AN)	89
3.15	Sorption isotherms for MeOH on XAD-2 (activity of MeOH)	90
3.16	Fractional swelling of XAD-2 using aqueous solution concentrations of OM	96
3.17	Fractional swelling of XAD-2 using aqueous solutions activities of OM	98
3.18	Combined fractional swelling-sorption for THF, AN, and MeOH	102
3.19	Combined fractional swelling-sorption for MeOH	103
3.20	Combined fractional swelling-sorption for AN	104
3.21	Combined fractional swelling-sorption for THF	105
4.1	Transmission Electron Micrograph of the inner part of XAD-2	117
4.2	Typical sorption kinetic curve	121
4.3	Diffusion of small solute molecules in polymers	125
4.4	Normalized rate of sorption of THF on XAD-2	134
4.5	Normalized rate of sorption of AN on XAD-2	135
4.6	Normalized rate of sorption of MeOH on XAD-2	136
4.7	Hypothetical rate curve for a monodisperse model	140
4.8	Comparative triexponential fitting (overall) of data for THF, AN, and MeOH up to 100 min	144

4.9	Swelling rate of a particle of XAD in a 4.94% w/w THF solution	146
4.10	Swelling rate of a particle of XAD in a 10.97% w/w THF solution	147
4.11	Swelling rate of a particle of XAD in a 52.24% w/w THF solution	148
4.12	Swelling rate of a particle of XAD in a 72.61% w/w THF solution	149
4.13	Swelling rate of a particle of XAD in a 100% w/w THF solution	150
4.14	Swelling rate of a particle of XAD in a different THF solutions (fittings)	151
4.15	Swelling rate of a particle of XAD in a 4.06% w/w AN solution	153
4.16	Swelling rate of a particle of XAD in a 8.10% w/w AN solution	154
4.17	Swelling rate of a particle of XAD in a 58.86% w/w AN solution	155
4.18	Swelling rate of a particle of XAD in a 71.05% w/w AN solution	156
4.19	Swelling rate of a particle of XAD in a 100% AN	157
4.20	Swelling rate of a particle of XAD in a different AN solutions (fittings)	158
4.21	Swelling rate of a particle of XAD in a 5.57% w/w MeOH solution	160
4.22	Swelling rate of a particle of XAD in a 16.17% w/w MeOH solution	161
4.23	Swelling rate of a particle of XAD in a 56.33% w/w MeOH solution	162
4.24	Swelling rate of a particle of XAD in a 75.82% w/w MeOH solution	163
4.25	Swelling rate of a particle of XAD in a 100% w/w MeOH solution	164
4.26	Swelling rate of a particle of XAD in a different MeOH solutions (fittings)	165
4.27	Effect of the OM on fractional swelling of XAD-2	168
4.28	Relative sorption rate of THF XAD-2 and the swelling rate of the polymer	171

4.29	Relative sorption rate of AN XAD-2 and rate of swelling	172
4.30	Relative sorption rate of MeOH XAD-2 and rate of swelling	173
4.31	Normalized composite plots for swelling and sorption rate	177

## List of Symbols

$a$	Distance between peak maximum and peak front (section 1.3.3)
$A$	Specific surface area ( $\text{m}^2/\text{g}$ )
$a$	Langmuir constant (section 3.2.2)
$a_i$	Activity of compound $i$
$A_{ij}$	Margules interaction parameter between compounds $i$ and $j$
$A_{\text{OM,L}}$	Activity of organic modifier in the liquid phase
AN	Acetonitrile
$b$	Distance between peak maximum and peak rear (section 1.3.3)
$b$	Langmuir constant (section 3.2.2)
$C_{i,\text{S}}$	Concentration of $i$ in the stationary phase (e.g. $\text{mol/g}$ , $\text{g/g}$ , mole fraction)
$C_{i,\text{L}}$	Concentration of $i$ in the mobile phase (e.g. $\text{mol/l}$ , $\text{g/g}$ , mole fraction)
$C_{\text{OM,S,v/w}}$	Sorbed concentration of organic modifier in volume/weight units
$C_{\text{OM,S,w/w}}$	Sorbed concentration of organic modifier in weight/weight units
$C_{i,t}$	Sorbed concentration of $i$ at time $t$ ( $\%w/w$ )
$C_{i,\infty}$	Sorbed concentration of $i$ at equilibrium ( $\%w/w$ )
$C_{\text{L,f}}$	Concentration of the liquid phase at equilibrium ( $\%w/w$ )
$d_p$	Particle diameter ( $\mu\text{m}$ )
$D$	Diffusion coefficient ( $\text{cm}^2/\text{s}$ )
$D_{\text{M}}$	Diffusion coefficient in the mobile phase ( $\text{cm}^2/\text{s}$ )
$D_{\text{film}}$	Film diffusion coefficient ( $\text{cm}^2/\text{s}$ )
$e$	Exponential
$f$	Fraction of stagnant mobile phase

$f_{ct}$	Function of
$F$	Fractional approach to equilibrium
$G_{ij}$	Interaction parameter between components $i$ and $j$
$H$	Average plate height (mm)
$H_{eddy}$	Plate height associated with resistance to mass transfer in the mobile phase (mm)
$H_{LD}$	Plate height associated with longitudinal diffusion (mm)
$H_M$	Plate height associated with resistance to mass transfer in the mobile phase (mm)
$H_{SM}$	Plate height associated with resistance to mass transfer in the stagnant mobile phase (mm)
$H_s$	Plate height associated with the adsorption on the surface of the stationary phase (mm)
$i_L$	Compound $i$ in the mobile phase
$i_s$	Compound $i$ in the stationary phase
$J$	Flux of component ( $\text{mol}/\text{cm}^2 \cdot \text{s}$ )
$K_D$	Distribution constant ( $\text{mL}/\text{g}$ )
$K_i$	Distribution coefficient of compound $i$
$k'_i$	Capacity factor of compound $i$
$\overline{k'}$	Average capacity factor
$k_r$	Desorption rate constant
$k_{ads}$	First order adsorption rate constant ( $\text{s}^{-1}$ )
$MW_{OM}$	Molar weight of organic modifier ( $\text{g}/\text{mol}$ )

MeOH	Methanol
$m_t$	Mass of polymer at time $t$ (g)
$m_0$	Mass of dry polymer (g)
$n_{i,s}$	Number of mols of $i$ sorbed onto the stationary phase
$n_{i,L}$	Number of mols of $i$ in the mobile phase
$N$	Number of theoretical plates
OM	Organic modifier
$P$	Specific pore volume (mL pore/mL bead)
$p$	Equilibrium vapor pressure of a liquid in a narrow pore
$p_s$	Equilibrium vapor pressure on a flat surface
$Q_{vv}$	Fractional swelling in volume-volume units
$Q_{vw}$	Fractional swelling in volume-mass units
$R$	Resolution (Chapter 1). Ideal gas constant (in all other places)
$r$	Pore radius (cm)
$r_0$	Radius of spherical particles
$t_r$	Retention time (s)
$t_0$	Retention time of unretained compound, dead time (s)
$t_{r,i}$	Retention time of compound $i$ (s)
$t_{w,i}$	Peak width of compound $i$ in time units (s)
$T$	Peak asymmetry ratio (section 1.3.3). Temperature (in all other places)
THF	Tetrahydrofuran
$U_0$	Linear velocity (cm/s)
$V_s$	Volume of stationary phase (mL)

$V_L$	Volume of mobile phase (mL)
$V_f$	Swollen particle volume (mL)
$V_i$	Dry-unswollen particle volume (mL)
$V_t$	Sphere volume (Chapter 3). Gel volume at time t (Chapter 4)
$V_0$	Time zero or initial gel volume
$V_\infty$	Equilibrium gel volume
$W_s$	Weight of stationary phase (g)
$W_{t,i}$	Peak width of compound i in time units (Chapter 1)
$W_{OM,i}$	Initial mass of organic modifier (g)
$W_{XAD-2}$	Mass of dry resin (g)
$W_{H_2O,i}$	Initial mass of water (g)
$W_{OM,f}$	Mass of organic modifier in the liquid at equilibrium (g)
$W_{OM,s}$	Sorbed mass of organic modifier at equilibrium (g)
$X_i$	Mole fraction of i
$z$	Direction of movement
$\alpha$	Relative retention (Chapter 1)
$\alpha_{ij}$	Non-randomness parameter
$\alpha_t$	Swelling ratio at time t
$\alpha_\infty$	Swelling ratio at equilibrium
$\delta c / \delta z$	Concentration gradient (M/cm)
$\phi$	Phase ratio (g/mL) (Chapter 1). Particle size (Chapter 2)
$\gamma$	Obstruction factor
$\gamma'$	Tortuosity factor



$\gamma_i$	Activity coefficient of component i
$\Delta r_0$	Film thickness (cm)
$\lambda$	Packing factor
$\mu_i$	Chemical potential of component i
$\mu_i^0$	Chemical potential of component i in the standard state
$\theta$	Contact angle (°)
$\rho_p$	Particle density (g/mL)
$\rho_{TW}$	True wet density (g/mL)
$\rho_{OM}$	Density of pure organic modifier (g/mL)
$\sigma$	Surface tension (dyne/cm)
$\tau_{ij}$	Interaction parameter between i and j
$\omega$	Packing factor
$\Omega$	Total fractional swelling

# **Chapter 1**

## **Introduction**

### **1.1 High-Performance Liquid Chromatography as a Separation Technique.**

High-performance liquid chromatography (HPLC) is a very efficient physical separation technique that allows fast separations of solute mixtures and yet gives both quantitative and qualitative information about the sample. It is based on the distribution of a solute between two phases. The stationary phase requires very small particles and hence a high pressure is required to force the liquid mobile phase through the column [1, 2]. There are various modes of liquid chromatography which differ in the nature of the stationary phase.

In polar adsorption chromatography, a relatively polar stationary phase is required. The stationary phase must possess a large surface area. Silica [3, 4], alumina [3, 5, 6], zirconia [7] and magnesium oxide [8] are typical solids used in this mode, silica being the most popular one. The mobile phase is relatively non-polar. The nature of the adsorption interaction of the sample molecules depends on the type of active site in the solid stationary phase [9]. The extent of adsorption provides the separation. In general, more polar compounds are eluted later than non-polar compounds.

In reversed phase liquid chromatography (RPLC), the stationary phase is a non-polar material while the mobile phase is a polar fluid. Non-polar compounds are eluted later than polar compounds [10, 11]. The RP stationary phase can be either a chemically

bonded phase (RPBP) or a solid polymer phase. Amberlite XAD-2 is a polymeric reversed phase stationary phase. Reversed-phase bonded-phases are the ones that are most widely used in the RP mode [12]. Polar bonded phases are also available. However, they are used for normal phase (NP) separations, in much the same manner as are polar adsorbents [13], rather than for RP separations.

When the stationary phase possesses ionic properties, i.e. it has ionic groups in its structure such as  $\text{NH}_3^+$  and  $\text{SO}_3^-$ , the chromatographic mode is referred to as ion-exchange chromatography (IEC). The interaction of the stationary phase ionic groups with those in the sample provides the separation [14-16].

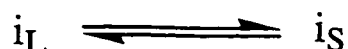
Size exclusion chromatography (SEC), sometimes referred as gel permeation chromatography (GPC) with organic solvents, and gel filtration chromatography (GFC) with aqueous solutions [17] separates molecules by their size. The smaller molecules can permeate the solid stationary phase and are eluted last. The larger molecules are excluded from small pores, so that they are eluted first.

Affinity chromatography is a chromatographic mode based on specific biochemical interactions between sample molecules and the stationary phase. A sample can only be sorbed if steric and charge-related conditions are satisfied, i.e. antigens and antibodies interactions [13, 18].

## 1.2 Retention and Equilibrium.

The separation of two or more components present in a sample is governed by the different rates of migration of the components along a chromatographic column and the spreading of molecules of each solute along the column. Differential migration is the basis of separation in chromatography.

The movement of individual compounds through the column depends on the equilibrium distribution of each compound between stationary and mobile phases. In that sense, differential migration is determined by those experimental variables that affect the distribution: composition of the mobile phase, type of stationary phase, temperature, and pressure [19, 20]. The distribution equilibrium of a sample compound “i” between a stationary phase “S” and a mobile phase “L” is given by:



Phase preference can be expressed by the distribution coefficient of compound i,  $K_i$ , [21] which represents the ratio of the equilibrium concentration of compound i in the stationary phase,  $C_{i,S}$ , to the concentration of i in the mobile phase,  $C_{i,L}$ , and is given by:

$$K_i = \frac{C_{i,S}}{C_{i,L}} \quad (1.1)$$

The capacity factor,  $k'_i$ , is defined as the ratio of total moles of i in the stationary phase,  $n_{i,S}$ , to the total moles of i in the mobile phase,  $n_{i,L}$ , at equilibrium:

$$k'_i = \frac{n_{i,S}}{n_{i,L}} \quad (1.2)$$

The capacity factor and the distribution coefficient are related by the phase ratio,  $\Phi$ , defined as the ratio of the quantity of phase “S” to the quantity of phase “L” in the chromatographic bed :

$$\Phi = \frac{V_S}{V_L} \quad \text{in volume-volume units} \quad (1.3)$$

$$\Phi = \frac{W_S}{V_L} \quad \text{in weight-volume units} \quad (1.4)$$

$$k'_i = \Phi \cdot K_i \quad (1.5)$$

$W_S$  = weight of stationary phase

$V_S$  = volume of stationary phase

$V_L$  = volume of mobile phase

The eluted compounds are transported by the mobile phase to the detector and recorded as approximately Gaussian shaped curves [22, 23]. The capacity factor can be obtained from the chromatogram by considering the column dead time,  $t_0$ , which is defined as the retention time of an unretained solute ( $k'_i = 0$ ). In other words, the time required by the mobile phase to pass through the column. The retention time,  $t_r$ , of a given retained compound is the time elapsed between injection and sample peak maximum or centre of mass [24, 25].

$$k'_i = \frac{t_r - t_0}{t_0} \quad (1.6)$$

### 1.3 Bandbroadening, Efficiency, and Resolution in HPLC.

The spreading of the initially narrow plug of sample which starts at the top of the column is caused by physical or rate processes [21, 24]. This phenomenon degrades separation. There are many reasons for bandbroadening to occur, including both intra- and extra- column processes. These will be discussed in the following subsections.

### 1.3.1 Efficiency and Resolution.

Band width in liquid chromatography is commonly expressed in terms of the theoretical plate number,  $N$ , of the column [1, 25]:

$$N = 16 \left[ \frac{t_{r,i}}{t_{w,i}} \right]^2 \quad (1.7)$$

$N$  = number of theoretical plates

$t_{r,i}$  = retention time of i.

$t_{w,i}$  = peak width, in time units, of i.

The average plate height,  $H$ , is obtained by dividing the length of the column,  $L$ , by the plate number [1, 25]:

$$H = \frac{L}{N} \quad (1.8)$$

$N$  measures the efficiency of a given column (at a given set of operation conditions). Small  $H$  values and large  $N$  values mean more efficient columns. The goal in liquid chromatography is to look for small  $H$  values in order to have large  $N$ .

In general,  $H$  is smaller for small particles and low mobile phase flow rates, less viscous mobile phases, high separation temperatures and small sample molecules. Therefore, large  $N$  and improved separations are favored by long columns and small particles [26]. To account for the total plate height, each of the bandbroadening processes has to be considered; i.e. [19, 27, 28]:

$$H = H_{eddy} + H_{LD} + H_M + H_S + H_{SM} \quad (1.9)$$

where  $H_{eddy}$ ,  $H_{LD}$ ,  $H_M$ ,  $H_S$ , and  $H_{SM}$  correspond to different bandbroadening processes that will be discussed in the next section.

The equations that support the mathematical treatment of the terms that contribute to peak tailing were developed for a large number of plates, or Gaussian peaks. This treatment assumes that, as independent processes, the effect of each one is superimposed on the moving zone centre to describe the overall peak shape.

Ultimately, efficiency is intimately related to resolution and an increase in efficiency will cause better resolution of the components of a sample. Resolution,  $R$ , is defined by [29]:

$$R = \frac{t_{r,2} - t_{r,1}}{\frac{1}{2}(W_{t,2} + W_{t,1})} \quad (1.10)$$



where  $t_{r,2} - t_{r,1}$  is the distance between the two band centres and  $(W_{t,1} + W_{t,2}) \cdot 1/2$  is the band width average between component 1 and 2.

$R$ , of two peaks is dependent on the relative retention,  $\alpha$ , the number of theoretical plates,  $N$ , and the capacity factor  $k'$ , and it is expressed as [21, 30]:

$$R \approx \frac{1}{4}(\alpha - 1)\sqrt{N}\left(\frac{k'_1}{1 + \bar{k}'}\right) \approx \frac{1}{4}\left(\frac{\alpha - 1}{\alpha}\right)\sqrt{N}\left(\frac{k'_2}{1 + \bar{k}'}\right) \quad (1.11)$$

$$\bar{k}' = \frac{k'_1 + k'_2}{2} \quad (1.12)$$

$$\alpha = \frac{k'_2}{k'_1} \quad (1.13)$$

Examination of equations 1.11 to 1.13 shows that, resolution improvements can be attained by: adjustment of the mobile phase composition in order to get larger  $k'$ ; increasing  $N$ , by using long columns; optimizing the experimental flow rate because  $H$  is a function of it [26]; and by increasing the relative retention,  $\alpha$ , which can be changed by using a different stationary phase. However, the change in the mobile phase is the first parameter that must be considered.

### 1.3.2 Bandbroadening in Liquid Chromatography.

Intra-column bandbroadening processes are of paramount importance in liquid chromatography. They are usually addressed as:

a) Eddy diffusion or multiple flowpaths. It is a non-uniform flow process. This arises from the multiple microscopic flowstreams that the mobile phase follows between different locations within the column. Sample molecules take different paths through the packed bed and, as a result, the sample zone gets broad. This is a non-uniform flow process.  $H_{eddy}$  is a function of the size and uniformity of the particles of packing in the column, and can be calculated from the following equation [26]:

$$H_{eddy} = 2\lambda d_p \quad (1.14)$$

$d_p$  = particle diameter

$\lambda$  = packing factor

Small and regularly shaped particles and uniformly packed beds give small eddy diffusion. If the particle diameter is small the sample molecule may spend less time in a given flow stream and differences among paths will be minimized. The packing factor,  $\lambda$ , accounts for uniformity of the packed bed. Large particles are easier to pack than small ones, so that  $\lambda$  is larger as the particle size decreases. In HPLC small particles are

mandatory, so that a compromise between  $\lambda$  and  $d_p$  must be found in order to get the minimum eddy term.

b) Resistance to mass transfer in the mobile phase. This is another type of non-uniform flow process. Molecules can spread in the flow stream. It refers to different flow rates for different paths of a single flow stream between surrounding particles. Liquid close to a particle moves slower with respect to the centre flowstream. This results in a spreading of the band [31].

The radial diffusion of the sample produces a relaxed non-uniform flow profile across the bed. Sample will diffuse from high concentration to low concentration regions. This process occurs at a finite rate which causes bandbroadening. A packing factor,  $\omega$ , must be considered in order to account for flow non-uniformities in packed beds. Usually,  $\omega$  is smaller for uniformly packed beds. The plate height due to this effect is derived by [28]:

$$H_M = \frac{\omega \cdot d_p^2 \cdot U_0}{D_M} \quad (1.15)$$

where  $U_0$  is the mobile phase linear velocity. As the diffusion coefficient in the mobile phase,  $D_M$ , increases the relaxation of the non-uniform flow profile is more efficient. On the other hand, the distance between particles is greater for large particles, so that bandbroadening is worse when large particles are used. Finally, for slow velocities of the

mobile phase, the sample molecules have more time to relax the non-uniform flow profile because lateral diffusion can occur more efficiently [32].

c) Resistance to mass transfer in the stationary phase. This is a non-equilibrium process. The bandbroadening contribution due to adsorption/desorption on the stationary phase is produced when the mobile phase flows down the column with a concentration different from the equilibrium concentration. The peak is broadened by the non-equilibrium processes associated with slow sorption/desorption kinetics. This contribution is related to the rate constant for sorption or desorption. The process is considered in terms of a desorption rate constant,  $k_r$ . The expression for  $H_s$  is [33]:

$$H_s = 2 \frac{k'}{(1+k')^2} \cdot \frac{U_0}{k_r} \quad (1.16)$$

d) Resistance to mass transfer in the stagnant mobile phase. This is a non-equilibrium process. The mobile phase contained within the pores of a particle is stagnant. Sample molecules move in and out of these pores by diffusion. Molecules diffusing a short distance and then returning to the moving mobile phase will move ahead of those molecules that diffuse a long distance inside the stagnant mobile phase. This contribution to the spreading of the moving band is called bandbroadening due to resistance to mass transfer in the stagnant mobile phase.

The resistance to mass transfer in the stagnant mobile phase is calculated by using the following expression [34-36]:

$$H_{SM} = \frac{fct(f, k_i') d_p^2}{\gamma' D_M} \cdot U_0 \quad (1.17)$$

For large particles, the distance that a molecule must diffuse through the pores to the particle surface will be longer, so that the degree of non-equilibrium will be larger. As  $D_M$  is larger, the faster the molecule will reach the surface and return to the mobile phase. If  $U_0$  is small there will be more time for the diffusion of the molecules and hence the non-equilibrium process will get closer to an equilibrium situation. The variable  $fct(f, k')$  is a function of the fraction of stagnant mobile phase,  $f$ , and of  $k'$ , the capacity factor. A tortuosity factor,  $\gamma'$ , corrects for the non-linearity in the path of the molecules, which will not necessarily travel in a straight line fashion [34]. In LC, the diffusion rate in the stagnant mobile phase in very small pores can cause large values of  $H_{SM}$  and low efficiencies. Liquid mobile phases with low viscosity are preferred because the larger  $D_M$  is more effective in relaxing non-uniformities in the flow profile ( $H_{SM}$  and  $H_M$ ). Lower stationary phase loadings, narrower range in particle sizes, and smaller particles contribute favorably to the overall plate height.

e) Longitudinal diffusion. When a molecule is in a fluid, the natural tendency is to diffuse randomly in all directions. This is not an important contribution to

bandbroadening at high mobile phase velocities but is significant at low mobile phase flow rates. Longitudinal diffusion,  $H_{LD}$ , occurs when molecules in the sample plug diffuse backward and forward from the center of the moving band. As the linear velocity,  $U_0$ , increases, this effect is reduced because the molecules have less time to diffuse during their transit down the column. The larger the diffusion coefficient, the more spread the sample zone gets because molecules diffuse faster. In packed beds, diffusion is affected by the presence of particles. Sample molecules finding particles in their way will encounter an obstructed path, which reduces the effective value of the diffusion coefficient. These effects are accounted for by the obstruction factor,  $\gamma$ . The longitudinal diffusion plate height term  $H_{LD}$  [37] tends to be very small in HPLC [38]. It can be calculated by:

$$H_{LD} = \frac{2\gamma D_M}{U_0} \quad (1.18)$$

As has been already mentioned, there are two processes to be considered in the mobile phase: non-uniform flow pattern (i.e.  $H_{eddy}$  and  $H_M$ ) and non-equilibrium (i.e.  $H_S$  and  $H_{SM}$ ). The non-equilibrium process is related to the adsorption that may occur when the sample front is traveling along the column. As the band is moving, the sample molecules will diffuse toward the particle as a result of sample sorption, and away from it as a result of sample desorption. This process requires some time to occur as the band keeps moving down the column, and thus contributes to bandbroadening. This process is

superimposed on the non-uniform flow profile and has the same dependencies. The non-equilibrium process arising from the mobile phase is less important than the non-uniform flow and is usually ignored.

The two non-uniform mobile phase flow pattern terms  $H_{eddy}$  and  $H_M$  are interrelated and have been assumed to be coupled. This coupled form is given by [37]:

$$H_{couple} = \left[ \frac{1}{H_{eddy}} + \frac{1}{H_M} \right]^{-1} \quad (1.19)$$

Both,  $H_{eddy}$  and  $H_M$ , only differ from one another in the nature of the process that relaxes the non-uniform profile: convection and diffusion. They do not operate independently. Equation 1.19 is known as the Giddings' equation. This is an approximation and a physical interpretation has been given. If  $H$  (total plate height) were dependent on the summation of  $H_M$  and  $H_{eddy}$  then for small diffusion coefficients in the mobile phase,  $H_M$  would be very large (equation 1.15), and therefore  $H$  would be also large. In this situation lateral diffusion (small diffusion coefficient) still operates to relax the flow inequalities, reducing  $H$ . Both terms act as a coupled term of the form shown in equation 1.19. At low  $U_0$ ,  $H_{eddy} \gg H_M$ , lateral convection (eddy term) is inefficient at relaxing the non-uniform pattern compared to diffusion, hence  $H_{couple} \approx H_M$ . At high  $U_0$ ,  $H_{eddy} \ll H_M$ , convection is more efficient than

diffusion, therefore,  $H_{couple} \approx H_{eddy}$ . The couple term can be applied in HPLC because

$H_M \approx H_{eddy}$  [39]. Finally, the overall plate height in a packed bed can be determined by

the summation of all the individual contributions previously described:

$$H = H_{LD} + \left[ \frac{1}{H_{eddy}} + \frac{1}{H_M} \right]^{-1} + H_S + H_{SM} \quad (1.20)$$

This final equation presents all the contributions to bandbroadening of eluted peaks in long columns where the efficiency is high. Compared to equation 1.9, this is a more realistic view, because of the coupling of the  $H_M$  and  $H_{eddy}$  terms, instead of considering them as independent effects.

The phenomena previously mentioned offer a wide view of the intra-column effects to bandbroadening. There are also extra-column factors that contribute to bandbroadening as the solutes enter or exit the chromatographic column. Some of these factors are large dead volume between column and detector, large sample volume, long detector response time, detector cell volume, and column-injector volume.

### 1.3.3 Tailing.

When eluted compounds are transported to the detector, in the ideal case, a Gaussian peak is recorded. Closer studies of a chromatographic peak show that the peak



shape usually is not symmetrical. When the rear part of a peak spreads out, it is called “tailing”. On the other hand, if the peak front is flatter than the rear, it is called “fronting”.

Peak asymmetry can be defined [24, 40] as the ratio of distances of rear to front of the chromatographic peak, measured from the peak maximum at 10% of the total peak height.

$$T = \frac{b}{a} \quad (1.21)$$

$a$  = distance between peak maximum and peak front measured at 0.1h

$b$  = distance between peak maximum and peak back measured at 0.1h

$h$  = total peak height

Tailing or fronting are indicative of a non-optimum chromatographic system. They reduce the column plate number and worsen resolution. There are a variety of conditions that enhance these notorious features. There can be mentioned:

a) Poorly packed columns having voids or unfilled pockets. In this case all bands show significant asymmetry.

b) Extra column volumes: detector volume, connecting tubings, injector-column and detector-column connectors. In this case early bands show greater tailing than later ones. Void effects show up even at low sample concentrations in the linear region of the sorption isotherms (see Chapter 3, section 3.2.1, below).

c) Column overload, in which case the column is not capable of separating any quantity of substances. When the quantity of sample increases, retention times and plate numbers begin to decrease, and band distortion becomes evident. This effect can be magnified by non linearity in the detector at high sample concentrations.

d) Incompatibility among the system compounds. This special case is known as chemical tailing. Some kinds of incompatibility could be a very low solubility of the sample in the mobile phase, or ionic samples on silica based reversed phase chromatography.

e) Heterogeneous retention sites or very active stationary phases in adsorption chromatography. At very low sample concentrations, the stronger sites are preferentially combined with sample molecules, but these sites are not overloaded and normal elution of sample bands is observed. When the strong sites become saturated the result is a very pronounced band tailing [41].

f) Mixed retention mechanisms. The most common band tailing results from stationary phases that allow more than one kind of retention (i.e., incomplete bonded

phase coverage of the silica surface that results in reversed phase chromatography with the organic coating) and adsorption onto the bare silica surface [4, 6, 42].

g) Unbuffered systems can lead to partial ionization of samples. Sample concentration varies between the band peak and the band tail, hence the degree of sample ionization also varies [42]. Micelle formation can also be included.

h) In liquid chromatography one important kind of tailing is that due to slow kinetic processes inside the stationary phase particles. Any slow process that retards the passage of a sample molecule in and out of the packing particles in the chromatographic column will produce broad peaks and eventually tailed peaks [34]. The slow processes that can be experienced by a sample molecule in relation to a packing particle have been summarized into five: film diffusion through the Nernst quasi static film around the particle [43, 44], pore diffusion into the stagnant mobile phase [27, 45, 46], surface diffusion [47], adsorption onto the solid surface [27] and microporous diffusion as seen in polymer packings [27, 48]. Each of the previously mentioned stages, except for adsorption and desorption, are mass transfer processes.

#### **1.4 Reversed Phase Liquid Chromatography.**

Reversed phase high performance liquid chromatography (RP-HPLC) is a powerful analytical technique widely used in different fields. The large number of available reversed phase packing materials is an indication of the increased use of this

mode. It has been classified as one special type of either adsorption or partition chromatography [49].

#### **1.4.1 Mobile Phases for Reversed Phase Liquid Chromatography.**

Methanol-, acetonitrile-, and THF- water mixtures have been the preferred choices for the mobile phase in the reversed phase mode. Mixed mobile phases are used because, if the mixture composition is changed, retention and selectivity can be varied. The mobile phase organic solvent, i.e. the organic modifier, has a noted effect in the selectivity of the stationary phase due to different interactions between solvent and solute [50, 51]. Relative phase polarity between the stationary and the mobile phase can be more quantitatively explained on the basis of the Hildebrand solubility parameter,  $\delta$ , or cohesion parameter [52], which is a composite indicator of possible intramolecular interactions that can occur among a solute, the mobile phase, and the stationary phase. The more similar the solubility parameters are, the more interaction occurs among them. The interactions are based on forces such as dispersion, dipole orientation, and hydrogen bonding [20, 52, 53].

#### **1.4.2 Stationary Phases for Reversed Phase Liquid Chromatography.**

Both chemically-bonded, silica based packing materials and polymeric packing materials are used as stationary phases in reversed phase liquid chromatography. The first silica packings [12], like the polymeric ones, were irregularly shaped and heterogeneous

but nowadays they can be prepared in a more controlled fashion. Some characteristics of each kind of packing are given as well as a comparison of them.

#### **1.4.2.1 Silica Based Stationary Phases.**

Usually RP-HPLC has been performed on silica based packing materials where an organic compound (mainly C-18 and C-8, n-alkanes) has been chemically bonded [50]. The bound molecule can also contain different functional groups which allows for a variety of polarities [3, 29, 54, 55].

Alkyl bonded phases are extremely non-polar phases which also have excellent mechanical resistance permitting the use of high linear flow rates of mobile phase [56]. They can be found in a variety of particle sizes, and those with 5-10  $\mu\text{m}$  particle diameter in a narrow particle size distribution are the most widely used [3]. They possess good mass transfer properties, producing narrow and symmetric peaks. More recently a new silica packing, with particle diameter of 3  $\mu\text{m}$ , has been introduced [57].

In the preparation of bonded phases, organic compounds, such as aromatic and linear alkanes (C2, C8, C18), are bound to the silica surface by siloxane linkages. Most common reactions are between an alkyl (or a substituted alkyl) chloro silane and the Si-OH group on the silica surface. Usually, silica and silane are slurried in toluene. An acid-acceptor catalyst (i.e., pyridine) [29, 58] is added to remove acids (HCl) generated during the reaction. The mixture is then refluxed for a few hours. Because not all Si-OH groups

are reacted in the previous step, due to steric effects, and because their presence is undesirable in the final packing [4, 12] (they produce tailing and low linear sample capacities), there is a last step in the synthesis process that is called “end capping”. This consists in treating the bonded particles with trimethylchloro silane (TMCS) in dry conditions to deactivate the residual polar Si-OH [59].

These packings present low stability when used at extreme pH values, so that their use should be restricted to a pH range of 2-8 [60, 61], although a new silica based packing has been synthesized and claimed to be stable between pH 1-12 [62, 63]. At higher pH values, the silica backbone dissolves. As a consequence, the separation properties change over time. At low pHs, the silanol groups are hydrolyzed, with the result that polar compounds are strongly retained, eluting with severe tailing [42, 64, 65]. This has been widely observed for amine separations [66, 67]. Charged molecules also show tailing due to polar interactions. Finally, when used under gradient elution conditions, columns may need re-equilibration before a next run [68].

#### **1.4.2.2 Polystyrene-divinylbenzene co-polymer (PSDVB) Stationary Phases.**

PSDVB co-polymers are reasonable alternatives to silica-based reversed-phase bonded-phases as a packing material. There are other polymeric packings currently used in HPLC but they will not be covered here [3, 5-8]. Polymeric packings are classified into microporous and macroporous polymers. Microporous (gels) are cross-linked polymers with a porosity determined by the amount of divinylbenzene cross-linker used in the polymerization process [56]. The lower the amount of this compound the softer the final

product (< 6% of divinylbenzene) which makes them inappropriate to be used in high pressure liquid chromatography.

Macroporous PSDVB's are co-polymers having macro-pores ( $\geq 50$  nm), meso-pores (2-50 nm) [69] and micro-pores (<2nm) with a high content of divinylbenzene [70]. The polymerization process has been described [71]. It is found that microgels are formed at the beginning of the reaction. Because of the presence of the solvent they swell and propagate. A cross-linked skeleton is so obtained. Porosity is controlled by using a diluent called the "porogen" [56], soluble in the monomer mixture but insoluble in the polymer. When the solvent is removed, spherical, rigid sorbent particles with permanent pores are obtained [72].

Polymeric chromatographic stationary phases are frequently used in a variety of applications. These include: the separation of metal-organic complexes in sea water [73], analysis of mixtures of methyl and propyl p-hydroxybenzoates in water and fat soluble ointment formulations [74, 75], pre-concentration of a wide variety of volatile organic compounds in air [76], purity control of erythromycin A [77, 78], purification of nucleic acids (DNA, RNA, T4 Ligase) [79], separation of carbon clusters  $C_{60}$  and  $C_{70}$  [17], separation of phosphorylated from dephosphorylated oligonucleotides up to 60 nucleotides in length on non-porous alkylated PSDVB [80-82], separation of weakly acidic organic molecules such as mono and dichlorophenols [55], separation of weakly organic bases and ampholites [60], as a medium to perform heterogeneous catalysis [83], and also in the study of the isolation of antibodies from complex biological matrices [84].

Hydrophobic polymer packings are very suitable for separations of polar as well as non-polar compounds. They possess a high tolerance to the pH of the mobile phases, and can be used over a wide range of pH (1-13). These PSDVB co-polymers remain stable over long periods of time. Due to the similarity in preparation and structure of PSDVB packings, different brands of polymers do not show important selectivity differences. PSDVB stationary phases are inexpensive, and different functionalities can be added to improve performance toward certain groups [85, 86].

There are many commercially available PSDVB packings from non-porous [79-81, 87] to macroporous [77, 88, 89]. They are sometimes functionalized to give a variety of polarities, which make them more or less water compatible [80, 89-91]. Hamilton PRP-1 [6, 65, 92], Amberlite series (XAD-2, XAD-4) [55, 60, 65, 91], and PLRP-S [74, 77, 88, 89, 93], are a few of the most used. They were reported to have very similar chromatographic properties [92, 94].

PSDVB packings show several characteristics that make them an excellent choice for HPLC. Mechanical stability, regular and narrow particle size, and inertness toward solvents, are a few of their attributes, but the most outstanding of them is the lack of silanol groups compared to silica packings. PSDVB chemical stability under extreme pH conditions is unmatched [56]. This allows for more selective separations of strong acids and bases. The hydrophobic surface can be altered to produce cation and anion exchangers [72] or less hydrophobic packings [67, 95, 96].



When organic modifiers are used their effects are not restricted to the mobile phase. Organic modifiers can also partition into the stationary polymer phase changing some of its properties [97], e.g.: 1) to “deactivate” the strong  $\pi$ - $\pi$  interaction of the sample with the polymer matrix by using a  $C_{18}$  group bound to the aromatic ring in the polymer, or 2) use of a small amount of a strong organic modifier (mixed solvent) to improve peak shape.

A characteristic usually found when these polymers are used in the reversed-phase mode is the lack of total rigidity of the polymer. Swelling of the polymer occurs in the aqueous organic solvent, due to the great hydrophobicity of these materials [65]. Preparation of more water compatible polystyrene-based packing materials by chemical derivatization to overcome shrinking and swelling when changing from water to aqueous organic solvent have been tried [85, 96]. Also, it has been found [6, 11, 87, 98-100] that aromatic compounds elute from the polymeric column with severe tailing or lower efficiencies than those obtained with silica based packing materials.

### **1.5 Excessive Bandbroadening on PSDVB.**

As mentioned before, efficiency in PSDVB columns is lower than that on silica bonded phases, as has been observed for polyaromatic hydrocarbons of low molecular weights [6, 56, 99]. Several interpretations of this phenomenon have been offered:

a) The shape of the eluted peaks showed marked dependency on the organic compound being used [101]. It has been attributed to the stagnant solutions in the pores of the packing, which reduce interactions between stagnant molecules and the mobile phase, and causing ultimately a poor elution. PSDVB carries aromatic rings along the pore surfaces; this will lead to strong  $\pi$ - $\pi$  interaction when separation of aromatic compounds is carried out [11, 99]. Depending on the molecular size and structure, some aromatics will be retained in a favorable position and their elution will be impaired.

b) On the other hand, the nature of PSDVB co-polymers makes them prone to swell and shrink depending on the cross-linking of the packing and the solvent used [102]. It has been assumed that the improvement observed in the shape of eluted aromatic compounds is due to swelling of the polymeric solid by preferential sorption of the organic modifiers based on their solubility parameters [99, 103]. Lower cross-linked regions, due to heterogeneity [104], will swell when in contact with organic compounds having solubility parameters close to that of the PSDVB [105]. So that, when a solvent gradient is used the expansion and contraction of the packing can cause channeling inside the column. This will eventually produce tailed peaks.

c) If the sample molecule can diffuse inside the micropores, and the ability of the eluent to penetrate those cavities is restricted, a process known as hindered diffusion [22, 106]. Poor elution is attained [107] unless a good modifier, such as THF [99, 103] is added to the eluent (swelling of the matrix). Micropores are present in all PSDVB due to the size of the aromatic rings. The presence of micropores in the copolymers was

suggested in a study using different PSDVB packings having different surface areas [108].

## **1.6 Overview of the Present Work.**

A study made on different PS-DVB copolymers suggests that the structure of their matrix is composed of two regions. The first region is a swellable, permeable, and low cross-linked polymer. The second region is a non-permeable, non-swellable, and highly cross-linked polymer [109]. Another study points out that the highly cross-linked regions have a permanent open structure [107] due to the existence of spaces between chains and bonds (micropores). Our results, which are to be explained later, agree with this latter observation since adsorption into micropores (highly cross-linked region) is possible depending on the adsorbate, and more specifically, on its solubility parameter. Solvation and swelling of the collapsed (when dry) low cross-linked regions possibly allow solutes to diffuse inside the microporous structure where no swelling can occur. Based on these interpretations, it would not be surprising that the more rigid regions of PSDVB (non-swellable) could sorb organic molecules which have an affinity for the polymer and that they experience severe hindered diffusion within the micropores.

This work covers two types of characterization of two types of processes: equilibrium and kinetics for both sorption and swelling of the PSDVB co-polymer Amberlite XAD-2. The swelling behavior of Amberlite XAD-2 was studied as a function of the solvent sorption onto the resin at equilibrium and under kinetic conditions for various binary mixtures of three organic modifiers (OM) in water: tetrahydrofuran (THF), acetonitrile (AN), and methanol (MeOH). The sorption isotherms of the organic modifiers from binary mixtures with water were measured using the batch equilibration

technique. Swelling of the particles was determined by microscopic measurements of the particle diameter in the aforementioned group of solvent-aqueous solutions.

A brief description of each chapter of this thesis is now given:

Chapter 2 lists all of the experimental procedures used in order to get the sorption isotherms and rate of sorption of THF, AN, and MeOH from aqueous solution on XAD-2, the equilibrium and rate of swelling of the XAD-2 resin in aqueous THF, AN, and MeOH solutions, and description of the apparatus used for the swelling measurements. Water uptake measurements on XAD-2 by Thermal Gravimetric Analysis is also presented.

Chapter 3 is focussed on the equilibrium studies. The results of water uptake are given. A very detailed interpretation of the sorption isotherms and swelling of the polymer is offered. Also, a combination of both types of experiments is attempted, i.e. swelling-sorption curves, in order to interpret the solid-solvent interaction.

Chapter 4 is concerned with the kinetic studies. Swelling rates of XAD-2 and the sorption rate of the OM<sub>s</sub> onto the XAD-2 resin are compared and interpreted. A mechanistic approach is suggested.

Chapter 5 gives the relevant conclusions of Chapters 3 and 4 and proposed future work.

The Appendix section has been divided into A, B, C, and D. Appendix A contains the packing procedure followed to prepare the Porapak-QS GC column employed in the GC experiments. Appendix B shows the calculation steps in order to get the concentration of organic modifier sorbed onto the solid. Appendix C gives tabulated data for all of the plots presented through this thesis. Appendix D gives a brief description of the Differential Scanning Calorimetry technique and the experimental approach to determine water presence in XAD-2.

## Chapter 2

### Experimental Section

#### 2.1 Introduction.

This section describes all the experiments that were carried out in this work, including the equilibrium and kinetic swelling measurements, as well as the sorption isotherms for the studied systems. The special cells, designed for the swelling measurements of single and multiple particles, are also presented.

#### 2.2 Sorbent Amberlite XAD-2.

PSDVB represents a series of non-polar co-polymers. They are organic materials, having macro ( $\geq 50$  nm) and meso pores (2-50 nm) [69] obtained in spherical form. A suspension polymerization technique is used so that spherical particles are obtained [70, 110]. Present in the suspension are [71]: a monomer such as styrene; a cross-linker (divinylbenzene); an initiator, which can produce a radical and initiates polymerization; and a porogen (an inert solvent), which is a good solvent for the monomer but a poor one for the polymer that is being formed in the reaction.

Porosity is controlled by using a porogen. When the solvent is removed, permanent pores exist in the spaces left and a rigid, macroporous sorbent particle with a high surface area and a hydrophobic surface is so obtained. The transition from macro to micro pores, ( $\leq 2$  nm, spaces between chains) is not discrete but rather gradual and this is

the origin of the heterogeneous nature of this type of polymer. These materials are not soluble in organic solvents. A synthetic approach is given in Figure 2.1 [1, 70].

Amberlite XAD-2 is a white PSDVB co-polymer sorbent produced in beads designed for the sorption of water-dissolved organic compounds, but it does not take up water without a previous treatment with organic wetting solvents. After treatment with an organic solvent, i.e. MeOH, XAD-2 can take up water in the voids or macropores. It has a high affinity for non-polar compounds such as THF and benzene. One laboratory application of this type of resin is as a support for reversed-phase liquid chromatography [111, 112]. Some properties of the Amberlite XAD-2 are given in TABLE 2.1.

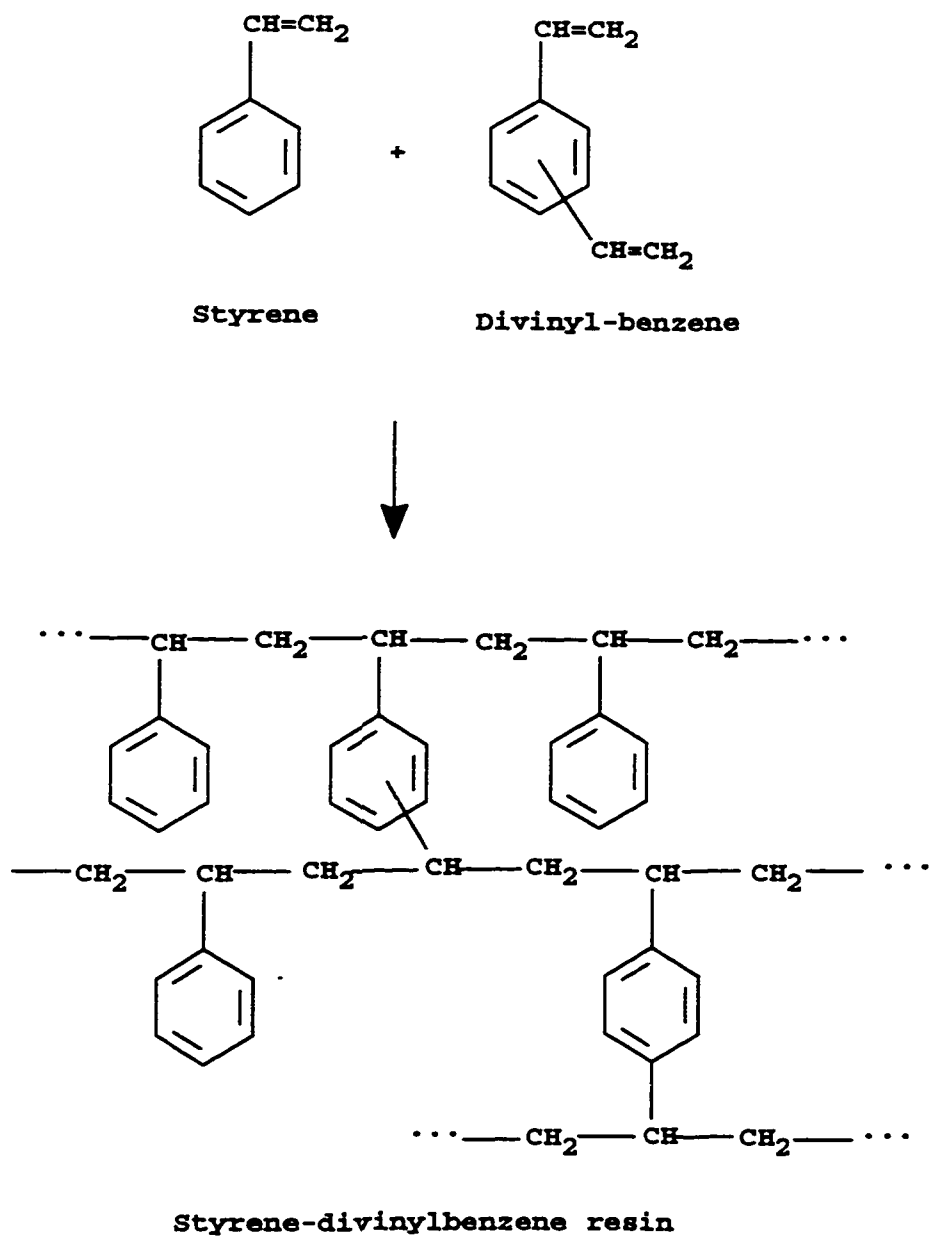


**Figure 2.1** Schematic of the general synthesis of Polystyrene-divinylbenzene co-polymers.



**TABLE 2.1 Physical properties of the Amberlite XAD-2 resin [112].**

<b>Property</b>	<b>Amberlite XAD-2</b>
<b>Physical Appearance</b>	<b>Spherical opaque white beads</b>
<b>Particle Size (selected) (<math>\phi</math>)</b>	<b><math>360 \pm 31 \mu\text{m}</math></b>
<b>Matrix Density</b>	<b>1.07 g matrix/mL matrix</b>
<b>Average Pore Diameter</b>	<b>90 Å (dry)</b>
<b>Specific Pore Volume (<math>P</math>)</b>	<b>0.40-0.45 mL pore/mL bead (dry)</b>
<b>Specific Surface Area (<math>A</math>)</b>	<b>330 m<sup>2</sup>/g (dry)</b>
<b>True Wet Density (in water) <sup>(a)</sup> (<math>\rho_{TW}</math>)</b>	<b>1.02 g wet particles/mL of particles</b>
<b>Packing Density</b>	<b>0.64-0.70 g dry-resin/mL of wet resin</b>

**(a) Macropores are filled with water.**

Amberlite XAD-2 (20-50 mesh, Fisher Scientific, lot 2-0218) was cleaned and fractionated by solvent elutriation by D. Gowanlock as previously described [113] and the  $(360 \pm 31 \text{ }\mu\text{m})$  diameter spheres were chosen. The particles were kept in methanol until needed. The slurry was filtered to remove most of the solvent, air dried and finally dried at 80°C overnight prior to use. The remaining portions of resin were stored in a stoppered bottle in a desiccator over Drierite until used.

### **2.3 Reagents and Solvents.**

Distilled-deionized water was obtained from a Barnstead NANOpure water filtration system (Boston, MA). 2-Propanol (2POH) (ACP Chemicals INC., Montreal, Canada), methanol (MeOH) (Fisher Scientific Co.), tetrahydrofuran (THF) (Caledon Laboratories Ltd., Georgetown, Ontario, Canada), and acetonitrile (AN) (Anachemia, Montreal, Canada) were reagent grade, and were carefully checked for purity by gas chromatography. All of the solvents were distilled and filtered through nylon 66 filters, 0,45  $\mu\text{m}$  pore diameter (Mandel Scientific Co. Ltd., Guelph, Ontario, Canada), before use. MeOH was kept in a glass bottle in contact with beads of the type 3A molecular sieve. THF was distilled in the presence of metallic sodium chips to eliminate any water sorption and collected in a dark glass bottle.

## **2.4 Water Uptake Measurements Using Thermal Gravimetric Analysis.**

Thermal Gravimetric Analysis is a technique widely used to determine weight loss from materials. PSDVB co-polymers are hydrophobic in nature [112], yet some have reported [14, 111] water uptake (w/w of dry co-polymer) for XAD-2 and other PSDVB co-polymers without solvent pre-treatment. As a starting point, it was very important to determine if any water was indeed sorbed by XAD-2.

### **2.4.1 Apparatus for Thermal Gravimetric Analysis.**

Thermal Gravimetric Analysis (TGA) of the Amberlite XAD-2 was carried out in a TGA meter (model Mettler TA 4000) which is composed of a Mettler thermobalance (model TG 50), a Mettler data processor (model TC11), and appropriate Mettler software for data analysis (model TA 72-PS 2100). A schematic picture is shown in Figure 2.2.

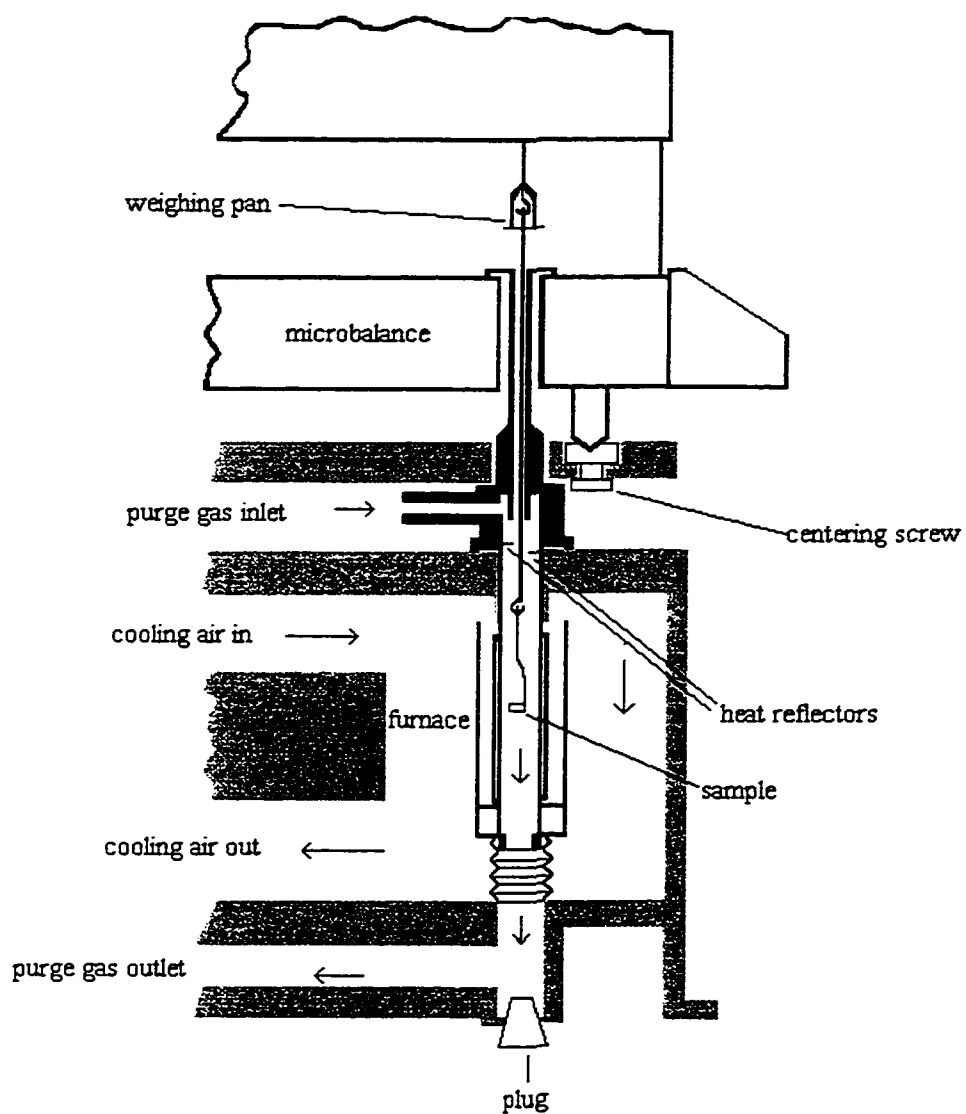


**Figure 2.2** TG50 Thermobalance for TGA measurements. Details of the construction of the furnace, the sample pan suspension and microbalance are shown.

### **2.4.2 Sample Preparation.**

TGA was performed in order to measure water uptake onto the XAD-2 particles. Two 5g vacuum dried XAD-2 samples were placed into petri dishes. A 4L- desiccator vessel, containing water at the bottom, was used as the container to provide the humid environment. The petri dishes were placed on the desiccator plate. This was closed at atmospheric pressure and stored in an oven, set at 35°C, for 45 days to allow equilibrium to be achieved.

### **2.4.3 TGA Measurements.**

Samples of XAD-2 from the previous step,  $\approx 20$  mg, were weighed into dry  $\text{Al}_2\text{O}_3$  crucibles. One crucible at the time was placed onto the thermobalance plate and lowered to the oven section by using a precision knob. The thermobalance oven, initially at 35°C, was then programmed to a 10°C/min heating rate. Weight variations were constantly registered until the final temperature was reached, which, in this experiment, was set at 300°C. A plot of weight loss versus temperature is obtained. This procedure was repeated for a dry sample, used as the blank, and a sample spiked with water to determine different types of water present, if any.

## **2.5 Uptake of Organic Modifier.**

In this section, two types of experiments will be described. The sorption of organic modifiers onto XAD-2 was studied in both kinetic and equilibrium conditions.

### **2.5.1 The Gas Chromatograph Apparatus.**

All of the chromatographic measurements were made in a Perkin Elmer 8500 gas chromatograph equipped with a Perkin Elmer GP100 Graphic Printer, using an in-house packed Porapak QS (mesh 50-80, batch 35, Chromatographic Specialties, Ontario, Canada) column, 3 m long and 2.163 mm internal diameter. Detection was achieved by using a Thermal Conductivity Detector (TCD).

### **2.5.2 Chromatographic Conditions for Multicomponent Samples.**

Optimal chromatographic conditions, carrier flow rate, column temperature, injector and detector temperature, were found for the three different mixtures used in this work in order to get a good resolution of the four components (air, water, organic modifier, and 2-propanol (2-POH) as an internal standard) which were present in each sample. TABLE 2.2 shows a summary of the optimal conditions.

**TABLE 2.2** Optimal gas chromatographic conditions for measurements of standards and samples. He was used as carrier gas. A Porapak QS column was used in all experiments. Details regarding column packing and conditioning can be found in APPENDIX A. The Thermal Conductivity Detector (TCD) was always set to the low sensitivity range (150 mA).

	MeOH/H <sub>2</sub> O/2-POH		AN/H <sub>2</sub> O/2-POH	THF/H <sub>2</sub> O/2-POH
Column temperature	T <sub>1</sub> =125°C	T <sub>2</sub> =220°C	T <sub>col</sub> =160 °C	T <sub>col</sub> =200°C
	t <sub>1</sub> =1.0 min	t <sub>2</sub> =1.5 min		
	Ramp = 30 °C/min		0	0
Flow rate	30 mL/min		30 mL/min	30 mL/min
Injector temperature	270 °C		250°C	275°C
Detector temperature	270°C		250°C	270°C
Injection volume	1µL		1-2 µL	1-2 µL
Run time	7 min		8 min	7 min

### **2.5.3 Thermostated Bath.**

To ensure a constant temperature while performing the sorption and swelling experiments, a constant temperature bath (Blue M, Magni Whirl constant temperature bath, Blue Island, Illinois, USA) was employed. It was composed of a stainless steel 30L bath, with a shaker platform attached to an electrical motor to shake the samples at different speeds. A thermometer was used to monitor the temperature inside the bath. The samples were fixed on this platform and immersed in the water. The bath was covered with a stainless steel lid that was easily removed for sample collection. The working temperature was maintained at  $(25 \pm 1)^{\circ}\text{C}$ .

### **2.5.4 Equilibrium Time Required in Sorption Experiments.**

Samples were prepared by adding approximately 60 mL of a 50% organic modifier (OM) in  $\text{H}_2\text{O}$  solution to approximately 10 g of vacuum-dried adsorbent in a glass-stoppered bottle (Figure 2.3). Samples were shaken at constant temperature. An aliquot was collected every 24 hours and analyzed by gas chromatography. The area ratio OM/ $\text{H}_2\text{O}$  was monitored until its value remained constant, demonstrating that equilibrium had been achieved.

### **2.5.5 Sorption Isotherm Experiments.**

A sample of dry XAD-2 (3.5 g for THF sorption and 10.5 g for each of AN and MeOH sorption) was weighed to the nearest tenth of a milligram in a tightly fitting glass-



stoppered flat-bottom cylinder (125 mL capacity) (Figure 2.3). This container consisted of a glass cylinder, (4cm of diameter, 13cm height) with a ground-glass lid, in which was attached a needle port with a multi-use Teflon faced liner (Alltech, Alltech Associates, Inc., 2051 Waukegan Road, Deerfield, IL.). This allowed the removal of microliters of liquid sample, avoiding the opening of the sorption container and evaporation of the volatile compounds. An accurately weighed amount of pure organic solvent was added to wet the particles. After a few minutes, distilled water was added to produce the required organic modifier concentration. The final weight was recorded. The cylinder was placed in the constant temperature shaker bath ( $25 \pm 1$  °C) under constant gentle agitation.

After three to four days, depending on the organic modifier used, which was sufficient time for equilibrium to be reached, three weighed aliquots of the supernatant liquid ( $\approx 3$  g) were taken and weighed into tared capped vials, to the nearest tenth of a milligram. Following this step, a known amount of 2-propanol, as internal standard (IS), was added to each vial. The amount of IS in each case was chosen so that the area ratio of the organic modifier GC peak to IS GC peak was close to one. Four injections of each of the triplicate samples were analyzed by GC.

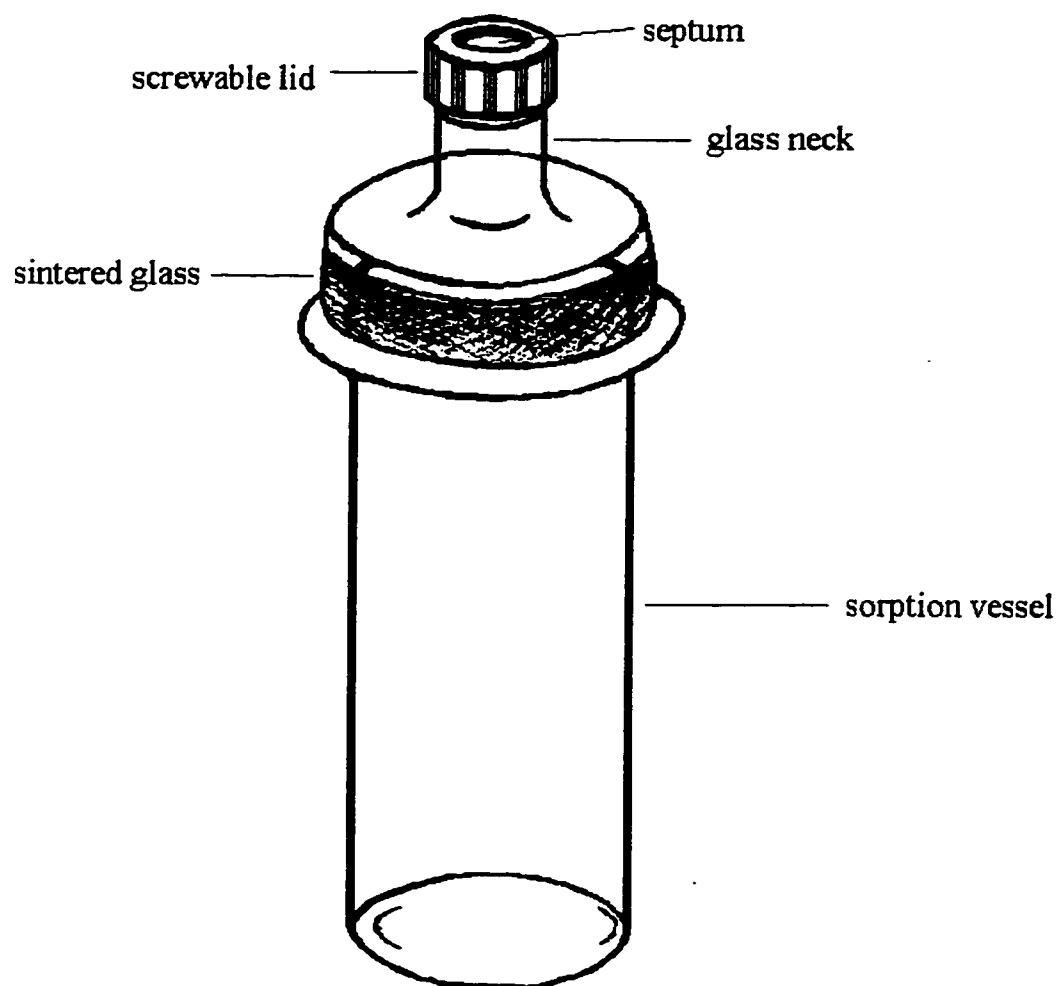


**Figure 2.3** Sorption flask for bath equilibration method.

A calibration curve was obtained by using several standards, prepared in the same way as the aliquots except that the resin was omitted.

Once the OM concentration of the aliquots was known, a mass balance equation for the solvent in solution was used to calculate the amount of OM sorbed. By subtracting the final amount of OM found in solution after equilibrium from the initial amount of OM used, the sorbed mass of OM was obtained. The concentration of OM in the solid phase was gotten by dividing the sorbed mass by the XAD-2 mass used in the batch.

#### **2.5.6 Sorption Rate Experiments.**

An amount of dry XAD-2 ( $\approx 10$ -14 g), weighed to a precision of the tenth of a milligram, was placed in the container shown in Figure 2.3, as previously described. The aqueous solution of organic modifier at the appropriate concentration, at  $(25 \pm 1)^\circ\text{C}$ , was added to the dry particles and the time was recorded as time zero ( $t = 0$ ). A control flask containing only aqueous organic solution (no particles) was used in each experiment to account for changes in the concentration other than sorption. Shaking was begun. Samples were collected with a 10  $\mu\text{L}$  gas chromatography syringe (Hamilton, Hamilton Company, Reno, Nevada) every 2 minutes during the first ten minutes of the experiment and after that, the time interval was increased to 10, 20, 40, etc., minutes, until equilibrium was reached. In each case, a sample of 1  $\mu\text{L}$  was withdrawn and immediately injected into the gas chromatograph for analysis. The calibration of the gas chromatograph was assessed by using various solutions of known concentration (%w/w)

of the aqueous organic modifier under study. The experiments were run until no change in the supernatant solution concentration was observed. A two point GC calibration curve was prepared.

## **2.6 Swelling Studies on Amberlite XAD-2.**

### **2.6.1 Apparatus for Swelling Measurements.**

The swelling of the XAD-2 particles was monitored by means of an E. Lietz/Wetzlar (Germany) optical microscope, equipped with a (170/-, 10:1, A 0.25) objective and an eyepiece with a graduated scale (10X, Baush & Lomb Opt. Co., USA). A stage micrometer (Fisher Scientific, catalog No. 16A, 12-579) was used for calibration of the eyepiece scale.

#### **2.6.1.1 Multiple Particle Measurements.**

When measuring multiple spheres, i.e. swelling equilibrium measurements, the particles were contained in a tightly stoppered specially designed glass cell. It is shown in Figure 2.4. The cell was very easy to tilt in order to make the particles contained in it change position. The cell has a total volume of 1 mL. The two openings in the cell permit washing the particles and changing solvent continuously. A porous glass frit prevents the particles from leaving the cell during washing or flushing. During measurement, the cell was sealed with Teflon stoppers. It did not need special attachments to be viewed under the microscope.

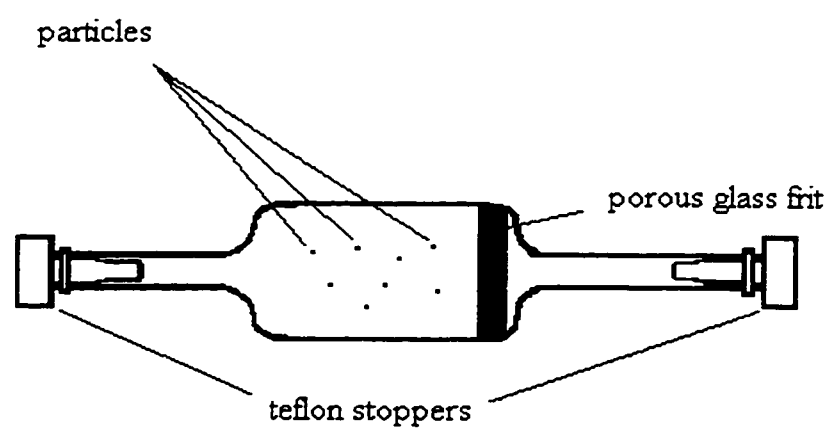


**Figure 2.4 Continuous flow cell for swelling measurements of multiple particles.**

### **2.6.1.2 Single Particle Measurements.**

In the kinetic approach, only one particle at the time was monitored in the swelling process. A cell was designed that allowed dynamic swelling measurements of a single particle under load, (see Figure 2.5). The cell rests over a hole in a aluminum plate ( $2.5 \times 7.5 \text{ cm}^2$ ). The cell itself is composed of a septum (Supelco, Thermogreen™ LB-2, 11.5 mm, Bellefonte, PA), with a 2mm diameter hole through it, which gives a volume of  $3.14 \times 10^{-3} \text{ cm}^3$  where the single particle will be at sight at all times. This septum is sandwiched between two microscope slides. The cell is topped with another aluminum plate with an 8 mm diameter hole through it, with the same diameter of the support, which is screwed to the bottom plate.

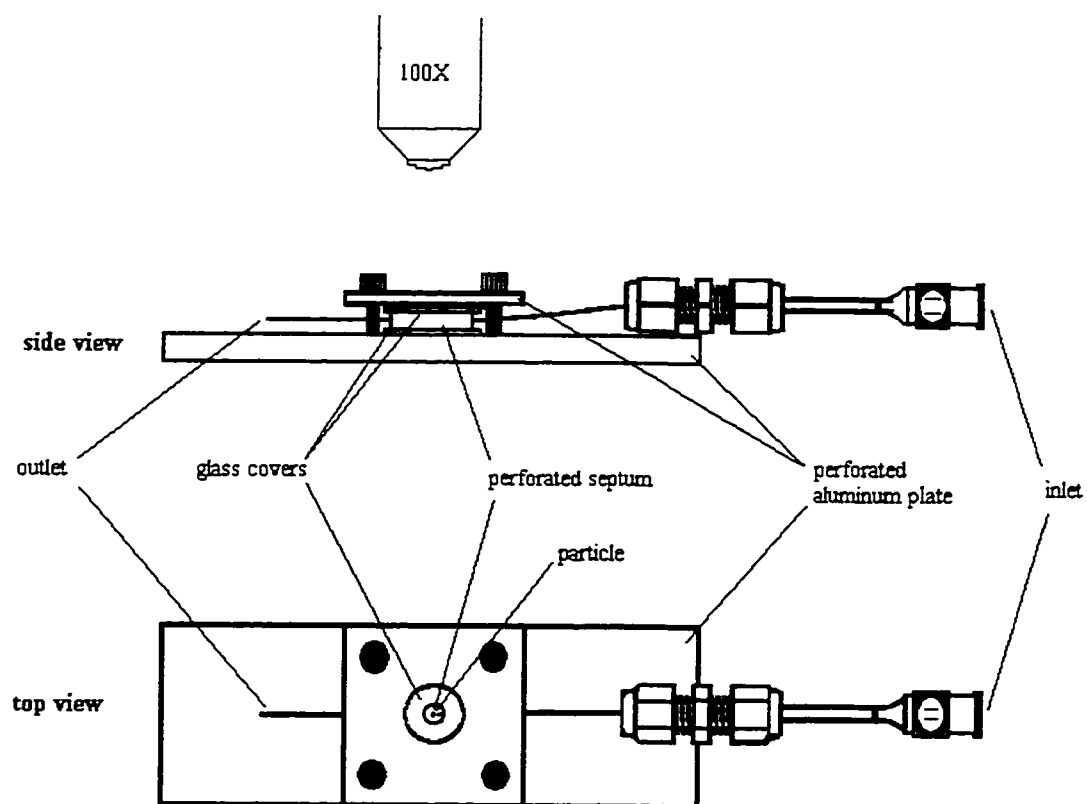


**Figure 2.5** Continuous flow cell for swelling measurements of a single particle.

## **2.6.2 Procedures for Swelling Measurements.**

Swelling of Amberlite XAD-2 particles was measured in both equilibrium and kinetic experiments. Glass beads were also used in order to get an optical blank for the system employed. Glass beads do not swell in any of the solvents employed in this work.

### **2.6.2.1 Equilibrium Swelling Measurements on XAD-2**

All of the particles used in the swelling experiments were chosen based on two requirements: spherical shape and similar dry diameter. Seven to ten particles were used in each experiment to account for differences between particles (i.e. cross-linking). They were placed in the cell shown in Figure 2.4. Since poly(styrene)-divinylbenzene copolymers (PSDVB) are highly hydrophobic, the dry co-polymer does not wet in pure water and does not take water into its macropores if the dry particle is contacted with water. Therefore, the particles were wet first with pure organic modifier [55], which caused them to swell to their maximum capacity in that particular solvent. Then, the organic modifier was removed completely by continuous injection of deionized-degassed water.

The particles were left in water until they stopped shrinking. The water was then removed and the cell refilled with a solution of known concentration of organic modifier in water (% w/w). The size measurements were taken after two hours by which time swelling equilibrium had been reached in all cases.



The polymer particles were measured in different positions to account for anisotropic swelling. Each particle was measured four times. This procedure was repeated for different concentrations of organic modifier, always going from low to high concentration.

To ensure constant supernatant concentration throughout the swelling process, the cell was filled to its maximum volume with the solution under study. The initial and final concentrations of organic modifier were checked by GC and found constant during the experiment. All swelling equilibrium experiments were studied at controlled temperature ( $25 \pm 1$ ) °C.

#### **2.6.2.2 Swelling Rate Measurements on XAD-2**

The swelling rate of an XAD-2 single particle, 340.8  $\mu\text{m}$ , was followed at ( $25 \pm 1$ )°C using the cell shown in figure 2.5. The dry particle was confined to the small volume in the cell. Pure methanol solvent was pumped through the inlet of the sample cell (5 min) in order to thoroughly wet the particle. The inlet of the cell was then connected to a syringe filled with deionized water and the particle was rinsed until it stopped shrinking. The excess water was then removed with a clean syringe. The swelling rate study was timed at the moment when the pumping of an aqueous solution of known concentration (% w/w) was initiated ( $t=0$ ) through the cell inlet. Readings were taken every 10 to 20 seconds during the first minutes of the swelling rate experiment. During each reading the flow was interrupted for a few seconds.

The diameter of the particle was recorded as a function of the contact time with the aqueous solution. Once the experiment was finished for a given concentration of the mobile phase, the swollen particle was rinsed with deionized water until the initial diameter was regained. Each swelling rate was measured at least twice in order to fill time gaps. The same procedure was repeated for different aqueous organic concentrations.

#### **2.6.2.3 Microscopic Measurements of Glass Beads in Solvents.**

To discard the possibility of any optical distortion or misreading of the particle diameter in different media, it was necessary to set up an experiment where those errors could be detected, if present. Six non-swellable Glass beads,  $\phi \approx 740 \mu\text{m}$ , were measured in the optical cells described in the previous section. The measurements were made in the same fashion as for the PSDVB. The glass beads were placed in air, water, and THF. The diameter in each medium was recorded three times for each particle.

## Chapter 3

### Equilibrium Sorption Isotherms of Organic Modifiers and Swelling of Amberlite XAD-2.

#### 3.1 Introduction.

The composition of the mobile phase is the most used parameter for controlling the retention in liquid chromatography. Some researchers have studied the effect of the organic modifier (in aqueous-organic mobile phases) on the distribution of a sample molecule between the two phases [114, 115]. To fully understand the processes taking place in a chromatographic column, it is necessary to determine the kind of interaction existing between stationary and mobile phases. Swelling of resins and sorption isotherms of different organic modifiers present in the mobile phase [116] have been investigated, in order to explain the behavior of polymeric packings.

In this work, the equilibrium sorption isotherms and swelling equilibrium curves were determined for MeOH, AN, and THF from binary aqueous solution on Amberlite XAD-2. Sorption isotherms are presented as the concentration of the sorbed organic modifier (OM) in g/gXAD-2 versus the concentration of OM in the equilibrium liquid phase in g/g and also as sorbed OM in g/gXAD-2 versus activity of the OM in the liquid phase. Swelling curves are presented as swelling ratio (defined in section 3.2.3.2) in mL/g XAD-2 versus the OM concentration in the equilibrium liquid phase in g/g and also as swelling ratio in mL/gXAD-2 versus activity of the OM in the liquid phase. In

addition, the isotherms and swelling curves have been combined, and are presented as the swelling ratio in mL/gXAD-2 versus concentration of the OM sorbed in mL/gXAD-2. The aim of this work is to understand the processes involved in polymer/solvent interactions, in terms of the PSDVB co-polymer structure.

## 3.2 Theory.

### 3.2.1 Distribution Coefficient Measurement.

When determining the sorption isotherm of a compound between two phases, the concentration of the solute in both phases at equilibrium is determined at several concentrations. The ratio of the concentration in the solid phase to the concentration in the liquid that is at equilibrium at any given concentration is called the distribution coefficient. Definition of the distribution coefficient has been given in chapter 1 (section 1.2, eqn.1.1), and is graphically presented in Figure 3.1. In the present context, the stationary phase is taken to be the polymer matrix, which includes the gel, the micropores, and the walls of the large pores (macro- and meso- pores), into- (or onto-) which sorption can occur. The liquid phase is taken to be bulk liquid which is present both in the solution outside the particles and in the solution that is present in the large pores (macro- and meso- pores). This definition of  $K_i$  is consistent with that which is used in chromatography, where the volume of mobile phase is taken to include the pore liquid (i.e. stagnant mobile phase).

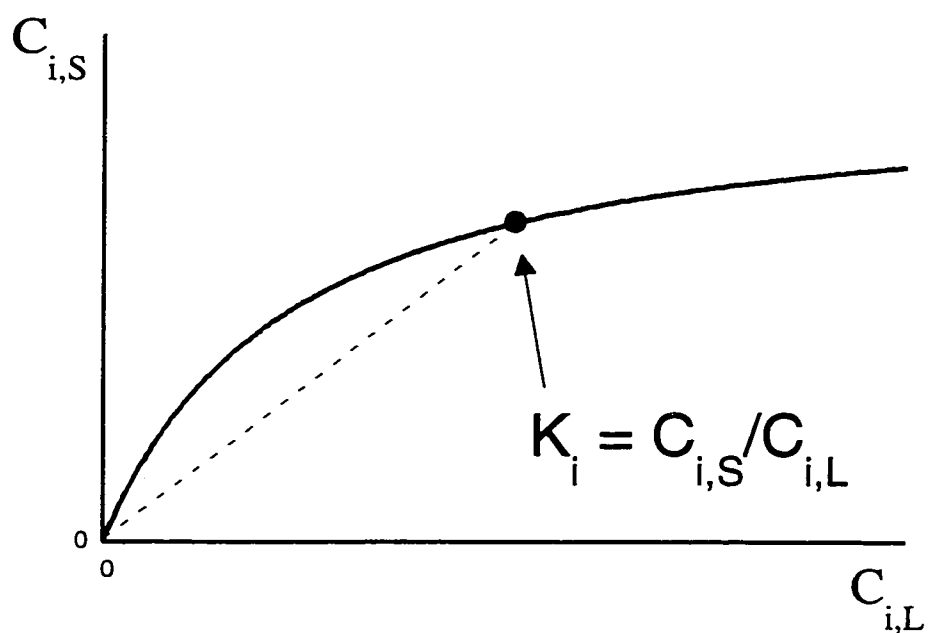


**Figure 3.1:** Relationship between distribution isotherm and distribution coefficient. The distribution coefficient,  $K_i$ , at any point on the isotherm is the ratio  $C_{i,S}/C_{i,L}$  (slope of dashed line).

There are a number of methods that can be used to determine sorption isotherms [43, 117, 118]. They can be divided into two categories: on-column and batch techniques. On-column methods include frontal analysis (non-equilibrium analysis) [103, 114, 117] and column equilibration [22, 106], in which a sample solution is constantly injected into a column, packed with a known amount of sorbent. In frontal analysis, the concentration at the outlet of the column is monitored until total breakthrough of volume (influent and effluent concentrations are equal to each other) of the sample is achieved. This process is repeated for each point in the isotherm using different concentrations. The column equilibration method [106, 119] resembles that of the frontal analysis, except that instead of continuously monitoring effluent concentration the amount sorbed at equilibrium after total breakthrough of the sample solution is eluted and measured.

In batch techniques for measuring sorption isotherms [48, 102, 120-125], several samples with known quantities of the sorbent, solute, and water are placed in closed bottles and are agitated for a time long enough to achieve equilibrium, in a temperature-controlled bath. A portion of the liquid is then taken from each bottle and analyzed to determine solute concentration in the liquid. The amount sorbed is calculated by a simple mass balance. The batch method was used in this work. Calculation of the distribution coefficients for each of the isotherms presented in this work is given in Appendix B.

### 3.2.2 Equilibrium Sorption Isotherms.

The relationship between the equilibrium concentrations of a component in the mobile and the stationary phases at constant temperature is known as the sorption isotherm [10, 126-129]. This is a plot of the concentration of the component,  $i$ , in the stationary phase,  $C_{i,S}$ , as a function of its concentration in the mobile phase,  $C_{i,L}$  (Figure 3.1).

The sorption isotherm is a collection of distribution coefficients, as mentioned in section 3.2.1 and defined in equation. 1.1. Each point on the isotherm represents a particular distribution coefficient and it is equal to the slope of the straight line traced from the origin to a specific point on the isotherm (dotted line in figure 3.1). If the isotherm is linear,  $K_i$  is a constant, independent of sample concentration. If the isotherm is curved, then  $K_i$  changes with sample concentration.

The shape of the sorption isotherm can be related to the shape of the elution peak in liquid chromatography. Figure 3.2 shows the three basic chromatographic peak shapes and their associated isotherms. A linear distribution isotherm produces a Gaussian peak (figure 3.2a), but there are two other basic shapes to be encountered; convex and concave shaped isotherms.

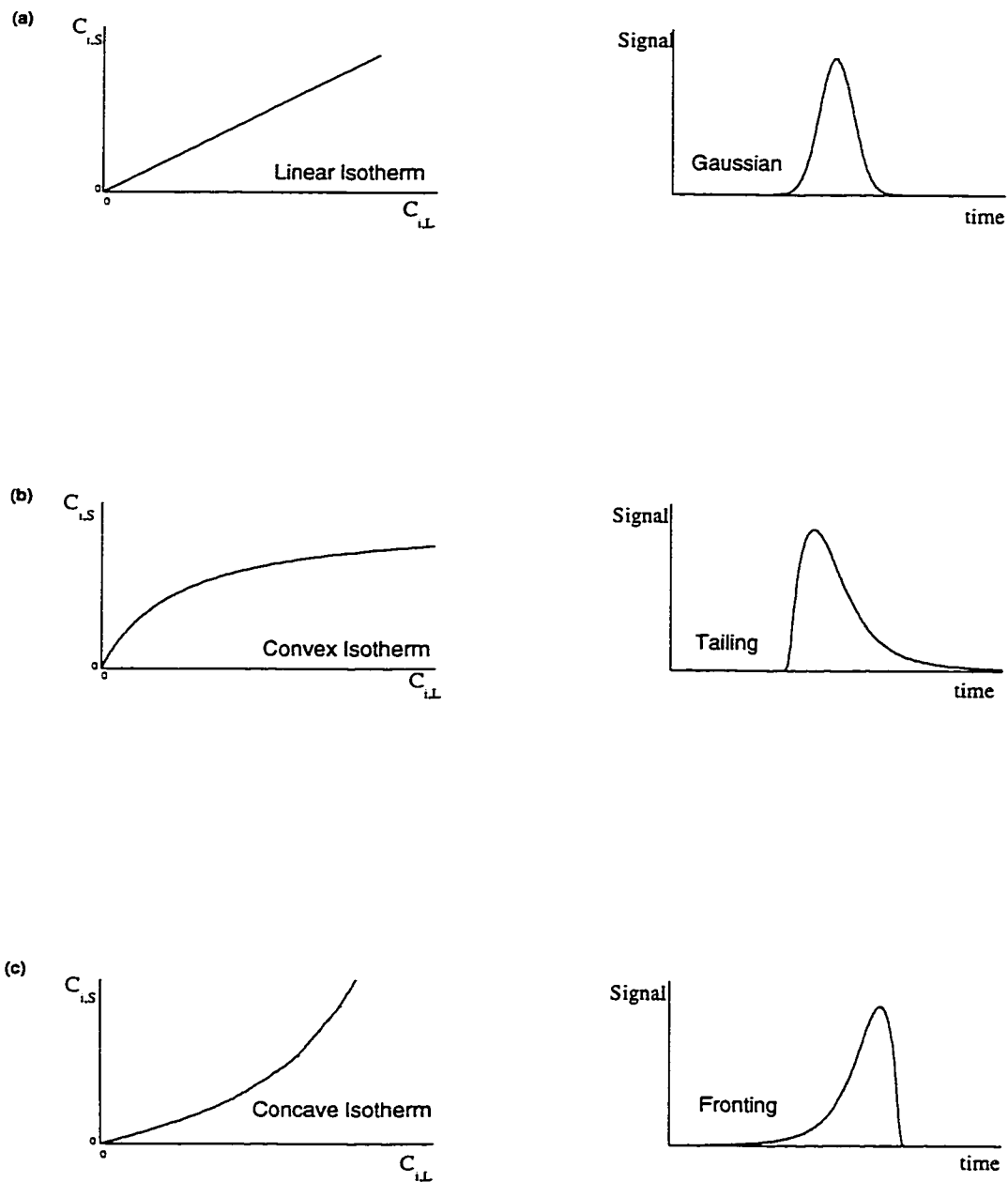


**Figure 3.2: Representation of the most common isotherms and their corresponding chromatographic elution peaks.**



In a convex isotherm,  $K_i$  decreases as  $C_{i,L}$  increases (figure 3.2b). In a concave isotherm,  $K_i$  increases as  $C_{i,L}$  increases (figure 3.2c). Both concave and convex isotherms become linear at very low solute concentrations,  $C_{i,L}$ . Depending upon the region of the isotherm where the chromatographic analysis is being performed, it will be referred as linear chromatography or non-linear chromatography.

Convex isotherms are the most widely observed isotherm shape. There are many mathematical models developed to describe them and the physical process taking place upon sorption. The Langmuir isotherm [126, 128, 130], for which a plateau is reached, is the most commonly cited and simple convex non-linear isotherm:

$$C_{i,S} = \frac{abC_{i,L}}{1 + bC_{i,L}} \quad (3.1)$$

where **a** and **b** are constants. The Langmuir isotherm was developed assuming an energetically homogeneous surface [131] where each site can hold only one molecule of sorbate, and the lateral interaction between neighboring sites is nil. One of the Langmuir isotherm features is that there is a monolayer restriction upon adsorption. Due to the nature of the model used by Langmuir, it is not surprising to find that many experimental data are not fit by the model. Some reasons for this are: more than one type of site is present; lateral attraction or repulsion between sorbed molecules; multilayer adsorption; and reorientation of sorbed molecules at high concentration [114, 128, 132, 133].

The Langmuir sorption isotherm is not a very suitable model for the sorption of organic modifiers on PSDVB due to their non-homogenous nature. If more than one energetic type of site on the surface is suspected, a more realistic approach would be to consider a modified Langmuir isotherm. In order to interpret sorption processes on heterogeneous packing materials, it is required to treat the adsorbent as having a continuous distribution of sorption energies [134]. There are a number of more complex isotherms that can be used, such as the multiple site Langmuir adsorption isotherm [135], Freundlich isotherm [136], the dual sorption model [137], Jovanovich-Freundlich isotherm [132], and others [114, 123, 138].

### **3.2.3 Polymer Swelling.**

Polymeric materials often swell in the medium in which they are used. Swelling and shrinking of these materials reflect the structure of the polymer.

#### **3.2.3.1 The PSDVB Structure.**

In order to understand what processes in the XAD-2 particle are really responsible for the bandbroadening and tailing observed in liquid chromatography, it is necessary to understand in more detail the structure of the PSDVB particles. The PSDVB matrix has been described as having different regions. In order to identify the terms that will be used along this work, Figure 3.3 and 3.4 identify the different regions encountered in a PSDVB bead and the chosen terminology.

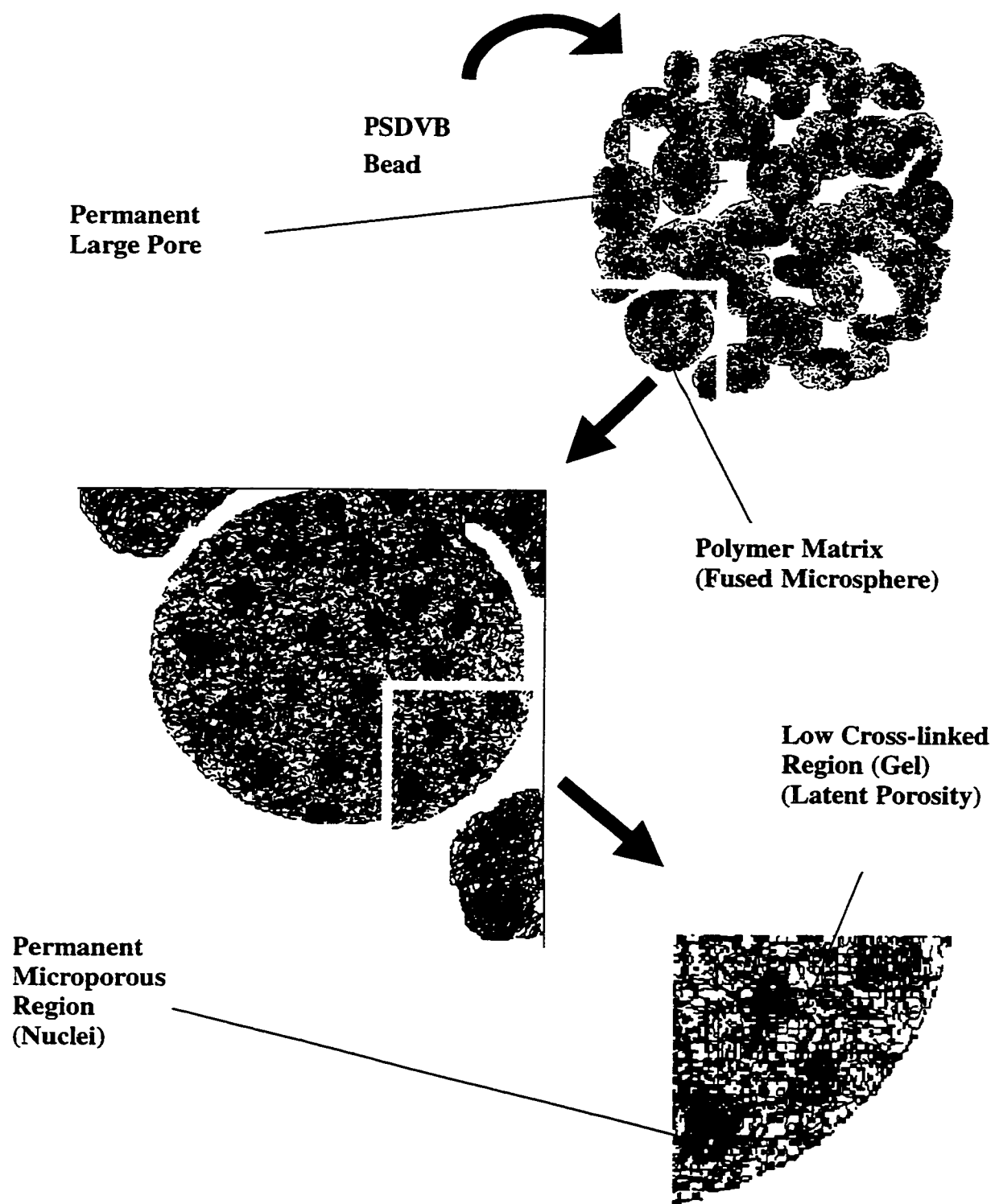


**Figure 3.3: Pictorial interpretation of the PSDVB structure.**

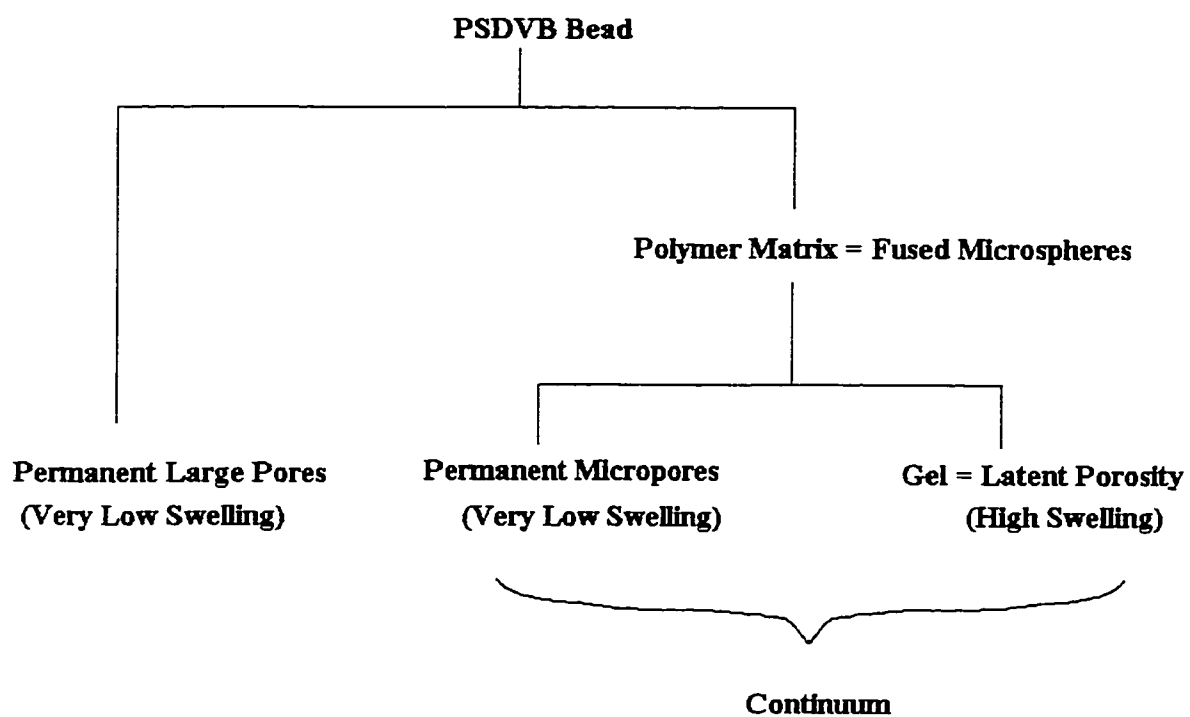


**Figure 3.4: Diagram of terminology describing the different regions in the PSDVB beads based on Figure 3.3.**

Figure 3.3, shows the interpretation of how a macroporous particle looks, i.e. Amberlite XAD-2, based on the findings of other researchers [70, 72, 95, 109, 110, 139-141]. The macroporous bead is comprised of microspheres. First to be formed during polymerization in a suspended drop of porogen solvent are the nuclei. These are very small and highly cross-linked due to the presence of the divinylbenzene, which is more reactive than the styrene monomer. As the concentration of divinylbenzene is depleted, a softer polymer is formed, called the gel region or latent-pore region. The nuclei grow together by forming linkages between them. In Figure 3.3 the density of criss-crossed lines represent the cross-linking density. These arrangements, consisting of enlarged nuclei by gel are called the microspheres. The low cross-linked gel region is collapsed when the polymer is dry [102], but during the polymerization, the chains are solvated and fully swollen. Toward the end of the process, a looser entanglement of chains and continued polymerization causes the microspheres to fuse together. The *polymer matrix* is defined as all of the polymerized PSDVB. The spaces between the microspheres are macro- and mesopores, usually referred to as the permanent macro-porosity. These large pores are present because they were occupied by porogen solvent late in the polymerization process. The cross-linking density is a continuum from high (nuclei) to low (between nuclei) with no well defined limits. In a dry particle, after the solvent and unreacted monomers are removed, the particle is composed of a collapsed low cross-linked gel region surrounding the highly rigid nuclei, and interconnected macro- and mesopores, left after removing the solvent (porogen).

The characterization of swollen polymer gels of different PSDVB copolymers showed that the structure of the polymer matrix is composed of swellable permeable low

cross-linked (gel) and non-permeable non-swelling highly cross-linked regions [107, 109]. The highly cross-linked region has a permanent open structure (permanent microporosity) [107] due to the existence of spaces between chains and bonds. The collapsed gel has a very high density of polymer chains but a low density of cross-linking. The terminology used in this thesis is summarized in Figure 3.3 and 3.4. It is important to note that there are potentially three sources of sorption that do not cause an increase in the external diameter of the particles, i.e. adsorption on macropore walls, sorption in permanent micropores, and sorption of gel which produces internal swelling (swelling of microspheres reducing macropore volume).

Research on the structure of these polymers has employed different techniques, i.e. NMR spectroscopy, fluorescence spectroscopy, infra-red spectroscopy, and pore distribution measurement in the swollen materials are a few of the techniques traditionally employed in order to get structural information.

$^1\text{H}$ -NMR measurements of  $\text{CHCl}_3$ , inside and outside the polymer matrix, showed the presence of two types of interactions, which supports the heterogeneity of PSDVB [139]. Two signals were observed for  $\text{CHCl}_3$  and their separation in chemical shift depended on the different environment around the  $\text{CHCl}_3$  molecules. As the pore size in the polymer increases, i.e. on going from a polymer free of micropores to macropores, the signal for the  $\text{CHCl}_3$  inside the polymer matrix gets closer to the signal for the  $\text{CHCl}_3$  outside the matrix in the macropores. Here, the opening of the collapsed dry structure upon  $\text{CHCl}_3$  sorption is not mentioned. Instead, the closeness of two types of  $\text{CHCl}_3$

signals was related to the different pore sizes in the matrix. The larger the pore the closer the inside and outside matrix signals get.

Two fluorescent probes, with structure and reactivity similar to those of polystyrene and divinylbenzene, were incorporated into the polymer matrix at low concentration by including them in a mixture of the monomers. It was found that both probes were actually incorporated into different microdomains, providing qualitative evidence for heterogeneity of the polymer matrix [104].

Determinations of pore size distribution of PSDVB co-polymers using size exclusion chromatography (SEC) have shown that an increase in the void volume is observed when a good solvent, such as THF, is used. This was attributed to the opening of the collapsed structure of the polymer chains, which expand and disentangle upon contact with the solvent [95, 142]. Nominally non-porous PSDVB packings (PRP- $\infty$  type) had an enormous increase in pore volume when swollen with THF compared to the  $N_2$  adsorption measurements made on dry (gel collapsed) particles. Ninety per cent of the pore volume found in the SEC study corresponded to micropores of about 3 nm in diameter.

### 3.2.3.2 Methods to Determine Polymer Swelling.

The swelling of polymer based stationary phases has been measured employing gravimetric, volumetric, and other techniques measuring a swelling related property, e.g., back pressure measurements.

Gravimetric swelling measurements, i.e. weight gain measurements, require that the excess solvent surrounding the particles be removed before the weight measurement is taken. Centrifuging the solid sample to remove wetting liquid and blotting are two of the methods used in this regard. Centrifuging was widely used in the past to determine the weight-swelling of different materials [143-145]. In this type of measurement, solvent uptake, instead of swelling, is the measured parameter. Blotting of polymer samples enmeshed in poly(tetrafluoroethylene) microfibers (composite samples) [146-149] was used by others. Composite samples were immersed in the solvent of interest and then removed and damp-dried between paper towels. The weight of liquid taken up by the enmeshed particles was used to calculate the corresponding specific volume (mL/g) of swollen composite, but no correction for solvent occupying non-swellaable zones of the composite sample, e.g. between particles, in permanent micropores in the PSDVB matrix, and into both macropore walls and volume, was made. The same approach was also studied on discs of polyacrylates and tea-bags containing the ground polymeric material [150]. Using the same experimental approach swelling was determined as the weight difference between swollen and dry polymer to weight of dry polymer. These works ignore the fact that the total uptake of solvent into a polymer sample does not necessarily causes an equivalent amount of swelling. As was mentioned earlier, the polymer matrix



possesses highly cross-linked regions that probably are not swellable but can still imbibe solvents. These techniques have been used by others [151-153]. Due to the uncertainties associated with the preparation of the swollen sample before the actual weight is taken, these techniques are not recommended.

The volume increase of a densely packed bed of resin particles (the height change of a polymer sample) on column has been attributed to swelling [102, 105, 144, 154] of the beads. This technique is flawed due to the assumption that the fractional void volume of the swollen bed is the same as it is in the dry bed. These type of measurements overestimate the degree of swelling caused by the solvent and exhibit lack of accuracy because they only provide a way to infer the swelling of the polymers. It is desirable to have a volumetric method in order to provide unambiguous swelling values, e.g. dimensional change measurement of the polymer bead, so that swelling can be related directly to bead volume and not from another property.

Some swelling studies have been reported using microscopic measurements of the particle [116, 140] and the volumetric swelling ratio was reported as the swollen to unswollen particle volume [155, 156]. In these studies, swelling is related to the diameter [116] or projected area [156] of the resin measured before and after swelling, by means of microscopic direct observation of the particles. This technique not only can accurately measure the polymeric spheres before, during, and after swelling, but also is very quick and only an optical microscope with a reasonable set of objectives is required. More sophisticated equipment can be added to make the procedure less dependent on human errors, i.e., addition of an image analyzer [155-157]. The usual factors that are found to

limit this sort of measurements are bead fracture upon swelling and diffraction effects. Also, small particles ( $d < 8\mu\text{m}$ ) require the special design of cells and moving stage to allow accurate reading of the dimension measured as found in our research group [158].

A less popular method to determine swelling of polymers is to calculate it from back-pressure measurements in packed beds [100, 159]. This is not a very recommendable method to obtain swelling data because it is totally indirect and may also depend on flow rate conditions, homogeneity of the packed bed, and particle size range.

In this work, equilibrium swelling was measured in THF/water, AN/water, and MeOH/water, at different concentration of the organic modifier. It is expressed as the ratio of volume change in the particle to the initial dry volume,  $Q_{VV}$ .

$$Q_{VV} = \frac{V_f - V_i}{V_i} \quad (3.2)$$

where  $V_f$  and  $V_i$  are the swollen and dry particle volume respectively. The sphere volume is given by:

$$V = \frac{\pi}{6} \phi^3 \quad (3.3)$$

where  $\phi$  is the sphere diameter. In the microscopic measurements, the measured property is the diameter of the particles in their initial (non-swollen) and final (swollen)

states. Substitution of (3.3) into (3.2) for the swollen ( $\phi_f$ ) and non-swollen ( $\phi_i$ ) diameters, gives the final swelling expression:

$$Q_{vw} = \left[ \left( \frac{\phi_f}{\phi_i} \right)^3 - 1 \right] \quad (3.4)$$

This expression can be converted to units of swollen volume per mass of XAD-2, by using the particle density,  $\rho_p$ , which in the case of Amberlite XAD-2 is calculated using the following derivation. From porosity,  $P$ , and true wet density,  $\rho_{TW}$  (TABLE 2.1):

$$V_{pore} = P \cdot V_{particle} \quad (3.5)$$

$$\rho_{TW} \cdot V_{particle} = g_{particle} + g_{H_2O} \quad (3.6)$$

Where  $V_{particle}$ ,  $V_{pore}$ ,  $g_{particle}$ , and  $g_{H_2O}$  are particle volume, pore volume, mass of dry particles, and mass of water in the pores of the particles, respectively. Because XAD-2 does not swell in water, and assuming water density is 1 g/mL, then:

$$\frac{g_{H_2O}}{\rho_{water}} = V_{H_2O} = V_{pore} = P \cdot V_{particle} \quad (3.7)$$

substituting (3.7) into (3.6):

$$\rho_{TW} \cdot V_{particle} = g_{particle} + P \cdot V_{particle} \quad (3.8)$$

and rearranging for

$$\frac{g_{particle}}{V_{particle}} = \rho_{TW} - P = \rho_P \quad (3.9)$$

Porosity and true wet density from TABLE 2.1 are (0.40 - 0.45) mL pore/mL dry-particle and 1.02 g/mL-particle in water. This gives a range of (0.62-0.57) g dry-particle/mL dry-particle and an average density,  $\rho_P$  of (0.60±0.01) g dry-particle/mLdry-particle. Knowing the density of particles, fractional swelling,  $Q_{vw}$ , can be defined as:

$$Q_{vw} = \left[ \left( \frac{\phi_f}{\phi_i} \right)^3 - 1 \right] \cdot \rho_p \quad (3.10)$$

Swelling due to organic modifiers in the mobile phase alone cannot provide enough evidence to understand polymer behavior. It is also necessary to know the sorption isotherms of the organic modifiers and correlate both swelling and sorption in

order to get more information. As suggested before, sorption and swelling are two different processes and as such, must be determined independently.

### 3.2.4 Activity Considerations for High Concentration Solutions.

The organic modifiers, THF, AN, and MeOH employed in the sorption and swelling experiments are used in a wide range of aqueous concentrations, ranging from 0 to 70% w/w, approximately. In order to interpret the results of these experiments, it is necessary to know the extent of polymer-solvent interaction. However, both organic modifier-resin and organic modifier-water interactions are involved in these experiments and these solutions are far from being ideal. In other words, Raoult's law does not apply. The organic modifier-water interactions, which affect the characteristics of the liquid phase, are concentration dependent [160-162]. A standard way to get results unaffected by the changes in interaction within the liquid phase is to use activities, rather than concentrations. In an ideal solution, all of the interactions among molecules are the same regardless of the concentration range. Contrarily, in real solutions, there are different interactions involving solute-solute, solvent-solvent, and solute-solvent molecular interactions. This causes deviations from the ideal behavior. The activity coefficient measures behavior deviations between a real and an ideal solution. Activity coefficients,  $\gamma_i$ , and activity,  $a_i$ , of a substance *i* are defined by [163]:

$$a_i \equiv \exp[(\mu_i - \mu_i^0)/RT] \quad (3.11)$$

$$\gamma_i \equiv \frac{\exp[(\mu_i - \mu_i^0)/RT]}{x_i} \quad (3.12)$$

$$a_i = \gamma_i \cdot x_i \quad (3.13)$$

where  $RT$  is the product of the ideal gas constant and temperature,  $\mu_i$  and  $\mu_i^0$  are the chemical potentials of component  $i$  in solution and of the pure substance  $i$ , respectively, and  $x_i$  is the mole fraction of component  $i$ . Activity is a dimensionless quantity whereas activity coefficients have inverse concentration units. The chemical potential  $\mu_i^0$ , in the standard state where  $a_i = 1$ , is a function of temperature and pressure, whereas  $\gamma_i$  is a function of temperature, pressure and concentration [164, 165]

It is important to specify those conditions where  $\gamma_i$  becomes equal to unity. There are two conventions commonly used for solutions of non-electrolytes. Convention I relates to the pure solute standard state. The activity coefficient of each compound approaches unity as its mole fraction approaches unity. Convention II is based on the extrapolated infinite dilution standard state. The activity coefficient of solute approaches unity as the mole fraction approaches zero. These conventions [163, 165] are based on Raoult's and Henry's laws respectively. Here only the pure solute standard state will be employed, which is a real state of the system.

The activity coefficients used here were calculated with the Margules Equation [166, 167] for methanol-water solutions, and with the Non-Random Two-Liquid Equation (NRTL equation) [166, 168] for acetonitrile-water and tetrahydrofuran-water solutions.

Margules Equation:

$$\ln \gamma_i = [A_{12} + 2(A_{21} - A_{12})x_1] \cdot x_2^2 \quad (3.14)$$

NRTL Equation:

$$\ln \gamma_1 = x_2^2 \left[ \frac{\tau_{21} \cdot G_{21}^2}{(x_1 + x_2 \cdot G_{21})^2} + \frac{\tau_{12} \cdot G_{12}}{(x_2 + x_1 \cdot G_{12})^2} \right] \quad (3.15)$$

where,  $x_1$  and  $x_2$  are the mole fractions of the organic modifier and water respectively, and  $A_{12}$ ,  $A_{21}$ ,  $G_{12}$ ,  $G_{21}$ ,  $\tau_{12}$ , and  $\tau_{21}$  are interaction parameters obtained from the literature [167-170], which are summarized in TABLE 3.1.

Depending on the system, the activity coefficient of a given component could be greater or less than unity. In a system showing positive deviations from ideality, like those represented in Figure 3.5, the activity coefficient, and therefore the escaping tendency of the molecules from solution, is greater than in an ideal solution of the same

**TABLE 3.1** Parameters for THF/water, AN/water, and MeOH/water for the calculation of activity coefficients using Margules and NRTL equations [170].

Binary Organic/water 1/2	Type of equation	Parameters	Definition	Value
MeOH/water	Margules	$A_{12}$ $A_{21}$	Adjustable parameter Adjustable parameter	0.6304 0.4237
THF/water	NRTL	$G_{12}$ $G_{21}$ $\tau_{12}$ $\tau_{21}$ $A_{12}$ $A_{21}$ $\alpha_{21}=\alpha_{12}$ $T$ $R$	$e^{(-\alpha_{12}\cdot\tau_{12})}$ $e^{(-\alpha_{21}\cdot\tau_{21})}$ $A_{12}/RT$ $A_{21}/RT$ $A_{12}$ $A_{21}$ Nonrandomness parameter Temperature gas constant	0.4355 0.3624 1.8141 2.2152 1074.8365 1312.459 0.4582 298 K 1.98721 cal/K.mol
AN/water	NRTL	$G_{12}$ $G_{21}$ $\tau_{12}$ $\tau_{21}$ $A_{12}$ $A_{21}$ $\alpha_{21}=\alpha_{12}$ $T$ $R$	$e^{(-\alpha_{12}\cdot\tau_{12})}$ $e^{(-\alpha_{21}\cdot\tau_{21})}$ $A_{12}/RT$ $A_{21}/RT$ $A_{12}$ $A_{21}$ Nonrandomness parameter temperature gas constant	0.56 0.4082 1.3105 2.0252 776.4673 1199.901 0.4424 298 K 1.98721 cal/K.mol



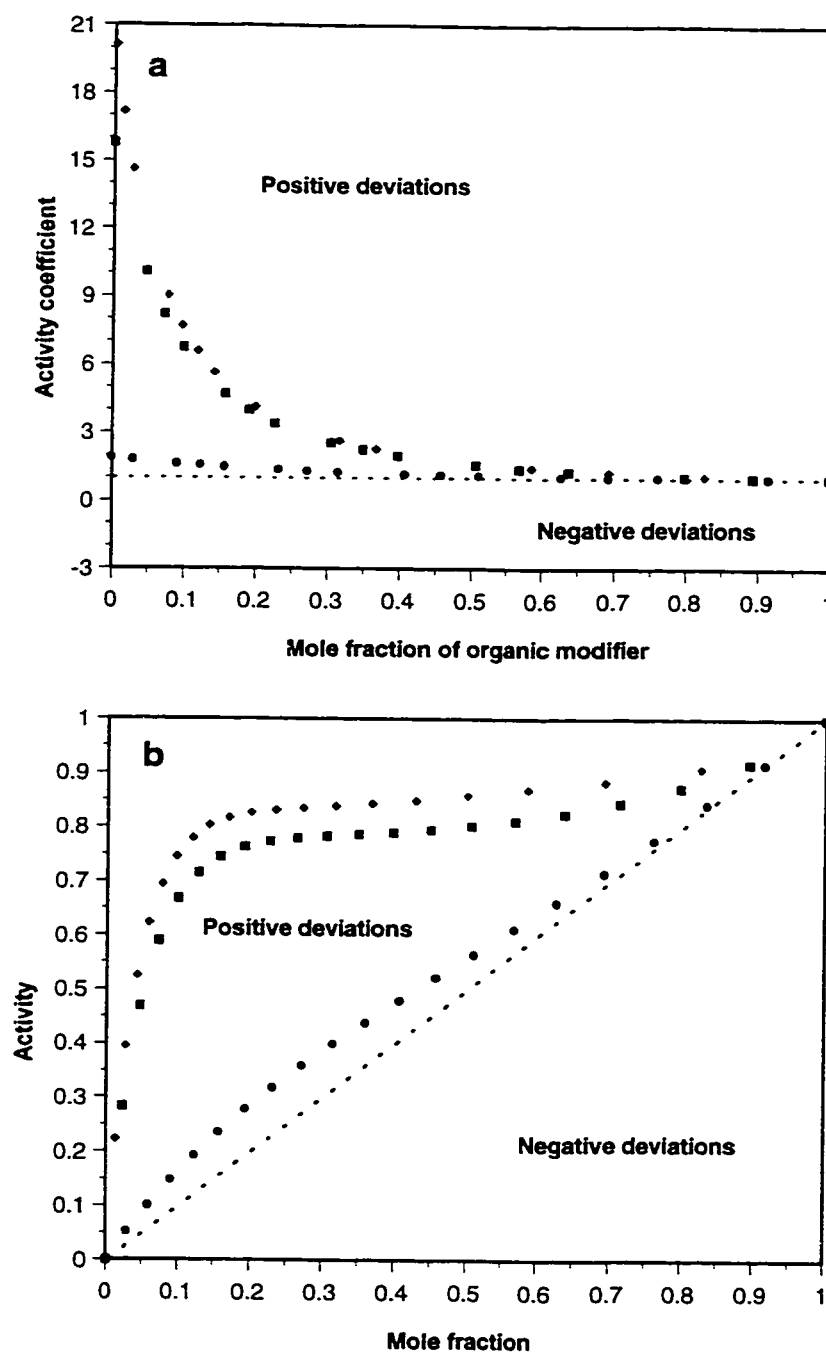


**Figure 3.5: Activity Coefficients,  $\gamma_i$  (panel a) and Activities,  $a_i$  (panel b), calculated by using the Margules (MeOH) and NRTL (THF and AN) equations, versus mole fraction,  $x_i$ , for: ( $\diamond$ ) THF, ( $\blacksquare$ ) AN, and ( $\bullet$ ) MeOH in aqueous solutions, (...) Ideal solution behavior. All of the binary solutions present positive deviation from ideality. Data in Appendix C, TABLES C.1 and C.2.**

concentration [164]. When negative deviations are present, the substance has a lower escaping tendency than in an ideal solution of the same concentration, and the activity coefficient is less than unity.

All of the binary solutions used in this work exhibit positive deviations from Raoult's law, especially the THF-water and AN-water solutions. If the solutions were ideal, then  $a_i = x_i$  and  $\gamma_i = 1$ , for all values of  $x_i$ .

### 3.3 Results and Discussion.

#### 3.3.1 Water Uptake on XAD-2

The TGA experimental results, discussed in the next section, confirm the literature claim [14, 111] that PSDVB co-polymers, and specifically the macroporous Amberlite XAD-2, have very little, if any, affinity for water. This was proven by the insignificant amount of water found in the XAD-2 samples after 45 days in a humid environment. A brief discussion of the thermograms is given below.

The weight loss was monitored in three different samples. Figure 3.6 and 3.7 show the results obtained from a nominally "dry XAD-2 sample", that was kept in a dry atmosphere after the vacuum drying process described in Chapter 2. The thermograms were recorded in nitrogen atmosphere between 35°C and 290°C. These plots suggest an

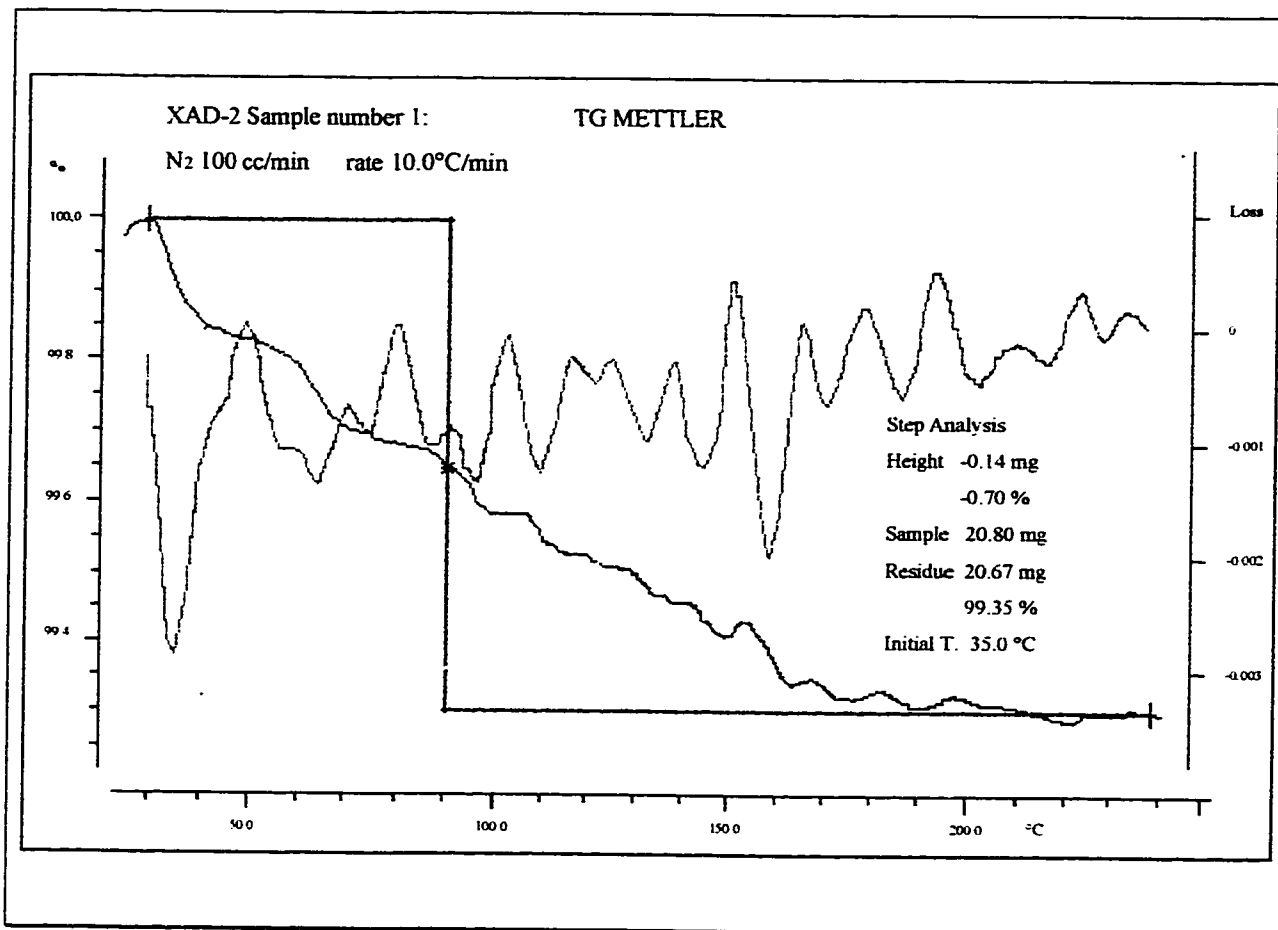


**Figure 3.6:** Thermal study of dry XAD-2. The red trace represents the direct weight loss of the sample (namely TG, or thermogravimetry) versus temperature. The green trace is the first derivative of the weight loss (namely DTG, or derivative thermogravimetry), versus temperature. The blue line is the weight loss measured. Temperature range: 35-240 °C. The raggedness in the red trace is measurement noise.

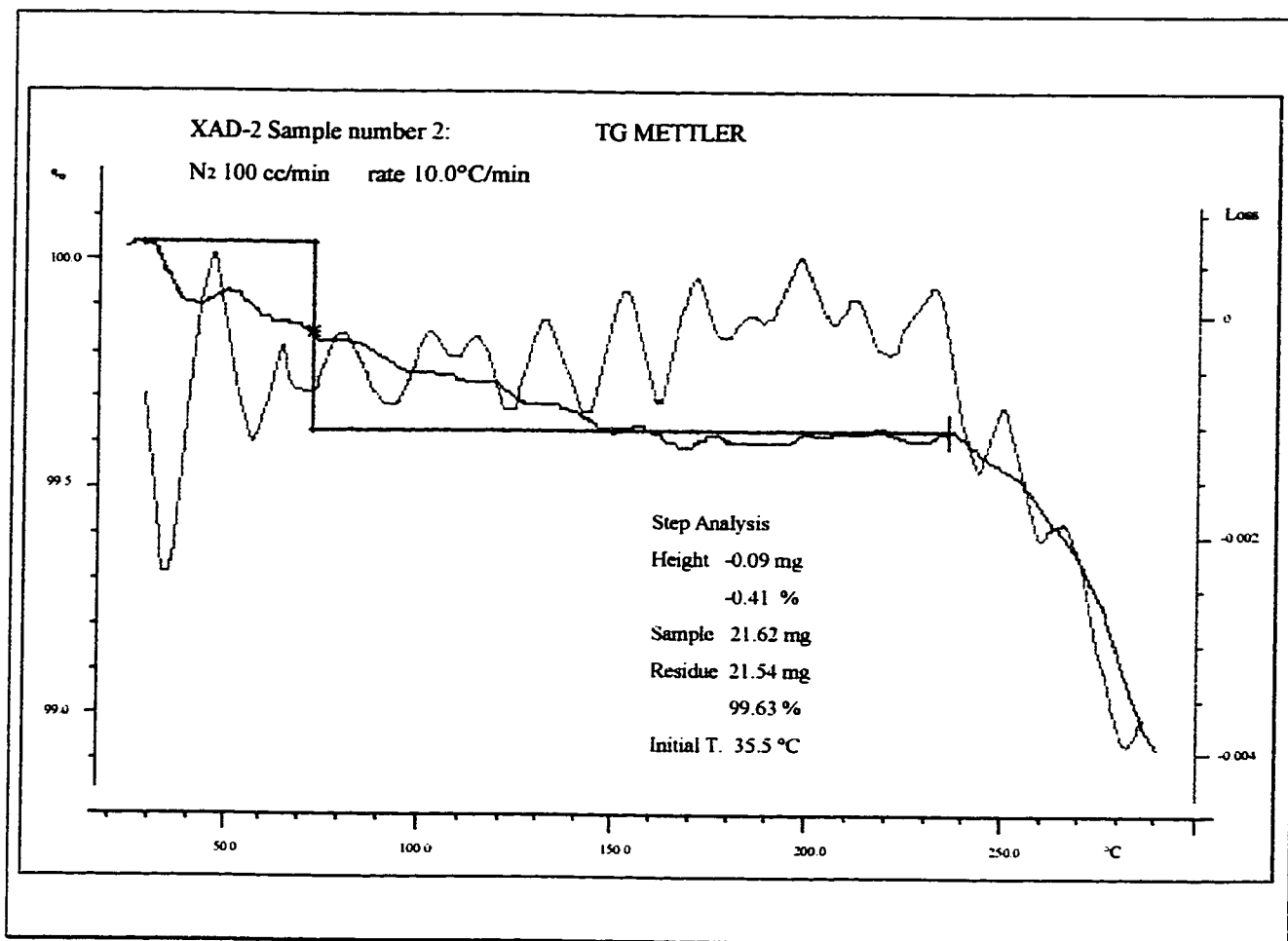


**Figure 3.7:** Thermal study of dry XAD-2. The red trace represents the direct weight loss of the sample (namely TG, or thermogravimetry) versus temperature. The green trace is the first derivative of the weight loss (namely DTG, or derivative thermogravimetry), versus temperature. The blue line is the measured weight loss. Temperature range: 35.5-290 °C. The raggedness in the red trace is measurement noise.

average loss of material from within the particles of  $(0.56 \pm 0.06)\%$  between  $35^\circ\text{C}$  and approximately  $240^\circ\text{C}$ . The expelled material has to diffuse toward the outside of the particles during heating, which explains the slow rate of weight loss observed. Both figures exhibit similar slopes in the range from  $35$  to  $200^\circ\text{C}$ . In figure 3.7, it can be seen that there is a strong decrease in the weight of sample when the temperature is increased beyond  $230^\circ\text{C}$ . This can be attributed to thermal degradation of XAD-2 [171]. These polymers are reported to be thermally stable up to approximately  $250^\circ\text{C}$  [112].

Figures 3.8 and 3.9, are the thermograms of a “humidified XAD-2 sample” (45 days at 100% relative humidity). The total average weight loss of  $(0.63 \pm 0.06)\%$  matches the results found in the two figures previously discussed. Taking into account the measurement error, the weight loss values displayed are the same. This confirms that the affinity of Amberlite XAD-2 for water is negligible as suggested by the non-polar nature of the PSDVB co-polymers [102, 112]. The water levels reported here are below those found in earlier measurements made on this kind of packing [14, 111].

A dry sample of XAD-2 was sprinkled with water forcing the sample to hold water on the surface, between its particles, and it was then subjected to TG. Figure 3.10 shows the weight loss of this, “water sprinkled XAD-2 sample”. The thermogram displays two main differences with respect to the ones previously discussed in Figures 3.6 through 3.9. Initially, there is a steep decrease in weight due to the evaporation of the water droplets that were on the surface of the sample. This is occurring at low temperatures. No diffusion from within the particles is occurring and only non-sorbed

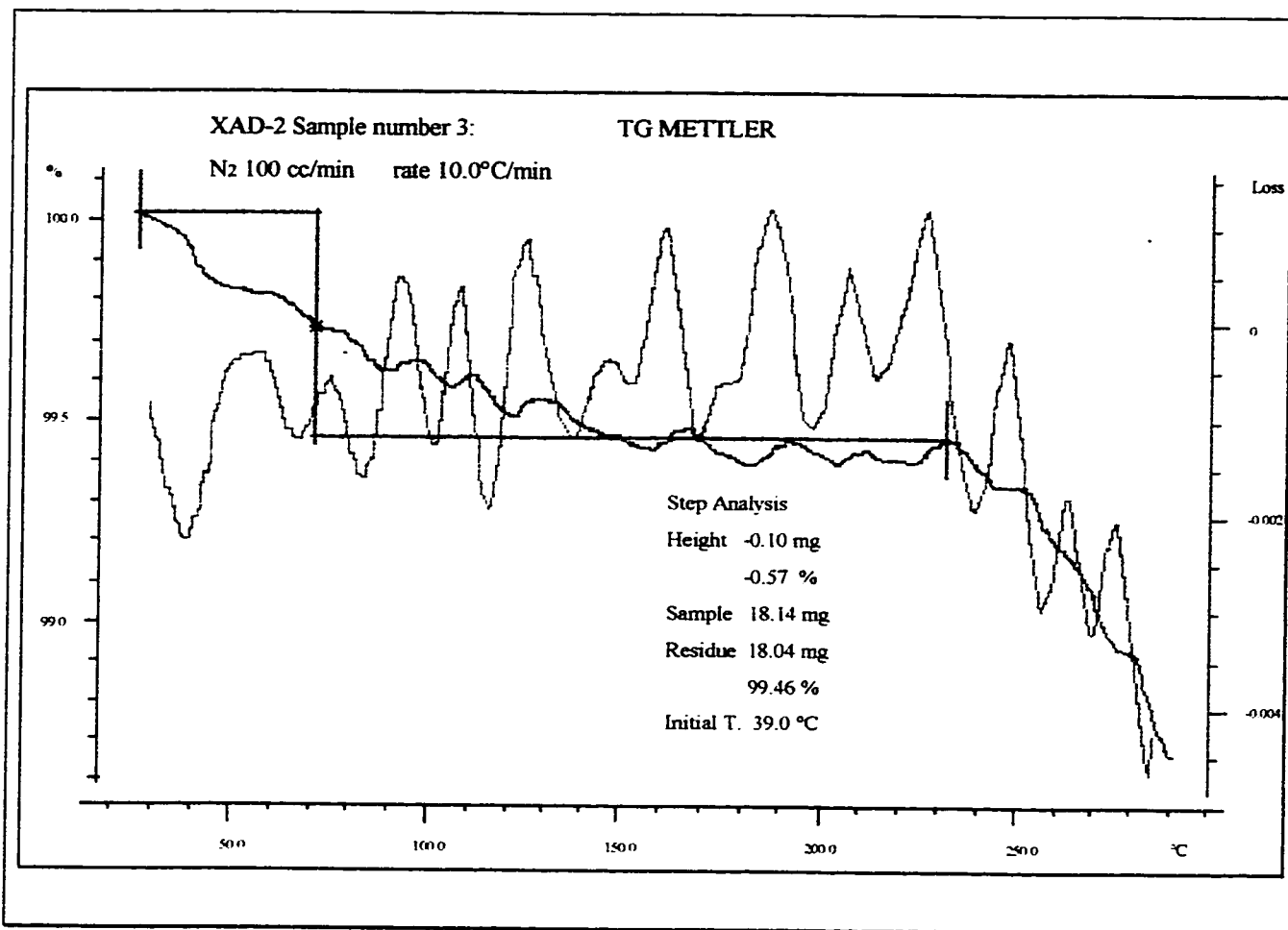


**Figure 3.8:** Thermal study of humid XAD-2. The red trace represents the direct weight loss of the sample (namely TG, or thermogravimetry) versus temperature. The green trace is the first derivative of the weight loss (namely DTG, or derivative thermogravimetry), versus temperature. The blue line is the measured weight loss. Temperature range: 39-290 °C. The raggedness in the red trace is measurement noise.

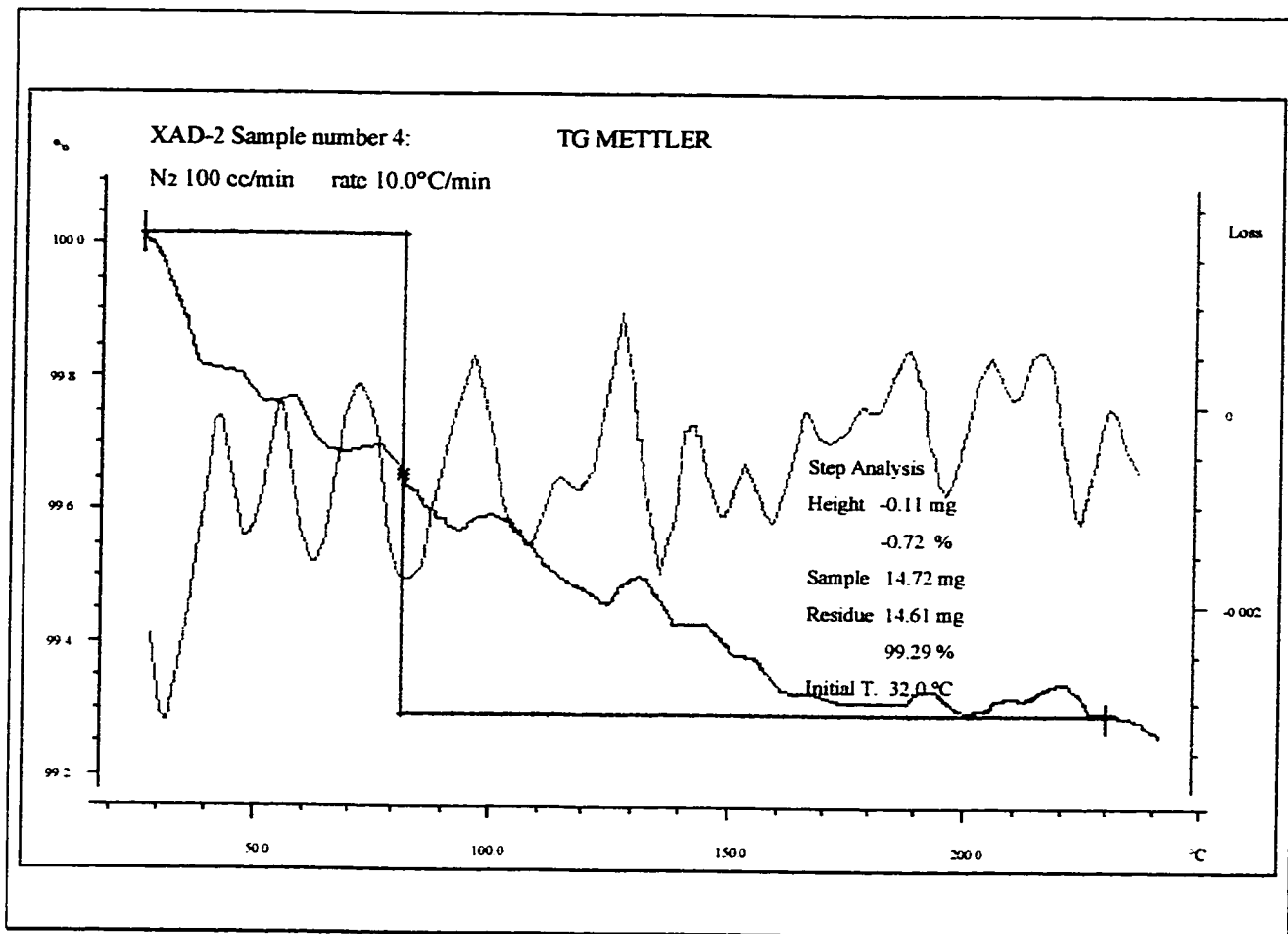


**Figure 3.9:** Thermal study of “humid XAD-2”. The red trace represents the direct weight loss of the sample (namely TG, or thermogravimetry) versus temperature. The green trace is the first derivative of the weight loss (namely DTG, or derivative thermogravimetry), versus temperature. The blue line is the measured weight loss. Temperature range: 32-240°C. The raggedness in the red trace is measurement noise.

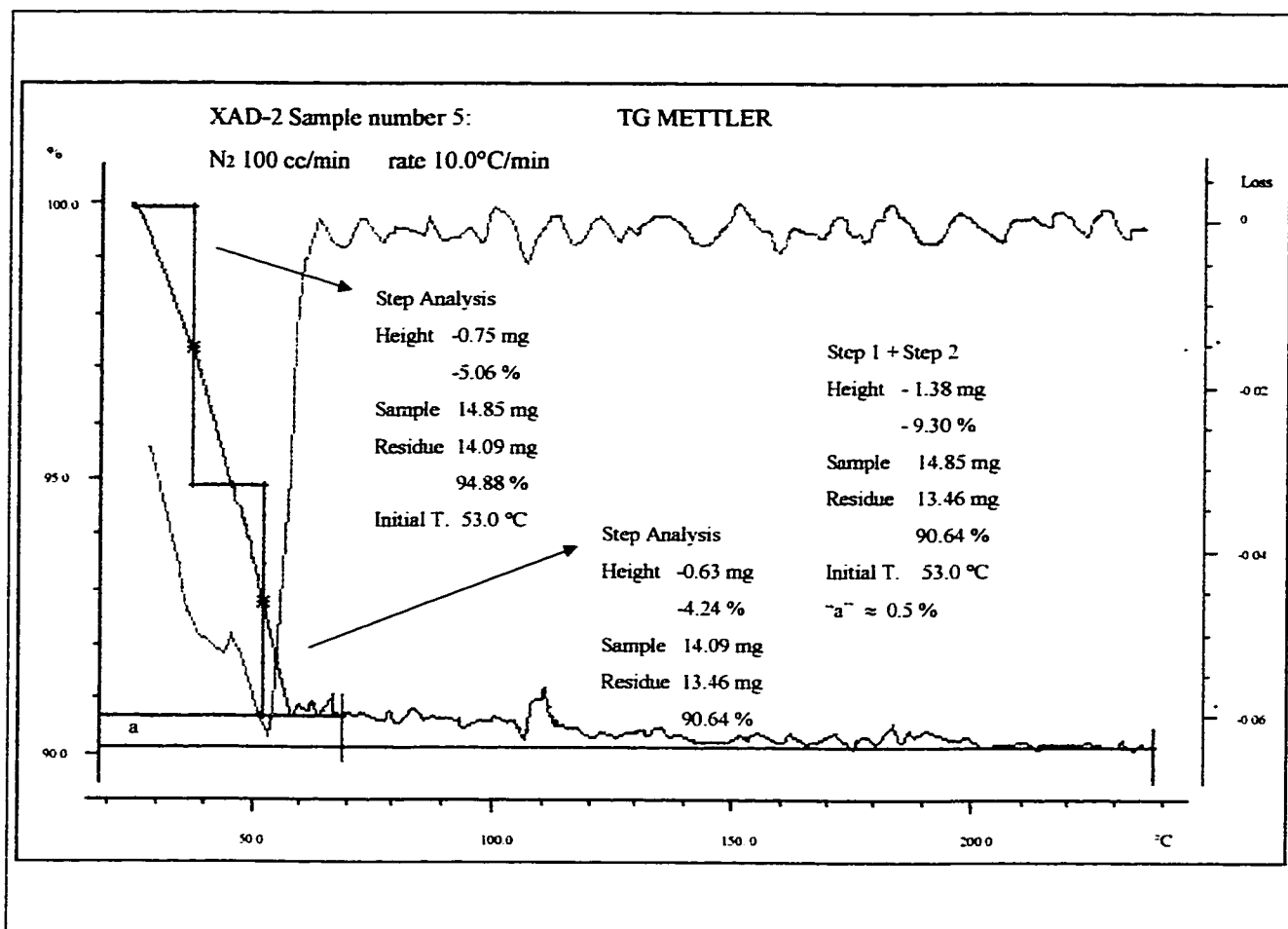


Figure 3.10: Thermal study of “water sprinkled XAD-2”. The red trace represents the direct weight loss of the sample (namely TG, or thermogravimetry) versus temperature. The green trace is the first derivative of the weight loss (namely DTG, or derivative thermogravimetry), versus temperature. The blue line is the measured weight loss. Due to the high weight loss, it was calculated in two step analysis, each one delimited by two maxima in the first derivative curve. Temperature range: 32-250°C. The raggedness in the red trace is measurement noise. The segment of the plot, a  $\approx 0.5\%$  weight loss, was manually evaluated.



water, that does not require high temperatures, evaporates. In the second region, that above 60 °C, there is a slow decrease in weight in the range of temperature between 60 to 240 °C, corresponding to an approximate  $(0.50 \pm 0.05)\%$  weight loss. This value coincides with the results found in the previous four thermograms for weight loss of material from within the particles that occurs very slowly [171]. Water evaporation from the surface and water diffusion from within the particles occurs simultaneously at the beginning of the thermal treatment, where the surface water evaporation is the dominant part.

Even though the Amberlite XAD-2 samples used in these studies had been cleaned and vacuum dried at 80°C until constant weight was obtained (Chapter 2), nevertheless, the thermograms show that there are still substances being expelled out of the polymer. This is because the uncertainty of the TG microbalance is very low,  $\pm 1 \times 10^{-6}$  g, while the uncertainty of the balance used to determine constant weight was  $\pm 1 \times 10^{-4}$  g. That means that the weight change observed in the thermograms could not be measured by using an analytical balance. The expelled materials could be strongly retained organic substances that can be removed only at higher temperatures [172]. These materials are usually residues from the polymerization process that failed to be removed by extraction with solvents [139, 141].

### **3.3.2 Sorption Isotherms on XAD-2 Using Aqueous Phase Concentrations.**

The sorption isotherms of THF, AN, and MeOH on Amberlite XAD-2 from aqueous solution were determined and are presented in Figure 3.11. Plotted in the figure

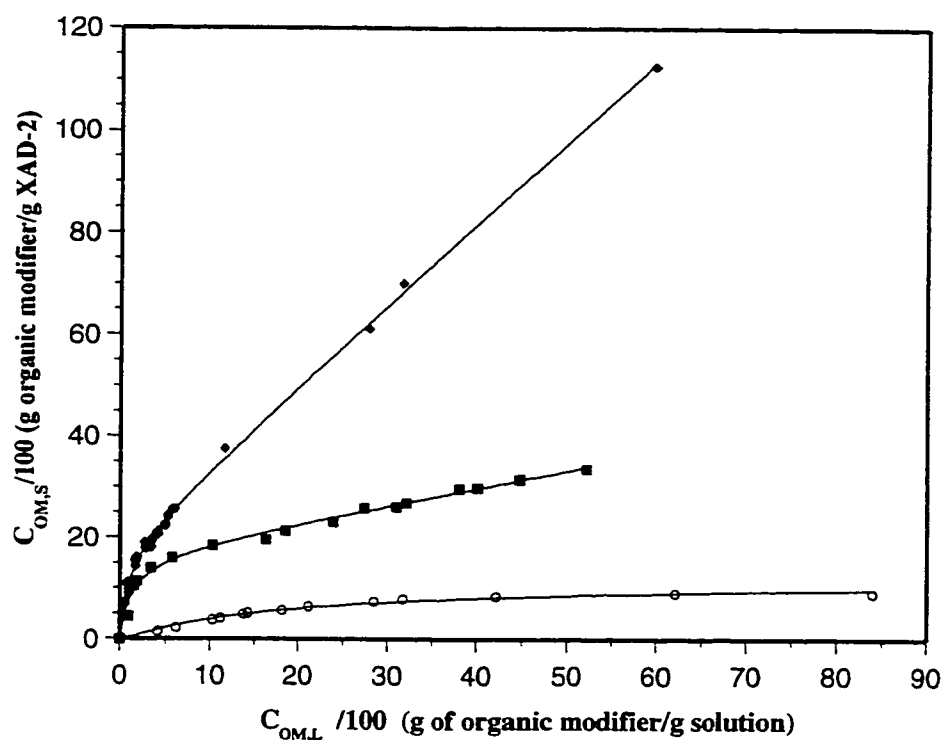


**Figure 3.11: Sorption isotherms for (♦) THF, (■) AN, and (○) MeOH on Amberlite XAD-2 from aqueous solution. Symbols represent experimental data. Lines represent the fittings to equations, 3.16 for THF and 3.17 for AN. MeOH isotherm was drawn by hand. Data found in Appendix C, TABLE C.3.**

is the equilibrium concentration of the organic modifier  $i$  in the polymer matrix solid phase,  $C_{i,S}$ , versus the equilibrium concentration of the organic modifier  $i$  in the liquid phase,  $C_{i,L}$ , keeping in mind that the liquid phase in question represents both outside the particle and inside the large macro- and meso- pores.

These sorption isotherms were measured up to 60 to 80 % organic modifier in the liquid phase depending on the organic modifier used. Further increase of the concentration was not pursued due to the high uncertainty in calculating the sorbed amount of organic modifier from a large initial content using the mass balance.

The analytical fittings (obtained with the shareware program CurveExpert 1.34, Daniel Hyams, Microsoft Corporation, 1997) for the isotherms are given by:

1) THF/water

$$C_{THF,S} = \frac{17.276 \cdot C_{THF,L}}{(1 + 0.9304 \cdot C_{THF,L})} + 1.5875 \cdot C_{THF,L} \quad (3.16)$$

2) AN/water

$$C_{AN,S} = \frac{12.2867 \cdot C_{AN,L}}{(1 + 0.7411 \cdot C_{AN,L})} + 0.3389 \cdot C_{AN,L} \quad (3.17)$$

THF (Figure 3.11), the best solvent among the ones used, has the largest distribution coefficients, followed by AN. Both of them fit a combined equation

resembling a Langmuir isotherm and a straight line (equations 3.16,  $R=0.998$ , and 3.17  $R=0.995$ ). The MeOH isotherm was drawn by hand.

Because high organic modifier concentrations are required in these studies, the sorption isotherms are not expected to be linear. The Langmuir sorption isotherm also fails in describing these systems because it assumes an ideal behavior of both the solution and the adsorbed layer. It does not take into account the secondary effects that are important at high concentration levels, i.e. interactions between adsorbed molecules and solvation effects. The continuing increase in sorption observed in the THF and AN isotherms at high concentrations of organic modifier suggests that there is a different environment in the porous particle (linear portion superimposed to the Langmuir isotherm). A particular adsorption model, called the associative-bilayer adsorption isotherm, has been developed by others [133]. It has a theoretical description for associations due to hydrophobic interactions, which yields a first term resembling the Langmuir isotherm, and a second term describing a linear region. In this model additional solute molecules associate with molecules already sorbed.

However, conformity of the THF and AN isotherms to equations 3.16 and 3.17 respectively, may be an artifact for reasons discussed in section 3.2.4 above. In the next section, the isotherm for each of the systems is presented as sorbed concentration of OM,  $C_{OM,S}$ , versus activity in the liquid phase,  $a_{OM,L}$ . The isotherm fittings are used latter in order to get accurate interpolation of the sorption data.

### 3.3.3 Sorption Isotherms on XAD-2 Using Aqueous Phase Activities.

The sorption isotherms on XAD-2 in THF/water, AN/water, and MeOH/water, using activities of modifiers in the liquid phase and weight/weight concentration units in the polymer phase are shown in Figure 3.12. When comparing isotherms from different solutes, it is not expected to find the same sorption levels at equal activity in the liquid. Molar sorption energies, molecular weights, and densities, and consequently the molar volume, vary among the compounds studied [123]. Use of weight/weight units for sorption in the polymer is not the best way to compare sorption levels. The use of volume/weight units is preferred since sorption of organic modifiers is to be compared to swelling. Because both the molecular weight and densities (and molar volumes) vary among the solvents studied these differences in physical properties imply that weight uptake is not the most fundamentally useful basis for comparison of sorption levels. Manipulation of the isotherm data provides additional insight. Conversion to a volumetric basis is useful [123]. It can be achieved by using molecular volume, which is independent of the state of matter, or liquid density where the molecules are in closer interaction than in the isolated state.

There are two ways to convert the mass of sorbed organic modifier into volume units. The conversion from weight/weight to volume/weight sorbed is achieved by using either one of the following equations:

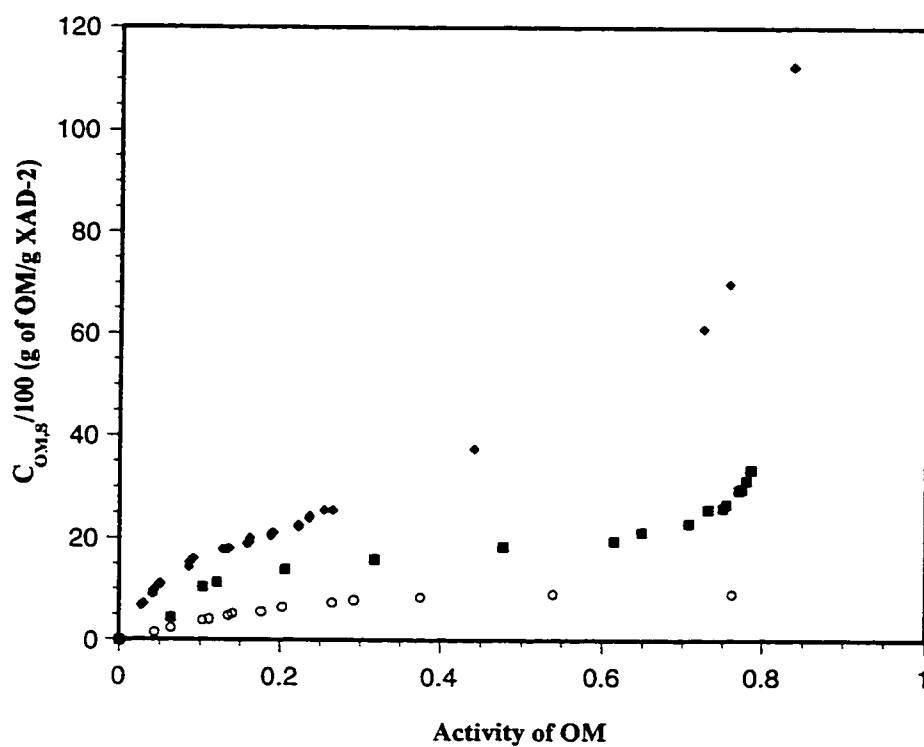


**Figure 3.12:** Sorption isotherms for ( $\diamond$ )THF, ( $\blacksquare$ ) AN, and ( $\circ$ )MeOH on XAD-2 from aqueous solution given as  $C_{OM,S}$  in g of sorbed OM per g of XAD-2 versus activity,  $a$ , of the OM in the liquid phase. Symbols represent experimental data. Data found in Appendix C, TABLE C.4.

$$C_{OM,S,v/w} = C_{OM,S,w/w} \cdot \left( \frac{V_{m,OM}}{MW_{OM}} \right) \quad \text{in mL /g XAD-2} \quad (3.18)$$

$$C_{OM,S,v/w} = C_{OM,S,w/w} \cdot \left( \frac{1}{\rho_{OM}} \right) \quad \text{in mL/gXAD-2} \quad (3.19)$$

where  $C_{OM,S,v/w}$  is the sorbed concentration of OM in volume/weight units,  $C_{OM,S,w/w}$  is the sorbed concentration of OM in weight/weight units,  $V_{m,OM}$  is the molar volume of OM in mL/mol calculated by using the shareware computer modeling software Molecular Modeling Pro™ 1.3 (WindowChem Software™ Inc., [www.windowchem.com](http://www.windowchem.com)),  $\rho_{OM}$  is the density of the pure OM at 25°C, and  $MW_{OM}$  is the molar weight of OM.

Figure 3.13, 3.14, and 3.15 show the sorption isotherms plotted on the basis of equations 3.18 and 3.19, for THF, AN, and MeOH, respectively. TABLE 3.2 summarizes all of the physical parameters used to convert the sorbed concentrations from g OM/g XAD-2 to mL OM/g XAD-2.

When the molar volume from Molecular Modeling Pro™ is used, there is the implicit assumption that all the sorbed molecules of organic modifier behave as if they were isolated, because the figure has been obtained from considering one isolated molecule. In other words, there is the assumption of ideal sorbed OM on the PSDVB

material (that can be adsorption, partition, or both [102]). This situation can be happening at very low sorbed amounts, but as the higher sorption levels are achieved, the general picture might be expected to be more in accordance with the density model, where the sorbed molecules resemble the liquid state. From now on, the concentrations of sorbed OM in mL/g calculated from density will be used. The reasons for this choice are related to the discussion that follows.

Figures 3.13 and 3.14 show a very high increase in the sorption of the organic modifier at high activity values. In gas/solid systems, where only one component interacts with the solid, i.e. uptake of methylene chloride on cellulose acetate [173, 174], this is a common behavior and has been addressed by using the interpretations of the B.E.T theory [126]. Sorption in more than one layer occurs within the small pores of the solid.

This behavior is called capillary condensation [176] in the high concentration range where a bulk phase of adsorbate is formed in the capillaries on the solid phase [123]. A liquid phase is formed at high pressures and a sudden increase of sorbed solute is reflected in the isotherm. In liquid-solid systems this type of isotherm is rarely seen [133]. This is because the solvent component of the mobile phase often also enters the pores and the equilibrium vapor pressure of the adsorbate is lower than that expected if only adsorbate molecules could get inside the solid. However, capillary condensation is possible if only one component (e.g., OM) enters the matrix. In such a case, the saturation vapor pressure will equal that of the pure liquid, that consequently will be at equilibrium with the sorbed molecules. In this case condensation can occur in the capillaries when the



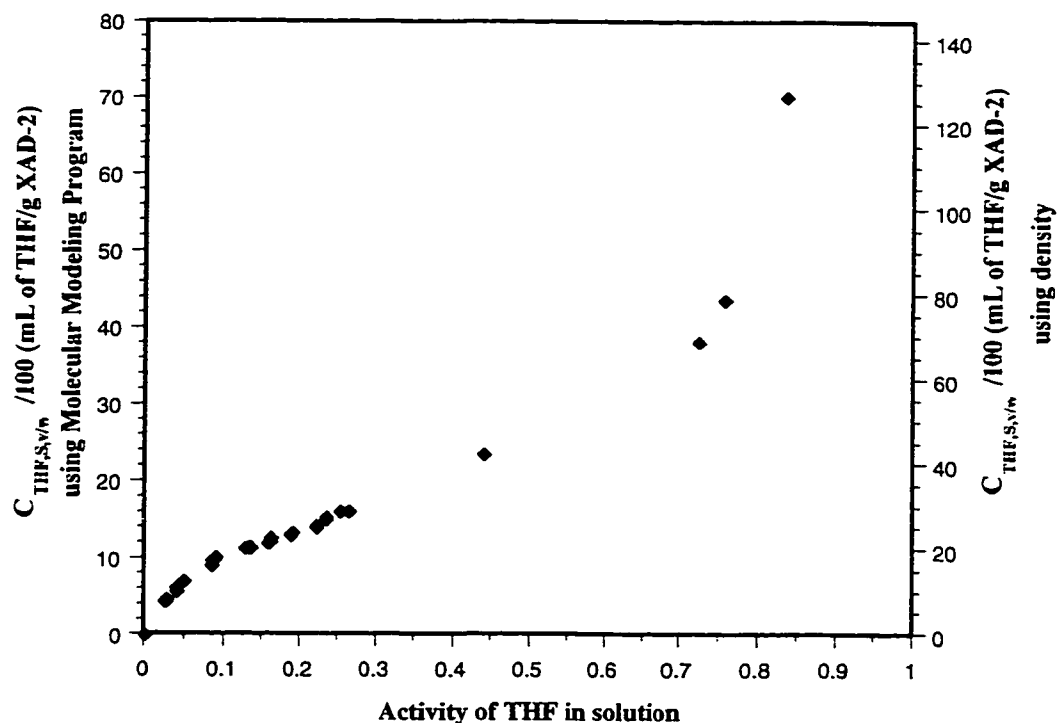


**Figure 3.13:** Sorption isotherm for THF on XAD-2 from aqueous solution given as ( $Y_1$  axis)  $C_{\text{THF},S,v/w}$  in mL of sorbed THF per g of XAD-2 by using eqn. 3.18 and ( $Y_2$  axis)  $C_{\text{THF},S,v/w}$  in mL of sorbed THF per g of XAD-2 by using eqn. 3.19 versus ( $X$  axis) activity,  $a$ , of THF in the liquid phase. Symbol ( $\diamond$ ) represents experimental data. Data found in Appendix C, TABLE C.5 and C.6.

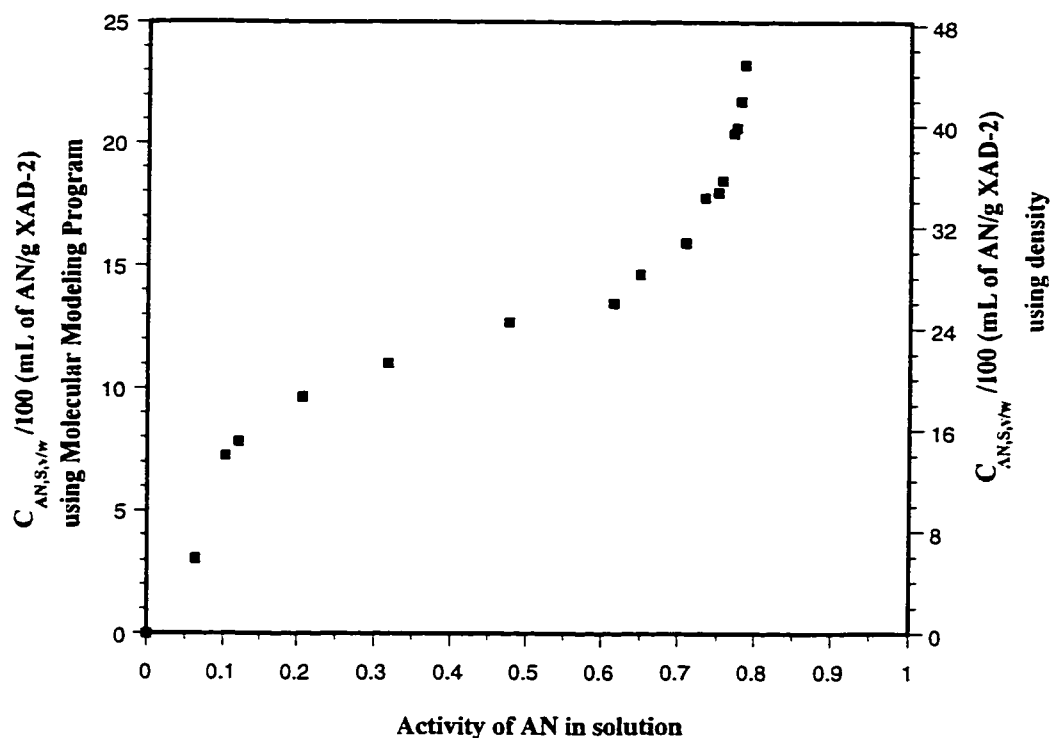


**Figure 3.14:** Sorption isotherm for AN on XAD-2 from aqueous solution given as ( $Y_1$  axis)  $C_{AN,S,v/w}$  in mL of sorbed AN per g of XAD-2 by using eqn. 3.18 and ( $Y_2$  axis)  $C_{AN,S,v/w}$  in mL of sorbed AN per g of XAD-2 by using eqn. 3.19 versus ( $X$  axis) activity,  $a$ , of AN in the liquid phase. Symbol (■) represents experimental data. Data found in Appendix C, TABLE C.5 and C.6.

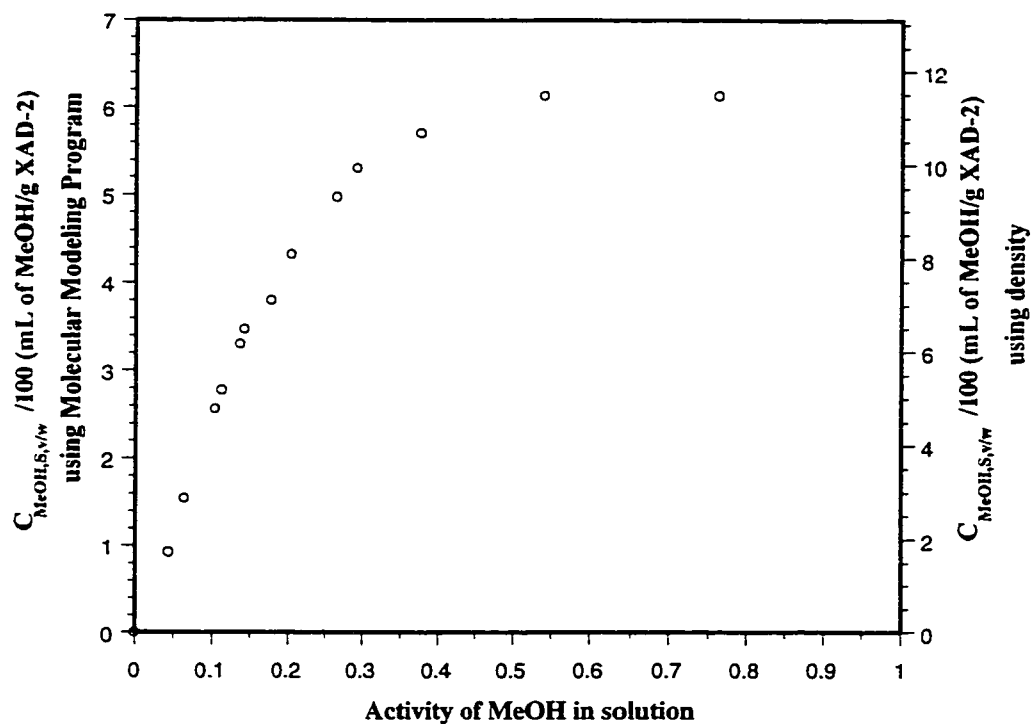


**Figure 3.15:** Sorption isotherm for MeOH on XAD-2 from aqueous solution given as (Y<sub>1</sub> axis)  $C_{MeOH,S,v/w}$  in mL of sorbed MeOH per g of XAD-2 by using eqn. 3.18 and (Y<sub>2</sub> axis)  $C_{MeOH,S,v/w}$  in mL of sorbed MeOH per g of XAD-2 by using eqn. 3.19 versus (X axis) activity,  $a$ , of MeOH in the liquid phase. Symbol (o) represents experimental data. Data found in Appendix C, TABLE C.5 and C.6.

**TABLE 3.2** Physical properties of OM used to calculate sorbed volumes. Densities are given at 25 °C [175]. Molar volume (a) are calculated from density values. Molar volume (b) were taken from Molecular Modeling Pro™ 1.3 (WindowChem Software™ Inc., [www.windowchem.com](http://www.windowchem.com)).

Organic modifier	Short name	Molecular weight (g/mol)	Density (g/mL)	Molar <sup>(a)</sup> volume (mL/mol)	Molar <sup>(b)</sup> volume (mL/mol)
Tetrahydrofuran	THF	72.1	0.8892	81.0841	44.9045
Acetonitrile	AN	41.05	0.7492	54.7918	21.7696
Methanol	MeOH	32.04	0.7866	40.7323	28.3982

partial pressure in the micropore approaches the vapor pressure of the pure liquid in the particles.

Capillary condensation occurs because the saturation vapor pressure of a pure liquid in a small pore is lower than the normal saturation vapor pressure of the liquid at equilibrium with the gas phase on a flat surface or in a big pore. This is in direct relationship with the surface tension of the liquid and is related by the Kelvin equation [47, 129]:

$$\frac{p}{p_s} = \exp\left(\frac{-2\sigma V_m \cos\theta}{rRT}\right) \quad (3.20)$$

where,  $p$  is the equilibrium vapor pressure of the liquid contained in a narrow pore of radius  $r$  (cm) ,  $p_s$  is the equilibrium vapor pressure of the same liquid exhibited at a plane surface,  $\sigma$  (dyne/cm) is the surface tension of the liquid,  $V_m$  (cm<sup>3</sup>/mol) is the molar volume of the sorbate,  $\theta$  (°) is the contact angle between the surface and the liquid,  $T$  (K) is the temperature, and  $R$  (8.3143x10<sup>7</sup> erg/K.mol) is the universal gas constant. The contact angle  $\theta$  is assumed to be zero for a liquid that wets the surface. For example, a contact angle of 10° will affect the exponential term by  $\cos(10) = 0.985$ , which is a change of 1.5% with respect to  $\cos(0) = 1$ .

For a given pore size, the smaller the exponential term is, the larger the ratio  $p/p_s$  will be in order to get capillary condensation. Micropores have been defined as those pores having a diameter  $< 2$  nm [69]. As an example, by choosing a micropore diameter of 2 nm (a radius of  $10^{-7}$  cm) for THF, AN, and MeOH the condition for capillary condensation to start can be calculated by using the Kelvin equation. The results are shown in TABLE 3.3

THF will reach the minimum  $p/p_s$  value ahead of AN and MeOH, in a pore of 2 nm diameter. This analysis can be applied to the high activity region observed in the isotherms of THF (Figure 3.13) and AN (Figure 3.14). AN condensation starts at an activity of approximately 0.65 while THF condenses at approximately 0.70. These results seem to contradict the Kelvin predictions, where THF would reach capillary condensation sooner than AN. In the studies presented here, the diameters of the pores in which condensation starts may not be fixed due to the capability of the PSDVB matrix to swell in these solvents. In the next section a discussion about the polymer swelling and its relationship to capillary condensation will be given. For now it must be mentioned that, AN (having a lower swelling effect on the matrix than THF) may be in a pore of smaller diameter than the one where THF is.

The minimum value of  $p/p_s$  for MeOH is much higher and therefore MeOH does not condense in those pores, based on the results obtained for MeOH (with the same swelling power that AN has up to an activity of approximately 0.45 for both), shown in TABLE 3.3.

**TABLE 3.3** Exponential term from eqn. 3.20 and  $p/p_s$  for THF, AN, and MeOH at 25°C as a function of pore radius and (e), and for a micropore-radius of 1 nm. Contact angles are assumed to be close to zero for solvents that wet the surface, then  $\cos\theta \approx 1$ .  $R$  is  $8.3143 \times 10^7$  erg/K.mol [175].

	$\sigma$ (dyne/cm)	$V_m^{(d)}$ (cm <sup>3</sup> /mol)	$\left( \frac{-2\sigma V_m \cos\theta}{rRT} \right)_{(\text{cm/r})}$	$p/p_s^{(e)}$
THF	26.40 <sup>(a)</sup>	81.0841	-1.728E-07/r	0.1776
AN	27.60 <sup>(b)</sup>	54.7918	-1.221E-07/r	0.2950
MeOH	21.85 <sup>(c)</sup>	40.7323	-7.184E-08/r	0.4875

(a) From ref. [177], (b) from ref. [178] [179], (c) from ref. [179], (d) Calculated from density values, (e) from eqn. 3.20.

### 3.3.4 Swelling of XAD-2 in Different Organic/Aqueous Solutions.

The particles used in the swelling studies swelled isotropically. This was verified by tilting the sample cell and measuring the particles in different positions. The initial and final concentrations of organic modifier before and after equilibrium swelling was reached, were checked by GC and found to be the same.

Figure 3.16 shows the swelling curves for XAD-2 in the three aqueous-organic solvent systems, plotted as fractional swelling per gram of particles,  $Q_{vw}$  versus concentration of the OM in the liquid,  $C_{OM,L}$ . Dots represent experimental data for all of these cases. The lines (Figure 3.16) for THF and MeOH are empirical analytical fittings given by:

$$Q_{vw} = \frac{8.6107 \cdot C_{THF,L}}{(1 + 0.2270 \cdot C_{THF,L})} + 0.0675 \cdot C_{THF,L} \quad (3.21)$$

$$Q_{vw} = -0.0624 - 0.0415 \cdot C_{MeOH,L} + 0.0136 \cdot (C_{MeOH,L})^2 \\ - 2.4 \times 10^{-4} \cdot (C_{MeOH,L})^3 + 1.26 \times 10^{-6} \cdot (C_{MeOH,L})^4 \quad (3.22)$$

These fittings were obtained with the shareware program CurveExpert 1.34 (Daniel Hyams, Microsoft Corporation, 1997). AN data could not readily be fit to a mathematical equation and the line in the figure was drawn by hand. It is interesting to note that equation 3.16 (isotherm fitting for THF) resembles equation 3.21 (fractional



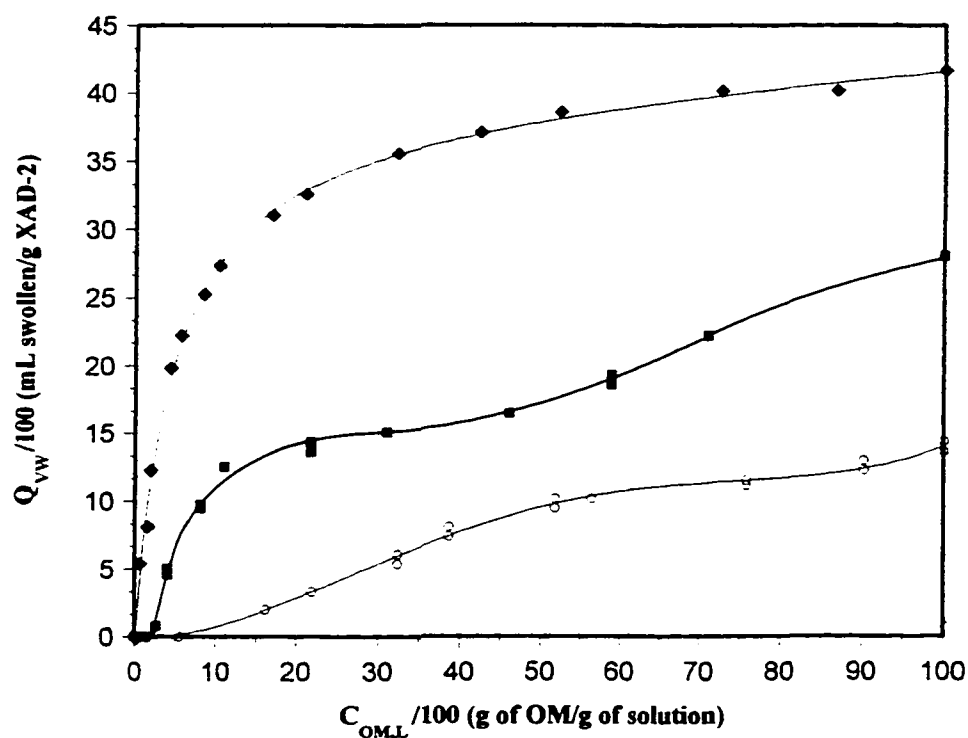


**Figure 3.16: Fractional swelling of XAD-2 using aqueous solutions concentration in the liquid phase of (♦) THF, (■) AN, and (○) MeOH. Dots represent experimental data. Fitting for THF and MeOH are given in the text (eqns 3.21 and 3.22). AN is represented with a hand draw trend line. Data found in Appendix C, TABLE C.7.**

swelling for THF) which was examined in section 3.3.2. These fittings are to be used in the next section for interpolation only.

Figure 3.17 shows the swelling equilibrium curves using the activity considerations previously discussed. THF and AN curves exhibit a region at high activity where a sudden increase in swelling is observed. For an activity of 0.7, AN has such a knee-point corresponding to a fractional swelling of 14% that increases steeply up to 22% when the solution activity is increased to 0.8. The fractional swelling due to THF at an activity of 0.7 in the solution is 33%, but the knee-point is not reached until an activity of 0.8, where the fractional swelling is 37%. Above 0.8, the fractional swelling gradually increases up to a value of 42 % at an activity of 0.85. Clearly at an activity of 0.7 in the solution, THF is in wider pores than those where AN is. The different environment in the particles is the reason why capillary condensation of AN starts at lower activities than THF. Condensation of AN into the capillaries formed upon swelling from the collapsed structure (close to the nuclei in the continuum), produces a pronounced increase in the particle diameter. This occurs in the matrix around the highly cross-linked nuclei, in the continuum, (compare with “non-swelling” description in Chapter 3, Figures 3.3 and 3.4) which has low cross-linking relative to the nuclei. The low cross-linking allows for large swelling and accommodates the excess liquid being formed. THF, being a better solvent for PSDVB, shows a less dramatic change on the observed swelling of XAD-2 in the region where activity varies between 0.8-1.0. At lower activities of OM in the liquid

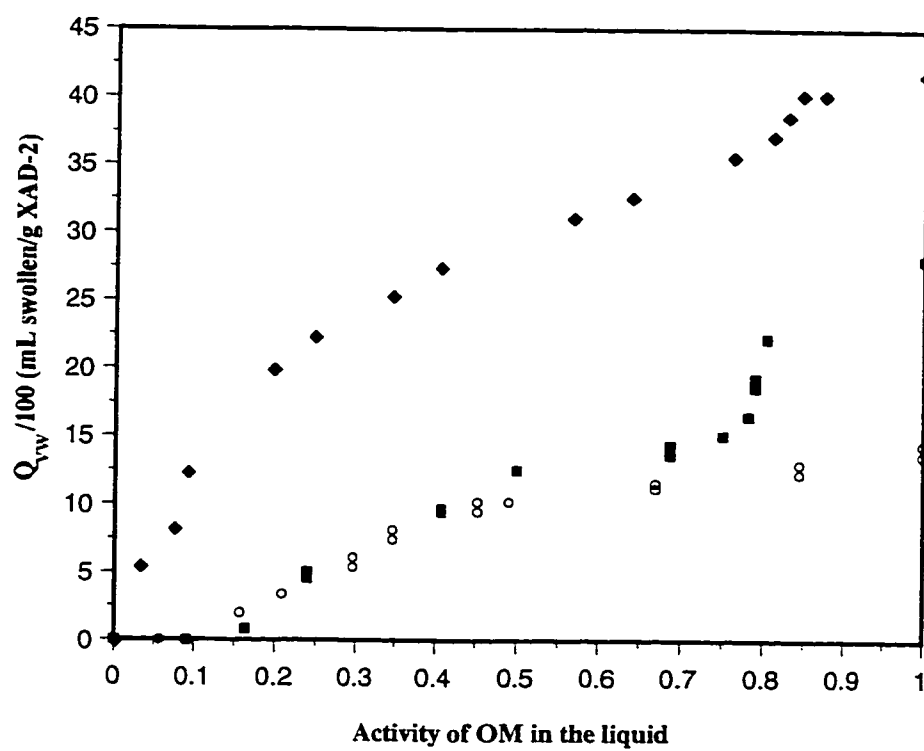


**Figure 3.17: Fractional swelling of XAD-2 using aqueous solution activities in the liquid phase of (◆) THF, (■) AN, and (○) MeOH. Dots represent experimental data. Data found in Appendix C, TABLE C.8.**

phase, THF swelling effect on the matrix is greater than that due to AN. At high activities of THF the swollen matrix possesses larger pore diameter and the volume increase of the particle due to capillary condensation of THF is not as large as it is for AN. Those latter regions in the plots correspond to the capillary condensation discussed in section 3.3.3.

It can be clearly seen that the PSDVB resin swells when in contact with the organic modifiers. At low activities ( $<0.5$ ) of organic modifier, the order of solvent swelling power observed is  $\text{THF} > \text{AN} \approx \text{MeOH}$ . At high activities ( $>0.5$ ) the order observed is  $\text{THF} > \text{AN} > \text{MeOH}$ . The maximum fractional swelling of XAD-2 in pure THF, AN and MeOH was 41.72, 28.22, and 14.02%, respectively. These results are in agreement with the trend expected based on the Hildebrand solubility parameters of the solvents and polymer [52]. THF ( $\delta=18.6 \text{ MPa}^{1/2}$ ) has a larger effect on the polymer than AN ( $\delta=24.3 \text{ MPa}^{1/2}$ ) or MeOH ( $\delta=29.7 \text{ MPa}^{1/2}$ ) [52, 53, 180] at any concentration due to the fact that its solubility parameter is closer to that of the PSDVB co-polymer ( $\delta=18.6\text{--}19.0 \text{ MPa}^{1/2}$ ) [181]. The results are also consistent with the observation that the void volume of columns packed with PLRP-S, a PSDVB co-polymer, decreases when using aqueous solutions of MeOH, AN, and THF as eluents, in that order [99], which may be due to the expansion of the particles inside the column.

Examination of the curves for AN and MeOH in Figure 3.17 reveals that over a small initial range of low concentrations, neither AN nor MeOH produces any swelling that can be measured by the experimental technique used here. At very low organic modifier concentration and high water content, the hydrophobic matrix of the XAD-2

resin does not swell because water cannot interact with it (water does not wet the polymer matrix). The solvent strength of those solutions (AN/water and MeOH/water) in the region of low concentration of organic modifier is not enough to permit the solvent modifier to cause any swelling and only adsorption on the walls of the macropores and mesopores or in the permanent micropores (in the highly cross-linked regions or nuclei) takes place. AN should have more affinity for the polymer matrix based on the solubility parameters alone as discussed in the previous paragraph and it may adsorb more on the surface, but the activity of the external solution is not enough to allow AN to penetrate inside and swell the polymer, or the swelling is only internal, reducing the macropore volume. THF solutions, on the other hand, will show a higher solvent strength at the same activity, and can be adsorbed on the macro- and mesopore walls and, at the same time sorbed in larger amount in the gel causing both internal and external swelling. Due to its great affinity for the polymer matrix, THF starts showing swelling of the gel at activities lower than 0.1 of the organic modifier in the equilibrium solution. Lower activities of THF were not used due to the high uncertainty in preparing the solutions.

### **3.3.5 Relationship Between Swelling and Sorption**

It has been suggested [102], that the swelling caused by certain organic compounds in polymer resins is related to the latent porosity of the polymer. Latent porosity has been defined as the pore volume available to organic compounds that wet the polystyrene surface and opens upon swelling. In the present terminology, latent porosity is due to the gel regions of the polymer matrix. In a polymer bead, the sorption of solvents occurs because of three effects as was mentioned before: adsorption on

macropore walls (that does not produce swelling), sorption by the gel region (accompanied by swelling), and sorption in permanent micropores (in the highly cross-linked regions which are capable of only a little swelling). The permanent microporous regions in the polymer bead, sometimes called nuclei, are very rigid and are poorly swollen even in good solvents. These regions are identified in Figure 3.3 and 3.4, and discussed in section 3.2.3.1. The relationship between sorption of organic modifier and the volume change experienced by individual particles can be interpreted in terms of the region of the particle on which sorption is occurring.

#### **3.3.5.1 Composite Plot of Sorption and Swelling at Equilibrium.**

A composite plot was prepared in which the equilibrium swelling of the polymer (vertical axes values interpolated from the swelling curves in Figure 3.16) is plotted versus the equilibrium solvent sorbed (vertical axes values interpolated from the isotherms in Figure 3.11). Isotherms and swelling plots considering activity instead of concentration could be also used in this way since the combined plot of swelling versus sorption is independent of both concentration and activity in the liquid phase. However, the shape of the activity-based plots (Figures 3.12-3.15 and 3.17) make accurate interpolation more difficult. The resulting plots are shown together in Figure 3.18 and separately in Figures 3.19, 3.20, and 3.21.

These curves have been divided into two or three regions, each of which has been fit with a solid straight line as shown in Figures 3.19, 3.20, and 3.21 to facilitate interpretation. TABLE 3.4 shows the slopes of the different regions for each of the curves

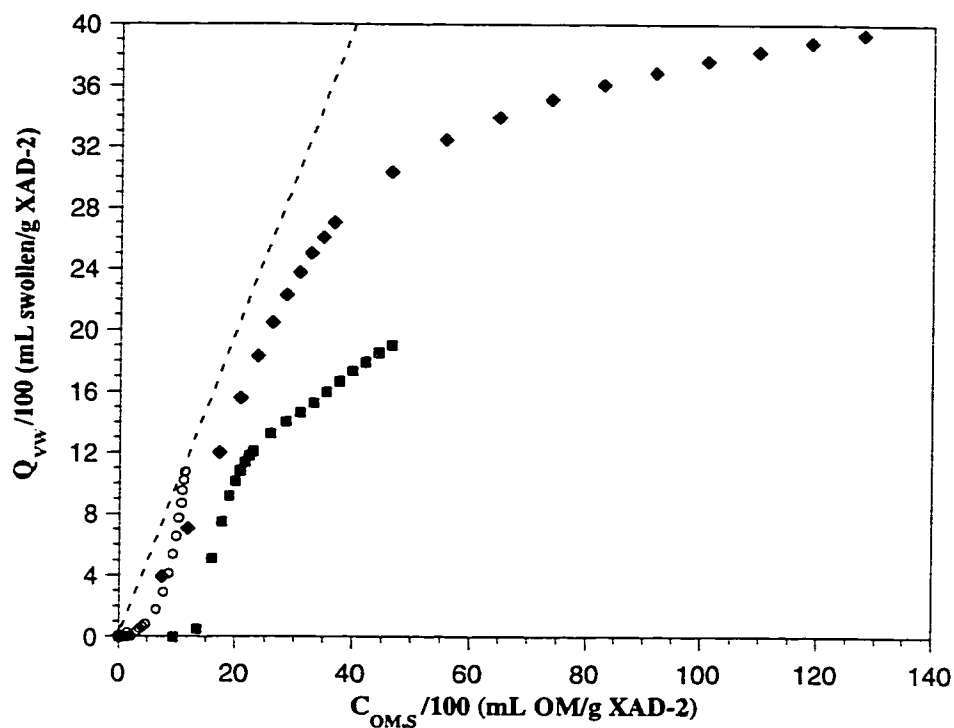


**Figure 3.18: Combined fractional swelling-sorption plots for ( $\diamond$ ) THF, ( $\blacksquare$ ) AN, and ( $\circ$ ) MeOH relating the swelling of XAD-2 caused by the organic modifier in mL/g versus concentration of sorbed organic modifier on the solid phase in mL/g, as calculated from the density of the pure solvent. Points were obtained by interpolation of the experimental curves in Figures 3.11 and 3.16. Broken line represents the 45° line (slope=1) which is the hypothetical case of a fractional swelling/sorption ratio of unity. Data found in Appendix C, TABLE C.9.**

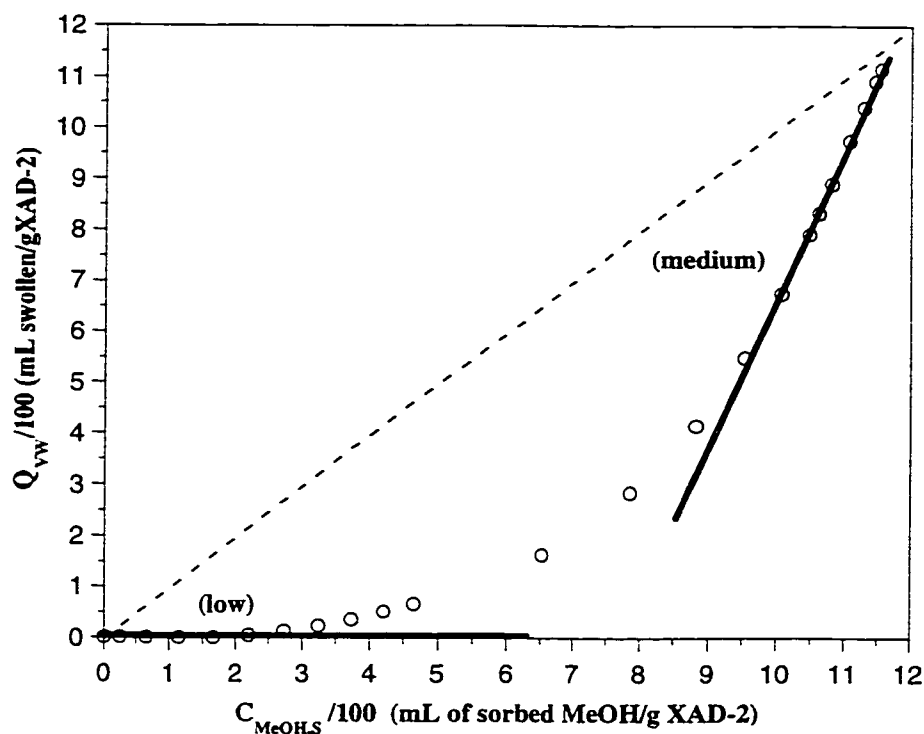


**Figure 3.19:** Combined fractional swelling/sorption plot for MeOH. Points are the same as in Figure 3.18. Low region slope = 0, Medium region slope = 1.89. Broken line represents the 45 ° line (slope = 1) which is the hypothetical case of a swelling/sorption ratio of unity. Data found in Appendix C, TABLE C.9.



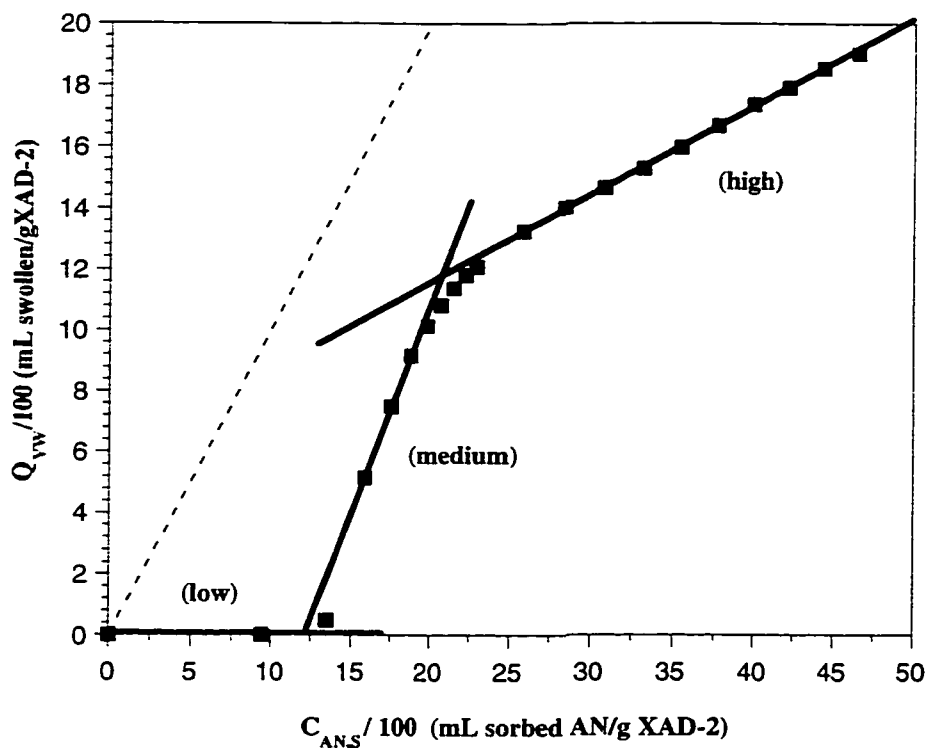


**Figure 3.20: Combined fractional swelling/sorption plot for AN. Points are the same as in Figure 3.18. Low region slope = 0, Medium region slope = 1.34, High region slope = 0.28. Broken line represents the 45° line (slope = 1) which is the hypothetical case of a swelling/sorption ratio of unity. Data found in Appendix C, TABLE C.9.**

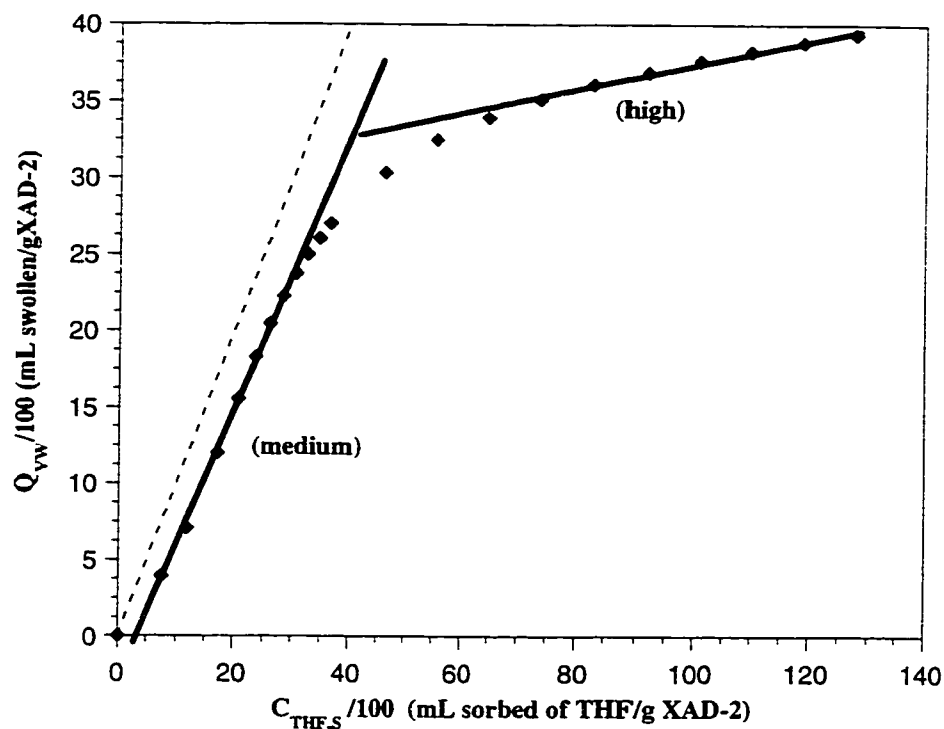


**Figure 3.21: Combined fractional swelling/sorption plot for THF. Points are the same as in Figure 3.18. Medium region slope = 0.94, High region slope = 0.08. Broken line represents the 45 ° line (slope = 1) which is the hypothetical case of a swelling/sorption ratio of unity. Data found in Appendix C, TABLE C.9.**

**TABLE 3.4** Characteristics of the fractional swelling – sorption curves shown in Figures 3.19, 3.20, and 3.21.

<b>Slopes</b>		<b>MeOH</b>	<b>AN</b>	<b>THF</b>
		0	0	---
	<b>Low</b>			
	<b>Medium</b>	<b>1.89</b>	<b>1.34</b>	<b>0.94</b>
	<b>High</b>	---	<b>0.28</b>	<b>0.08</b>
<b>Activity Last point</b>		<b>0.76</b>	<b>0.79</b>	<b>0.83</b>

as well as the activity values of the last point in each plot. Their interpretations are given in the following sections.

### 3.3.5.2 Structure Interpretation of PSDVB.

All of the plot features suggest that the sorption-fractional swelling of this kind of polymer could be taking place in three different stages at the same time. One of these processes is dominant over the others for a given OM. Consistent with the structure proposed in Figures 3.3 and 3.4, these stages are considered to be adsorption onto macropore walls, partition into the low cross-linked gel-region of the polymer matrix, and sorption onto the permanent microporosity in the highly cross-linked regions of the polymer matrix.

*The first region of Figures 3.19, 3.20, and 3.21 (the low  $C_{OM,S}$ ).* In the low  $C_{MeOH,S}$  (Figure 3.19) and  $C_{AN,S}$  (Figure 3.20) sorption occurred without causing swelling (slope = 0, TABLE 3.4) but THF (Figure 3.21) swells the polymer bead even at the low sorption levels.

The zero slope region for AN goes up to  $\approx 12\%$  in the low  $C_{AN,S}$  of Figure 3.20. From the sorption isotherm (Figure 3.14), the activity of the liquid solution at equilibrium with  $C_{AN,S} \approx 12\%$  (mL sorbed/gXAD-2) (no swelling) is  $\approx 0.09$ . The zero slope at low  $C_{THF,S}$  was not observed because data could not be collected at activities lower than 0.03. For THF (Figure 3.13) an activity of 0.09 corresponds to  $\approx 17\%$   $C_{THF,S}$  in the polymer.

This larger concentration inside the polymer produces external swelling that can be measured on the outside. The possibility of internal swelling cannot be neglected [102, 103]. Internal swelling can be pictured as the swelling in the microspheres that reduces the macropore volume without showing external change in the bead dimensions. Because the THF concentration inside the particle is high enough, adsorption onto macropore walls and sorption into the gel [102] causing external swelling are occurring simultaneously. This could be the reason why the region having zero slope is very small at low  $C_{\text{THF},S}$  in the combined fractional swelling-sorption plot. At very low THF sorption, swelling occurs because this solvent has great affinity for the polymer matrix. Partition into the polymer is energetically favorable compared to adsorption on the surface [109, 182] because more interaction between sorbed molecules and polymer chains takes place.

From Figure 3.19, the  $C_{\text{MeOH},S}$  in the zero slope region goes up to  $\approx 3.5\%$  (mL sorbed/gXAD-2). From the known BET surface area of XAD-2 (TABLE 2.1) a monolayer will be covered by  $3.7\%$  (mL sorbed/gXAD-2) of MeOH. Based on these calculated figures, the sorption of MeOH is taking place on the macropore walls, and neither partition into the gel nor sorption into permanent micropores occurs, as expected. This is not the case for AN (Figure 3.20) which shows a zero slope region going up to  $\approx 12\%$  (mL sorbed/gXAD-2). Calculation of monolayer coverage shows that it is obtained at  $4.1\%$  (mL sorbed/gXAD-2) of AN. This result shows a difference between monolayer coverage and maximum sorption before causing swelling, i.e.  $12\% - 4.1\%$ , of  $\approx 8\%$  (mL sorbed/gXAD-2). The extra sorbed volume observed for AN in the region with zero slope

then can be assigned to the presence of AN in two regions, micropore sorption which are non-swelling regions of the matrix, or sorption into the gel causing internal swelling. For THF, a monolayer should be obtained at a  $C_{\text{THF},S}$  of 4.4% (mL sorbed/gXAD-2). It seems that a monolayer of THF is not obtained before partition of this OM starts (Figure 3.21).

Others have reported [183] that, if the difference in the solubility parameters between the polymer and the organic solvent is  $\leq 1.6 \text{ (MPa)}^{1/2}$  they are considered equal. The solubility parameters for THF, AN, MeOH, and PSDVB are 18.6, 24.3, 29.7, and 18.6-19.0  $\text{(MPa)}^{1/2}$  [52, 181] respectively. This means that THF and PSDVB have the same solubility parameter, so that interactions of THF with the polymer are the strongest and this OM penetrates the matrix at low  $C_{\text{THF},L}$ , which explains why sorption onto macropores cannot be distinguished at low  $C_{\text{THF},S}$ . It may be possible that at very low THF sorption, ( $C_{\text{THF},S} < 7\% \text{ mL/gXAD-2}$ ) some adsorption occurs that is not accompanied by partitioning, but data were not obtained in this range (Figure 3.21). For AN and MeOH the difference in their solubility parameters with that of the polymer is too big and sorption onto macropore walls is preferred. A monolayer may be completed for both before any partition into the matrix takes place. Swelling requires extra sorption energy to disentangle the chains in the low cross-linked gel region of the polymer, responsible for swelling.

*The second region of Figures 3.19, 3.20, and 3.21 (the medium  $C_{\text{OM},S}$ ).* In this  $C_{\text{OM},S}$  region the less crosslinked (gel) region of the polymer matrix, (the so called latent pore region) [102]), is swollen as the sorption of solvent increases [11, 65, 107, 184]. The

dominant process in this region is partition of OM into PSDVB matrix. In a given  $C_{OM,L}$ , the swelling will be greater in less cross-linked regions of the gel. In addition, increasing  $C_{OM,L}$  causes increased swelling of a region in the gel having a given cross-linking density (up to a maximum). This continuum of cross-linking between nuclei in the polymer matrix (Figure 3.3 and 3.4) is true for all three OMs. An OM having a solubility parameter closer to that of the polymer matrix causes greater swelling for a given gel cross-linking density.

*The third region of Figures 3.19, 3.20, and 3.21 (the high  $C_{OM,S}$ ).* The predominant process taking place in the high  $C_{OM,S}$  range is sorption into the permanent micropores in the polymer matrix and capillary condensation. Micropores are in the rigid portions of the bead, so that even though OMs with solubility parameters close [153] to that of the polymer are sorbed, their sorption causes only a small change in the external diameter of the bead. In Figures 3.20 and 3.21, both AN and THF seem to approach a plateau in the high  $C_{OM,S}$  region, while MeOH stops swelling the polymer without reaching this “high  $C_{OM,S}$ ” region. The knee where the slope changes from the medium to the high region is obvious for both AN and THF. MeOH stops swelling the polymer approximately at the same value that AN reaches the knee ( $\approx 12\%$  fractional swelling). In section 3.2.3.1, Figures 3.3 and 3.4, the structure of PSDVB was discussed, a bead was defined as having a continuum in cross-linking density between the rigid microporous nuclei. Thus, the rigid microporous region actually would include cross-linking densities that, while relatively high, are low enough to allow some external swelling with the highly solvating OMs. This would be reflected in the external diameter of the particle and

is seen in the AN and THF plots (Figures 3.20 and 3.21). The interaction of THF with the polymer is much larger than that of AN because its solubility parameter is much closer to that of PSDVB than is that of AN, as discussed in *The first region of Figures 3.19, 3.20, and 3.21 (the low  $C_{OM,S}$ )*. More penetration into slightly swellable microporous regions lead to a lower slope in the high  $C_{OM,S}$  region.

The medium  $C_{OM,S}$  region (TABLE 3.4) slopes follow the order  $\text{MeOH} > \text{AN} > \text{THF}$ . This can be understood as follow. At a given medium  $C_{OM,S}$ , assuming that sorption onto the macropore walls has been completed for all three OM's, in the case of MeOH ( $\text{MeOH } \delta = 29.7 \text{ MPa}^{1/2}$ ) [52], the worst solvent for PSDVB ( $\text{PSDVB } \delta = 18.6\text{--}19.0 \text{ MPa}^{1/2}$ ) [52, 181], it is possible that very few molecules, if any, are sorbed in the permanent micropores due to the high solubility parameter of this solvent compared to the solubility parameter of PSDVB. For AN ( $\text{AN } \delta = 24.3 \text{ MPa}^{1/2}$ ) [52], which is a better solvent for PSDVB, some small fraction of the solvent molecules present in the polymer matrix are sorbed (at equilibrium) on the micropores due to the larger affinity between AN and PSDVB. For THF ( $\text{THF } \delta = 18.6 \text{ MPa}^{1/2}$ ) [52], the best solvent among the ones used, a large fraction of molecules are sorbed onto the permanent micropores, because the solubility parameter difference between THF and PSDVB is very small [153], so that the interaction between matrix and OM is favored. If not only sorption (partition) into micropores but also adsorption onto the macropore walls takes place as initially assumed, the residual fraction of molecules sorbed in the low cross-linked gel increases in the order  $\text{MeOH} > \text{AN} > \text{THF}$ , causing a large swelling of that region. This is clear, that the swelling produced will also follow the trend  $\text{MeOH} > \text{AN} > \text{THF}$ , and a large slope in the medium



region is obtained in the same order. For MeOH that process stops without producing a further effect when larger sorption levels are reached, i.e. a plateau in the isotherm (Figure 3.12), not swelling of highly cross-linked regions [109], can occur when poor solvents, like MeOH, are considered.

The absolute slopes of the swelling versus sorption curves in the second (medium) regions (Table 3.4) may be  $> 1.0$  mL swollen/mL of OM sorbed, even if the values used for the molecular volumes (based on densities of the pure solvents) are directly applicable. This is because measured swelling includes enlargement of the macro- and meso- pores (which are filled with bulk aqueous/organic liquid having the same composition as the extra-particle liquid), as well as enlargement of the polymer matrix (which contains sorbed organic modifier). The net effect is that water occupies part of the extra volume caused by the enlargement of the macro- and meso- pores. This volume occupied by water is not represented in the sorption isotherm, which only includes the organic modifier that is in the polymer matrix.

Differential Scanning Calorimetry (DSC) was used in order to determine if water was sorbed in the polymer matrix. If water were present in the matrix, this solution would be enriched in OM with respect to the solution present in the macro- and meso-pores (at equilibrium with bulk solution). In this case, two freezing points for water would be expected at temperatures below  $0^{\circ}\text{C}$  (i.e., freezing point depression for water due to the presence of OM). DSC was run on XAD-2 particles equilibrated with water, in one case, and with 50/50 THF/water (g/g) in the second case. The results are presented in appendix

D in which it is seen that only one peak is obtained for water in 50/50 % THF/water in, which is interpreted as water only being present in one region of XAD-2, i.e. macro- and meso-pores. THF/water was chosen for the DSC studies because THF produces the greatest swelling of XAD-2.

Capillary condensation is very evident in the combined plots for AN and THF. Its onset coincides with the start of the high  $C_{OM,S}$  linear region (marked on Figures 3.20 and 3.21). The process of capillary condensation is accompanied by a strictly linear increase in swelling, as though the driving force for continued condensation of the OM with itself is large enough to stretch the cross-linked polymer chains in the rigid micropores. The slope of this line is smaller than in the second region, in which the swelling is due to additional solvation of chains in the gel region (i.e. to solvation-induced chain disentanglements). At a certain  $C_{OM,S}$ , e.g. 25% (Figures 3.18, 3.20, and 3.21), THF is in a more swollen matrix, i.e. bigger pores on average, than those where AN is at the same  $C_{OM,S}$ . This is evident from the highest values of  $Q_{vw}$  for THF. Thus, the onset of capillary condensation for THF starts at a high value of  $C_{OM,S}$  as discussed in section 3.3.4. The smaller slope of the THF line in this third region, compared to the AN line, reflects the fact that solvation-induced swelling is already much greater for THF than for AN by the time that capillary condensation starts.

### 3.3.6 Effect of the Solvent Present in the Mobile Phase on Efficiency and Peak Symmetry.

It has been observed that tailing on PSDVB can be reduced by using organic modifiers in the mobile phase. Addition of acetonitrile and tetrahydrofuran have been extensively used to improve peak shape in liquid chromatography. The improvement has been correlated with the degree of swelling of the copolymers. PRP-1, a PSDVB packing for RP-HPLC, showed decreased permeability in the series MeOH>AN>THF [92] that was interpreted as an increased swelling of the copolymer [99, 159].

A similar trend has been found in a comparative study of ODS-silica and on a macroporous PLRP-S column in the separation of homologous alkylarylketones [101]. In the ODS-Silica column, the resolution obtained with THF-water (40:60, i.e.  $\approx 0.8$  activity THF) was equivalent to the resolution obtained with AN-water (50:50, i.e.  $\approx 0.8$  activity AN) or MeOH (70:30, i.e.  $\approx 0.56$  activity). However, for PLRP-S 90% MeOH (90:30, i.e.  $\approx 0.8$  activity MeOH) was needed to give a resolution close to that gotten with a 40% THF solution [101]. However, all the peaks eluted from the polymeric column using the 90% MeOH eluent were tailed (poor symmetry) and broad (low efficiency), compared to those eluted with 40% THF.

In order to interpret the results reported in that work [101], calculations of the activity of the OMs in the solutions employed as eluents in that study using Margules and NRTL equations (equations 3.14 and 3.15) were performed. Comparing the swelling

of the polymer (in the gel) in those activity regions shows that THF and AN produce swelling in the more stiff regions of the PSDVB matrix in accordance with another literature report [99] and this work, and both must have a relatively close effect on the efficiency of the eluted sample solutes that were sorbed onto the micropores of the matrix. Increasing the MeOH activity from 0.56 to reach an activity value of 0.8 causes an increase in the swelling of the polymer by only  $\approx 3\%$ . A chromatogram shown in that study exhibited peaks more tailed for the 90:10 MeOH:water than the ones using 40:60 THF:water. Based on this analysis, little improvement in efficiency can be gained by increasing the MeOH/water ratio to 90:10, because MeOH cannot either swell or occupy the highly cross-linked regions in the nuclei to the extent that THF does, so that diffusion of sample solutes out of these OM-free regions must be slow. This reasoning is supported by the results presented in the separation of n-alkylbenzenes in a PRP-1 column [103]. There a 98:2 MeOH:water mixture did not improve column efficiency compared to 54:46 THF:water or 86:14 AN:water mixtures.

### 3.3.7 Conclusions.

The results of this chapter show that adsorption into micropores (highly cross-linked region) is possible depending on the adsorbate molecule, and more specifically, on its solubility parameter. Solutes diffuse inside the permanent microporous structure where not much swelling can occur. The rigid regions of PSDVB (non-swellaable) may sorb organic molecules having a tight fit between the polymer chains, if the sample solubility parameter is close to that of the PSDVB matrix.

## Chapter 4

### **Sorption Rate of Some Organic Modifiers from Binary Solution and the Rate of Swelling of Amberlite XAD-2**

#### **4.1 Introduction.**

The pore structure of macroporous PSDVB copolymers is described in section 3.2.3.1 and illustrated in Figures 3.3 and 3.4. In addition to the permanent macroporosity that arises from the spaces left by the porogen during the polymerization process, there is also a large fraction of the total porosity due to permanent micropores, which are the spaces between the highly cross-linked regions in the polymer matrix. Figure 4.1 shows a transmission electron micrograph of a thin section of XAD-2. In this figure, macropores can be seen (white areas). Their size is comparable to that of the microspheres (dark areas). Micropores are too small to be observed even at a magnification of  $\times 172,000$ . Diffusion of solutes into the macropores is a fast process due to the large size of the pores. The concentration of the solution in the macropores is then assumed to be the same as the one in the bulk solution.

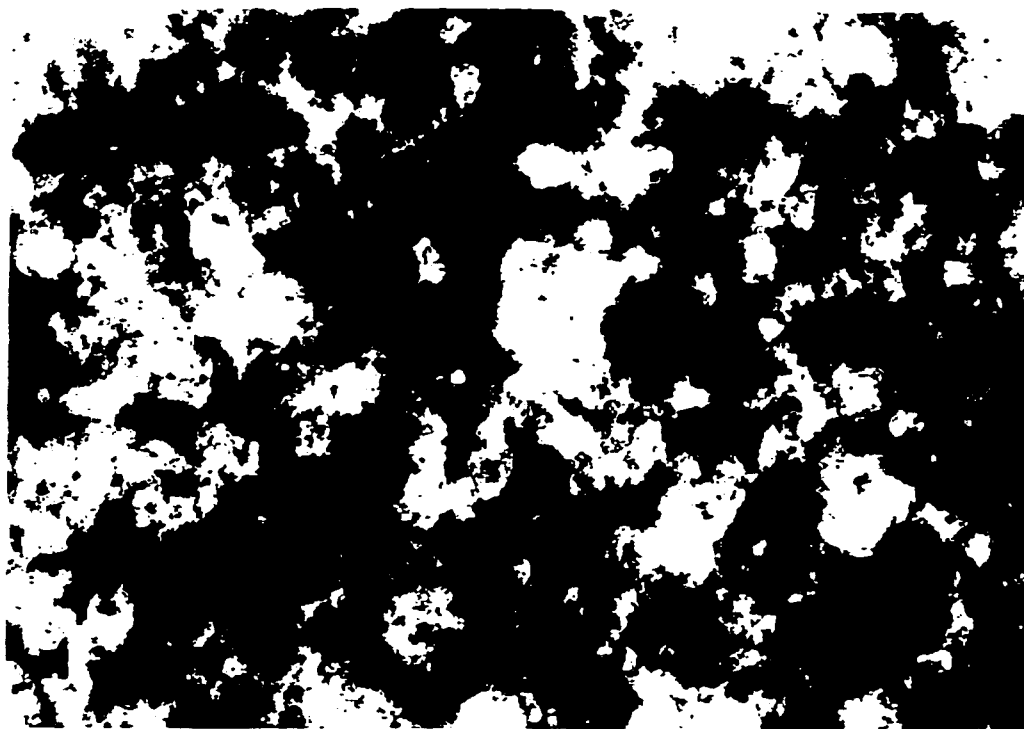


**Figure 4.1** Transmission Electron Micrograph of the inner part of an XAD-2 particle of the XAD-2 (x172,000 in a scale of 1 mm = 5.7 nm). White regions correspond to macropores between microspheres. Dark regions correspond to the solid matrix. Micropores have sizes that cannot be observed by this technique.

In this chapter the swelling kinetics of XAD-2 during sorption of THF, AN, and MeOH modifiers from an aqueous liquid phase is studied, as well as their rate of sorption. The method used for the sorption rate studies was the finite bath technique. For the swelling rate studies, the shallow bed technique was followed. Results of these experiments and their discussion are given at the end of the chapter.

## **4.2 Theory**

### **4.2.1 Kinetic Processes in Porous Media.**

The transport of a solute molecule from the bulk solution, near the particle, to the inner regions has been described as a combination of the following processes: extra-particle mass transfer (i.e. film diffusion) [185] [186], intra-particle mass transfer, and intra-particle chemical kinetics (i.e. adsorption) [26]. Adsorption can be divided into chemical and physical adsorption. Chemical adsorption is irreversible and true chemical bonding of the adsorbed molecules (adsorbate) with the surface takes place. An activation energy is required. Only a monolayer can be formed due to the requirement of a chemical site. Physical adsorption is reversible (does not involve chemical reactions) and may lead to surface coverage in more than one layer of adsorbate. Equilibrium is achieved rapidly since no activation energy is required. Adsorption onto non-polar stationary phases is considered to be a fast process.

#### 4.2.1.1 Sorption and Diffusion into Porous Materials.

Film diffusion is an extra-particle process in which the molecule of adsorbate diffuses through the stagnant film of mobile phase surrounding the particles. If this is the rate controlling step, or the slow step, the overall sorption rate, assuming spherical particles, will be described by [43, 186, 187]:

$$\frac{C_{i,t}}{C_{i,\infty}} = 1 - e^{-Rt} \quad (4.1)$$

$$R = \frac{3D_{film}}{r_0 \Delta r_0 K_D \rho_p} \quad (4.2)$$

where  $R$  is the rate constant,  $C_{i,t}$  and  $C_{i,\infty}$  are the sorbed amounts of solute  $i$  at time  $t$  and at equilibrium respectively,  $r_0$  is the radius of a spherical particle,  $\Delta r_0$  is the film thickness,  $K_D$  is the distribution constant of sample  $i$  between solid and liquid phase in mL/g,  $\rho_p$  is the particle density in g/mL, and  $D_{film}$  (cm<sup>2</sup>/s) is the diffusion coefficient in the film. Film diffusion can be accelerated by faster agitation of the particles or by using high flow rates.

Intraparticle processes include: pore diffusion through the stagnant mobile phase filling the big pores (meso- and macropores) [45, 46, 48, 186], surface diffusion of the



adsorbed solute molecule on the walls of the macropores [46, 47], and diffusion through the matrix, including gel and micropore diffusion. [44, 46, 48]. All of these steps are mass transfer terms.

Another intraparticle process is the adsorption step itself, where the solute molecule passes from the liquid to the solid matrix [46]. This is considered to be a fast step [188]. If the sorption rate were the rate controlling step, the following equation may apply:

$$\frac{C_{i,t}}{C_{i,\infty}} = 1 - e^{-k_{ads}t} \quad (4.3)$$

where  $k_{ads}$  is the first order adsorption rate constant.

Desorption of a molecule from the particle will involve all of the previously mentioned steps in reverse. All of the processes mentioned, except for film diffusion, contribute to the intraparticle sorption rate. A typical sorption rate curve is shown in Figure 4.2.

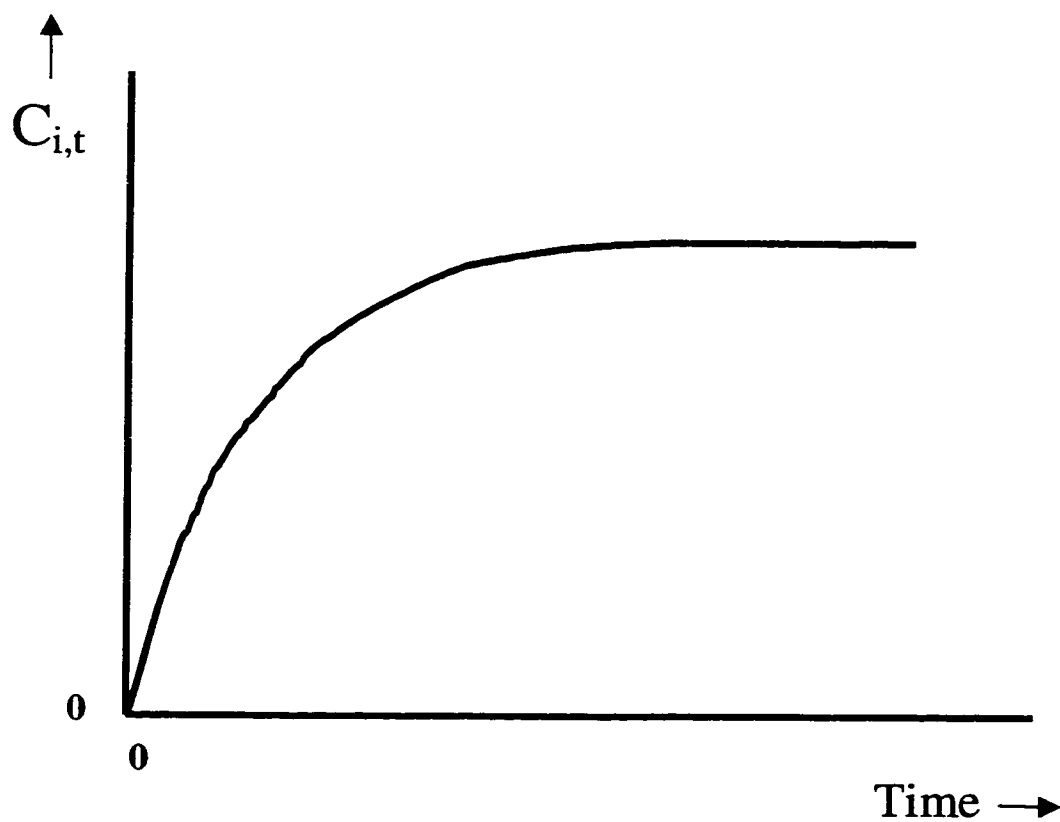


**Figure 4.2** Typical sorption kinetic curve.  $C_{i,t}$  is the amount of sorbed solute at time  $t$ .

#### 4.2.1.2 Swelling Kinetics of Polymeric Materials.

When structural change of the resin occurs upon sorption, it is difficult to distinguish between transport mechanisms, i.e. surface diffusion and pore diffusion [120]. Before a description of the swelling of polymers is given, it is necessary to introduce some concepts.

Diffusion in an isotropic medium, whose structure and diffusion properties are the same in all directions, is based on the hypothesis that the rate of transfer of diffusing molecules through unit area of a section is proportional to the concentration gradient measured normal to the section. This statement is known as Fick's first law [27, 187, 189]. Its mathematical form is given by:

$$J = -D\partial c / \partial z \quad (4.4)$$

where  $J$  is the flux of the component ( $\text{mol}/\text{cm}^2.\text{s}$ ),  $D$  is its diffusion coefficient ( $\text{cm}^2/\text{s}$ ) which may depend on concentration in polymeric systems, and  $\partial c / \partial z$  ( $\text{M}/\text{cm}$ ) is the concentration gradient. In some cases, e.g. diffusion in dilute solutions, the diffusion coefficient can be taken as constant. When diffusion into polymers is the case, the diffusion coefficient depends on concentration. The negative sign arises because diffusion occurs in the opposite direction to that of increasing concentration.

The diffusion behavior in polymers sometimes cannot be described by Fick's law, especially when the adsorbate substance causes large swelling of the polymer [189]. Deviations from Fick's law diffusion are associated with the finite rates at which the polymer swelling occurs when adsorption or desorption of adsorbate molecules takes place. The non-Fickian behavior can be related to the influence that the changing polymer exerts on solubility and diffusional mobility, or to the stress inside the polymer, opposing the advance of the adsorbate.

#### **4.2.2 Rate Controlling Processes.**

The sorption process will be influenced by the swelling of the polymer matrix. Swelling may be slower or faster than the diffusion process. A useful classification has been proposed [190] according to the relative rates of diffusion and relaxation in polymer systems. They are: Case I, relaxation rate  $\gg$  diffusion rate; Case II, relaxation rate  $\ll$  diffusion rate; and anomalous diffusion [191] where relaxation rate = diffusion rate.

##### **4.2.2.1 Case I.**

Case I (rate  $\propto kt^n$ ,  $n=1/2$ ) diffusion or Fickian diffusion establishes that the rate of diffusion is much less than that of relaxation of the polymer chains [190, 192]. Fickian diffusion applies Fick's law to the distribution of solvent in a gel sample during swelling. These systems are controlled by the diffusion coefficient. Soft polymers will adjust so quickly to the presence of the adsorbate that they do not have an effect on the diffusion

coefficient. Diffusion of solutes in polymers can be envisioned as diffusion of the small solute molecules into a concentrated polymer solution.

Figure 4.3 pictures the changes of the concentration dependent diffusion coefficient in several systems versus polymer weight fraction [193, 194]. The features of Fickian diffusion when controlled by a (sorbed) concentration dependent diffusion coefficient on polymers can be summarized as follows. (i) At the early stages, close to the initial times, the amount of sorbed solute is directly proportional to the squared root of time. This characteristic has been found to be true regardless of the relationship between diffusion coefficient and concentration. (ii) At larger times, the curve starts flattening and slowly approaches equilibrium. These have been observed in many experimental curves [195, 196]. (iii) Increases of diffusion coefficient with increasing sorbed concentration of a good solvent (due to a decrease in the viscosity [194]) does not have an obvious effect on the shape of the sorption rate curve, and it is basically linear. (iv) When diffusion coefficient increases with sorbed concentration over a large range of concentrations (from very low to final large concentrations), sorption is a much faster process than desorption. The contrary occurs if the diffusion coefficient decreases with increasing concentration.

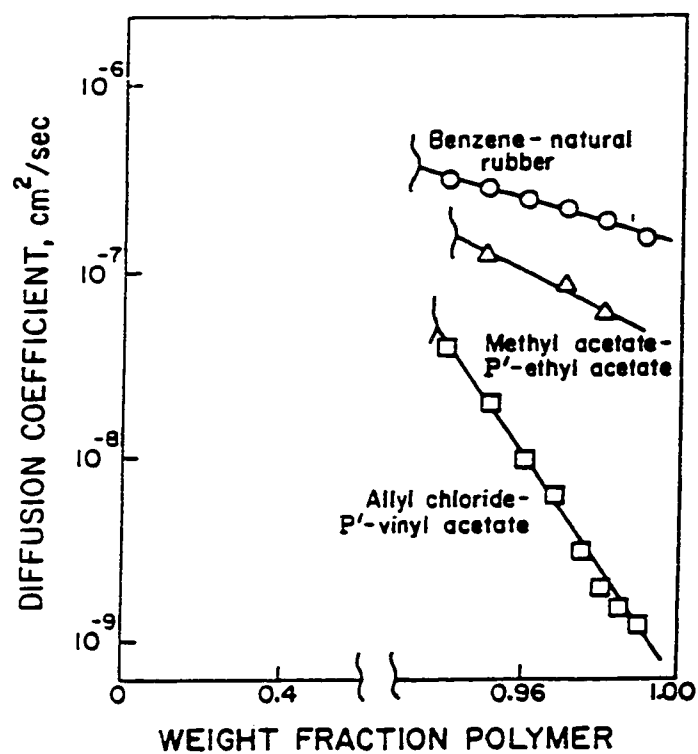


Figure 4.3. Diffusion of small solute molecules in polymers [193, 194].

The experimental swelling curves for many polymers undergoing large volume changes show a sigmoidal shape when the fractional approach to equilibrium versus the squared root of time is plotted. A recent model has been developed that provides short time solutions for moderate volume change [197] for spheres, slabs and cylinders. In this work, this model could not be applied to the experimental data because there was not enough data at short times. In this model the parameters  $F$  and  $\Omega$  characterize the system at various times.

$$F = \frac{V_t - V_0}{V_\infty - V_0} \quad (4.5)$$

$$\Omega = \frac{V_\infty}{V_0} \quad (4.6)$$

where  $F$  is the fractional approach to equilibrium,  $V_t$ ,  $V_0$ , and  $V_\infty$  are the gel volume at time  $t$ , initial, and final (equilibrium) respectively, and  $\Omega$  is total fractional swelling. For swelling,  $\Omega > 1$ ; for collapse  $\Omega < 1$ , and  $\Omega = 1$  represents solvent uptake without change in volume; i.e. classical Fickian solutions for slabs, cylinders, or spheres. For small  $\Omega$ , the curves of  $F$  vs  $\sqrt{t}$  are initially linear, but sigmoidal for larger  $\Omega$  values. For  $\Omega \geq 2.5$ , there is always an inflexion point present.

#### 4.2.2.2 Case II.

In Case II (rate  $\propto kt^n$ ,  $n=1$ ) diffusion the rate of diffusion is much greater than that of the relaxation process. These systems are controlled by the constant velocity of the advancing solvent (penetrant) front which limits the penetration of the advancing compound and sets the division between swollen and unswollen polymer [189, 192]. This is characterized by linear kinetics and a sharp diffusion front. This front is preceded by a region of adsorbate at low concentration, which forms a precursor to the front, and results from essentially Fickian diffusion into the rigid material ahead of the front. The front is a consequence of the strong dependence of solubility parameters and diffusion coefficient on concentration. The velocity of the front is controlled by the time required for disentanglement (relaxation kinetics) of molecular chains (mechanical deformation of the polymer), not by Fick's law [198-200].

Three boundaries can be observed in the front [189]. The inner boundary marks the limit of the advancing liquid, the outer boundary shows the limit of the swollen polymer, and the intermediate boundary is between the swollen and unswollen regions of the polymer. Case II diffusion sometimes occurs in the dissolution of polymers by a good solvent [193, 194].

With mixed solvents superposition of Case II and Case I swelling. has been observed. An example [190, 191] was reported for mixtures of MeOH (responsible for the Case I contribution) and acetone (responsible for the Case II contribution) in contact



with highly cross-linked polystyrene. If similar rates of diffusion and swelling are present, the rate equation describing the global process is:

$$\Delta\omega = k_1 t^{1/2} + k_2 t \quad (4.7)$$

where  $\Delta\omega$  is the total weight increase of the solid phase,  $k_1$  is the Case I swelling rate constant, and  $k_2$  is the Case II swelling rate constant.

The swelling kinetics of polymers has been often adequately described by [140, 152, 156, 201, 202]:

$$\alpha_t = \alpha_\infty [1 - e^{-kt}] \quad (4.8)$$

$$\alpha_t = \frac{m_t - m_0}{m_0} \quad (4.9)$$

where  $\alpha_t$  and  $\alpha_\infty$  are the swelling ratio at  $t$  and at equilibrium,  $k$  is the swelling rate constant,  $m_t$  is the mass of swollen polymer at time  $t$ , and  $m_0$  is the mass of dry polymer.

### 4.2.3 Sorption and Swelling Rate Measurements.

The actual rate of swelling of polymeric materials under the effect of organic compounds has not been studied as often as the rate of solvent sorption. In many cases [120, 152, 203, 204], sorption rates have been measured but swelling rates have been reported, assuming a direct proportionality between volume sorbed and volume swelling, over the whole rate curve. This assumption is not generally true.

Swelling and sorption are two distinct processes and can be independently determined as shown in Chapter 3. By using different experimental approaches, one can provide evidence for swelling rate only.

Different experimental approaches have been employed to measure sorption and swelling rates. For sorption rate measurements, column chromatography [117, 205], spectroscopy [206, 207], determination of sorbed compounds in finite or infinite bath [47, 208] and shallow bed [44, 106, 113] conditions are the most common ones. For swelling rate measurements, some studies have been done using optical microscopy [116, 140, 155-157, 173], where the increase in one of the dimensions of the solid is measured; measurement of column volume increase [120, 144, 154]; evaporation of liquid from composite films [203]; or weight increase [143, 145, 153, 182, 209] of swellable materials have also been experimentally measured. All of the reported swelling methods, except for the microscopic measurements, are by no means real swelling measurements. All of them are flawed by the assumption of equality between sorption and swelling.

In this work the sorption rate was followed by using the finite bath method and the sorbed concentration was measured by analysis of the liquid phase. Swelling kinetics was performed in the shallow bed method and the volume increase of a particle was calculated from measurements of the particle diameter. These techniques are described in the next sections.

#### **4.2.3.1 Finite Bath Method.**

In this mode, a known amount of the sorbent is confined in a vessel. The liquid phase containing the sorbate is added and the mixture is rapidly stirred. The amount of solute sorbed by the sorbent is measured as a function of time [43, 46, 47]. This can be done either by periodically withdrawing small amounts of the sorbent, eluting the sorbed compound and quantifying it, or by periodically withdrawing small fractions of the liquid phase and analyzing it for the solute. Then by mass balance of solute, the amount sorbed is calculated by difference. A plot of the sorbed mass per unit weight of solid versus time is the sorption rate curve.

The amount of solute sorbed will determine the conditions for the batch experiment [43, 47]. If the amount sorbed by the solid is small, the concentration of solute in the liquid phase is approximately constant and is frequently called “infinite bath conditions”. Here the sorption rate must be followed in the solid phase. Conversely, if the fraction of solute sorbed by the solid is high the experiment is said to be under “finite bath conditions”.

In this work, sorption rate of organic modifiers onto XAD-2 was determined by using "finite bath conditions" in the batch mode. The sorption rate was monitored in the liquid phase. Studies in "infinite bath conditions", where elution is required was not attempted because of the uncertainties related to the removal of external solution that usually remains as liquid bridges between the particles [156], as a result of capillary forces. Using the "finite bath conditions" approach, and calculating sorption by difference, eliminates the extra experimental step of removing the solution filling macropore spaces (void volume).

The finite bath method is troublesome to use in swelling kinetics experiments. The particles have to be in constant agitation so that the Nernst diffusion film will be very thin and the concentration gradient in the solution surrounding the particles will be zero. The swelling of polymeric materials is very fast and microscopic measurements of the particle dimensions require static particles so that they can be rapidly focussed and measured. If the solution is in agitation the time it takes to bring them to focus from a large space, e.g. cell shown in Figure 2.4, is too long.

#### **4.2.3.2 Shallow Bed Method.**

In the shallow bed mode a small column, 0.5 mm height [106] is filled with the sorbent and a known concentration of solution is forced to flow through the bed at a high flow rate such that, at all times, the concentration of solute at the effluent is nearly the same to that in the influent solution. This means that all of the particles contained in the column will be in contact with the initial concentration at all times. This is a special case

equivalent to infinite bath conditions. The contact time between the two phases is changed by varying the time that the solution is passed through the bed.

For the swelling studies in this work, the shallow bed flow conditions and microscopic determination of the particle diameter were used to determine the swelling rate of XAD-2 under the effect of different organic modifiers. The diameter increase of a single XAD-2 particle was measured as a function of time. The fractional swelling at different times was calculated as described in Chapter 3. The apparatus used in the swelling kinetic experiments was described in Chapter 2, Figure 2.5.

#### **4.2.4 Effect of the Mobile Phase on the Sorption Kinetics of Organic Solutes in HPLC**

Poor efficiency has been linked to hindered diffusion of solutes in and out the micropores (not seen in Figure 4.1, sketched in Figure 3.3) [107]. The mobile phase used has a great influence on the efficiencies observed in several studies [11, 99-101]. THF, AN, and MeOH have been traditionally used as components of the mobile phases in RPLC.

Partition of solutes (between the liquid and the solid phase) occurs at a certain rate that is determined by the physical processes that take place inside the polymer particle as mentioned in section 4.2.1. The mobile phase effect on tailing is related to swelling of the polymer when using a good solvent due to better solvation of the surfaces. Swelling of the polymeric packing is favorable in a chromatographic separation, e.g. improved

efficiency and less tailing, in the elution of aromatic compounds from such columns. It is possible to think that as the OM, present in the liquid, is sorbed, not only swelling of the packing occurs but also blocking of highly energetic sites, i.e. permanent micropores, where sample molecules could be trapped. The blocking of these sites inhibits the solute from being sorbed there, so that tailing and broadening could be reduced. It has been also interpreted that as the packing swells [100], some small pores open from their collapsed state and hindered diffusion decreases, leading to better efficiencies.

### **4.3 Results and Discussion.**

The sorption rate of THF, AN, and MeOH onto the XAD-2 resin and the rate of swelling of the resin under the effect of these modifiers were studied at several aqueous solution concentrations of organic modifiers. Swelling rate was studied by using the shallow bed mode whereas sorption rate was measured by using the finite bath mode.

#### **4.3.1 Rate of Sorption of OM from Aqueous Solutions by XAD-2.**

Figures 4.4, 4.5, and 4.6 show the rate of sorption of THF, AN, and MeOH on XAD-2 respectively. All these plots have been normalized by using the equilibrium value. This was obtained by leaving particles in contact with the respective solution for a 4 day-period and taking the measurement after that. The initial concentration of OM in the solutions employed to measure sorption were 35.83, 35.46, and 34.07 %w/w for THF,

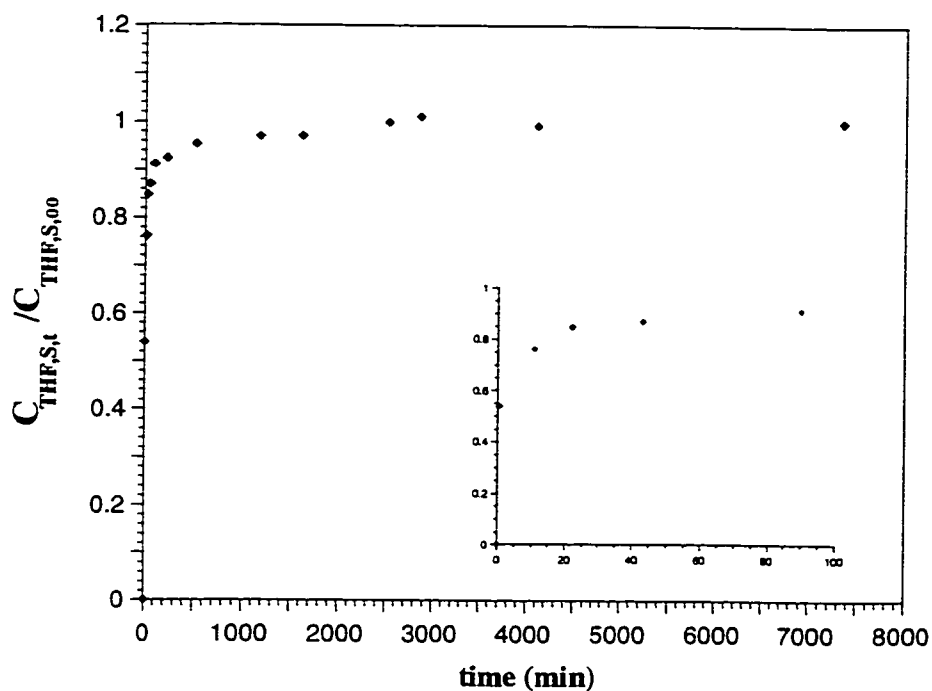


**Figure 4.4** Normalized rate of sorption of THF on XAD-2 using finite bath conditions. Symbols represent experimental data. Small plot shows low sorption times.  $C_{\text{THF},L,i}=35.83\%$  (g/g),  $C_{\text{THF},L,f}=29.44\%$  (g/g). Data found in Appendix C, TABLE C.10.

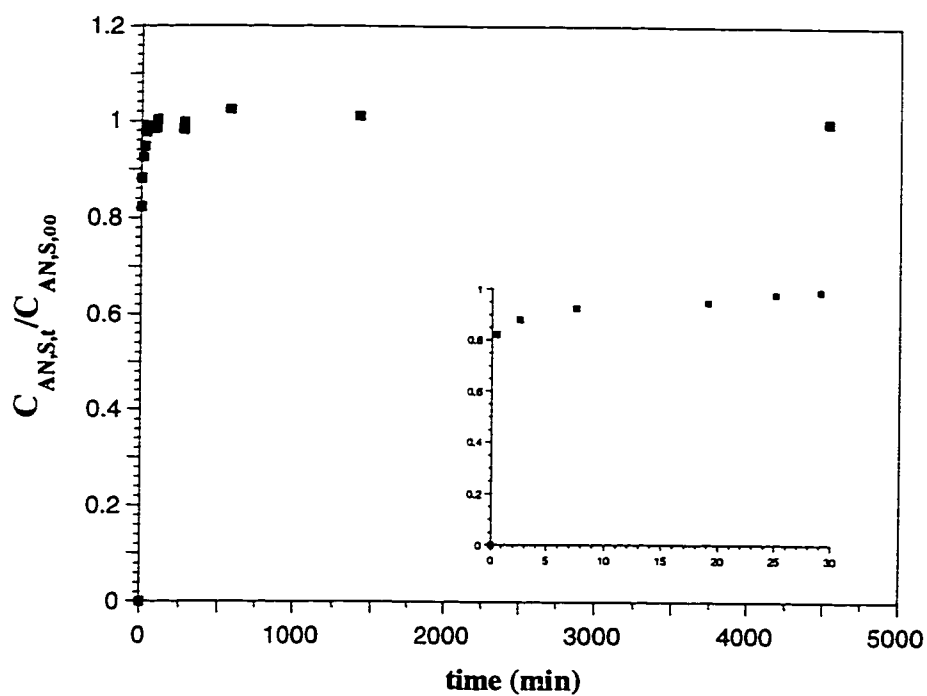


**Figure 4.5** Normalized rate of sorption of AN on XAD-2 using finite bath conditions. Symbols represent experimental data. Small plot shows low sorption times.  $C_{AN,L,i}=35.46\%$  (g/g),  $C_{AN,L,f}=31.99\%$  (g/g). Data found in Appendix C, TABLE C.11.



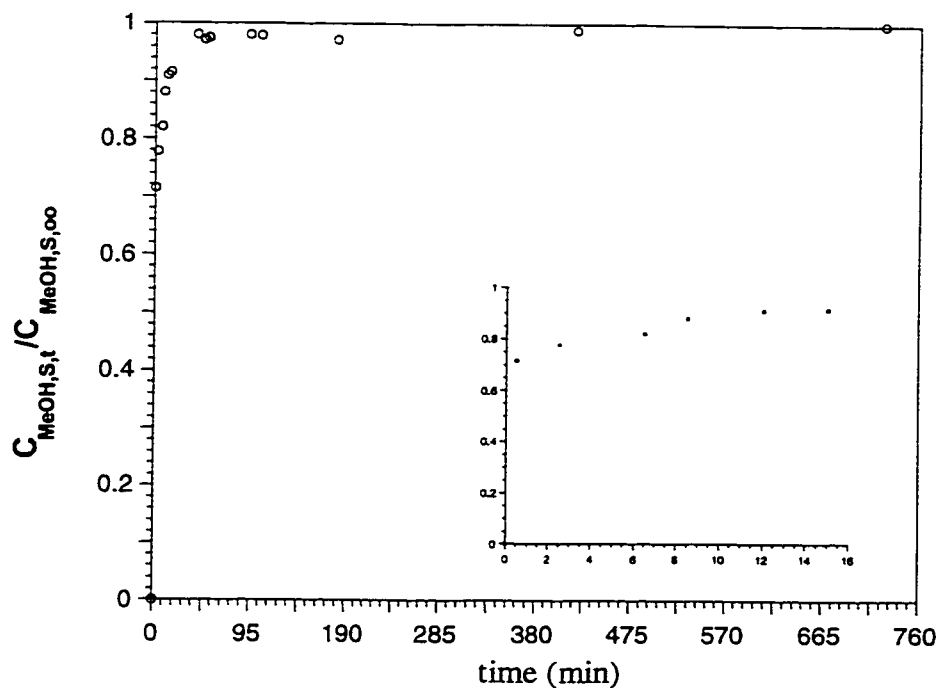


**Figure 4.6** Normalized rate of sorption of MeOH on XAD-2 using finite bath conditions. Symbols represent experimental data. Small plot shows low sorption times.  $C_{\text{MeOH},L,i}=34.07\%$  (g/g),  $C_{\text{MeOH},L,\infty}=33.14\%$  (g/g). Data found in Appendix C, TABLE C.12.

AN, and MeOH respectively. It can be observed that 90% of the equilibrium concentration (solid phase) recorded was reached in approximately 2 hours for THF, 30 min for AN, and 20 min for MeOH, respectively. The total change in the liquid concentration (initial versus equilibrium concentrations) was  $\approx 20\%$  for THF,  $\approx 10\%$  for AN, and  $\approx 3\%$  for MeOH. The final concentrations in the liquid phase after equilibrium had been reached were 29.44, 31.99, and 33.14 %w/w for THF, AN, and MeOH respectively. The concentrations of organic modifier in the liquid phase used to obtain the sorption rates and their corresponding activities are given in TABLE 4.1. In Figure 3.12, it can be observed that activity values (where the solutions employed were chosen) for THF and AN are very close to the isotherm region where capillary condensation starts. The activity value for MeOH is located in the region where the isotherm starts flattening (plateau).

**TABLE 4.1 Activity of the initial and equilibrium solution used to determine sorption rate of the organic modifiers on XAD-2 by using Margules and NRLT equations to calculate activity coefficients and activities (equations 3.14 and 3.15).**

	$C_{OM,L,0}$ (%w/w)	$C_{OM,L,\infty}$ (w/w)	$a_0$	$a_\infty$
<b>THF</b>	35.83	29.44	0.784	0.740
<b>AN</b>	35.46	31.99	0.765	0.754
<b>MeOH</b>	34.07	33.14	0.311	0.303

An overview of the different parts of these plots is given as follows. At initial times, less than 1 minute, the curves exhibit a sharp increase in the sorbed concentration (Figures 4.4, 4.5, and 4.6). Data could not be collected at times below 30 seconds. At very low times, the sorbed amounts of the organic compounds are small. The sorbed amount is obtained by subtracting the initial absolute amount of solvent employed in preparing the solution from the amount present in the solution at the time of sample withdrawal. The result of subtracting these two figures is a very small number. In the low sorption region, uncertainties are very large because of this way of calculating sorbed concentration (by mass balance).

A hypothetical limiting rate curve (Figure 4.7) was calculated for one of the organic modifiers, i.e. THF, by using a monodisperse model for homogeneous spheres [189, 210] and for infinite bath conditions. This is a model in which diffusion through only the pore liquid is assumed and the retardation effect of adsorption on diffusion rate is ignored. The equation employed in these calculations is:

$$C_{THF,S,t} = C_{THF,S,\infty} \left( 1 - \frac{6}{\pi^2} \sum_{n=1}^{\infty} \frac{1}{n^2} e^{(-n^2 Bt)} \right) \quad (4.10)$$

$$B = \frac{\pi^2 D}{r^2} \quad (4.11)$$

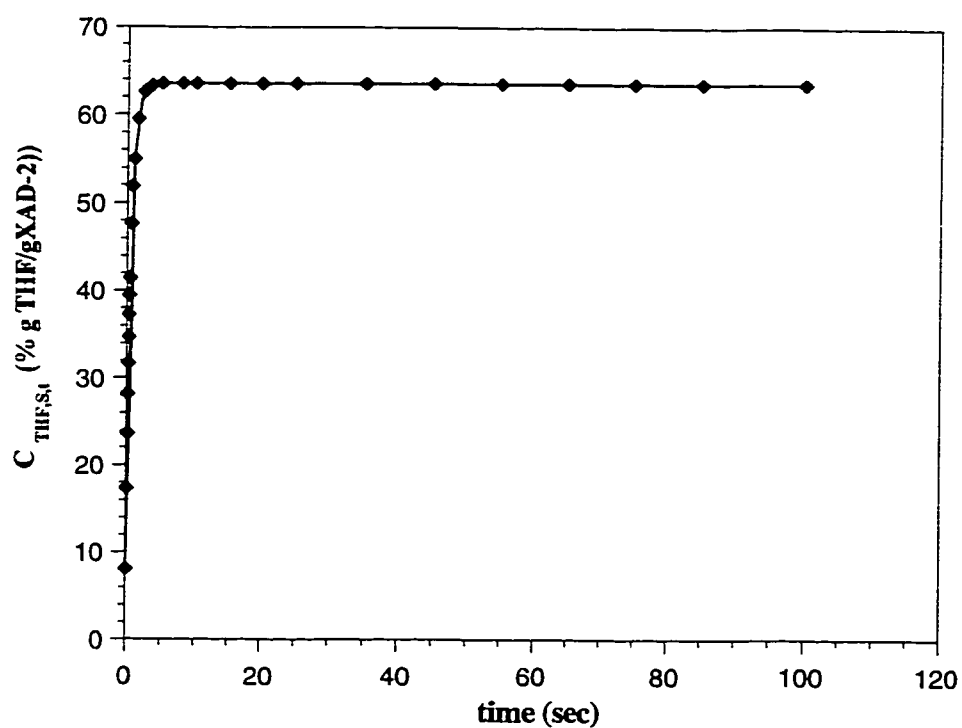


**Figure 4.7** Hypothetical rate curve calculated from a monodisperse model [189] by using a particle diameter of 360  $\mu\text{m}$  and a diffusion coefficient of  $5 \times 10^{-6} \text{ cm}^2/\text{s}$  (equation 4.10 and 4.11). Data found in Appendix C, TABLE C.13.

where  $C_{THF,S,t}$  is the macropore uptake at time  $t$ ,  $C_{THF,S,\infty}$  is the macropore uptake at equilibrium,  $D$  is the diffusion coefficient of the sorbate (in this case is taken as  $\approx 5 \times 10^{-6} \text{ cm}^2/\text{s}$  for diffusion in macropores, no hindrance and no adsorption retardation), and  $r$  is the radius of the spherical particles (XAD-2 particle diameter of  $360 \text{ }\mu\text{m}$ ). Curves of this type for AN and MeOH will show the same shape and time dependence because the diffusion coefficient is assumed to be the same for all of the organic modifiers in free solution. The only difference between the last two hypothetical (not shown) curves in comparison to the one for THF is the height of the  $C_{OM,S,t}$  values in the Y axis. The THF hypothetical plot shows that equilibrium should be reached in less than two minutes if hindrance and sorption retardation were not present.

The sorption of these solvents approaches equilibrium very slowly. Equilibrium is reached at 4000 min ( $\approx 3$  days) for THF (Figure 4.4), 1500 min ( $\approx 1$  day) for AN (Figure 4.5), and 120 min (2 hours) for MeOH (Figure 4.6). For the equilibrium studies, solutions were left 4 days to be sure equilibrium was reached. This slow approach to equilibrium can be interpreted as hindered diffusion into the polymer matrix. Hindered diffusion of MeOH, THF, and AN is probably occurring in micropores in the highly cross-linked region of the polymer matrix.

Sorption rate data for all three organic modifiers were fit to an empirical triexponential equation. This empirical general equation is shown below (equation 4.12). Figures 4.8, 4.9, and 4.10 show these fittings for THF, AN, and MeOH respectively.

$$C_{OM,S,t} = C_{OM,S,\infty} - C_1 * e^{-k_1 t} - C_2 * e^{-k_2 t} - C_3 * e^{-k_3 t} \quad (4.12)$$

This is a purely empirical equation, which has no physical significance. Its properties and use have been discussed and justified in previous studies in this laboratory [106, 113] as the mentioned equation can accurately predict elution chromatographic peaks.

The three empirical triexponential fits for THF, AN, and MeOH are shown in equations 4.13, 4.14, and 4.15. The regression coefficients ( $R^2$ ) obtained for the fittings are 0.9996, 0.9989, and 0.9989 for THF, AN, and MeOH respectively.

$$C_{THF,S,t} = 62.35 - 34.38e^{-6.3400t} - 19.98e^{-0.1017t} - 7.998e^{-0.0059t} \quad (4.13)$$

$$C_{AN,S,t} = 27.09 - 22.97e^{-5.9640t} - 3.17e^{-0.0702t} - 0.94e^{-0.0060t} \quad (4.14)$$

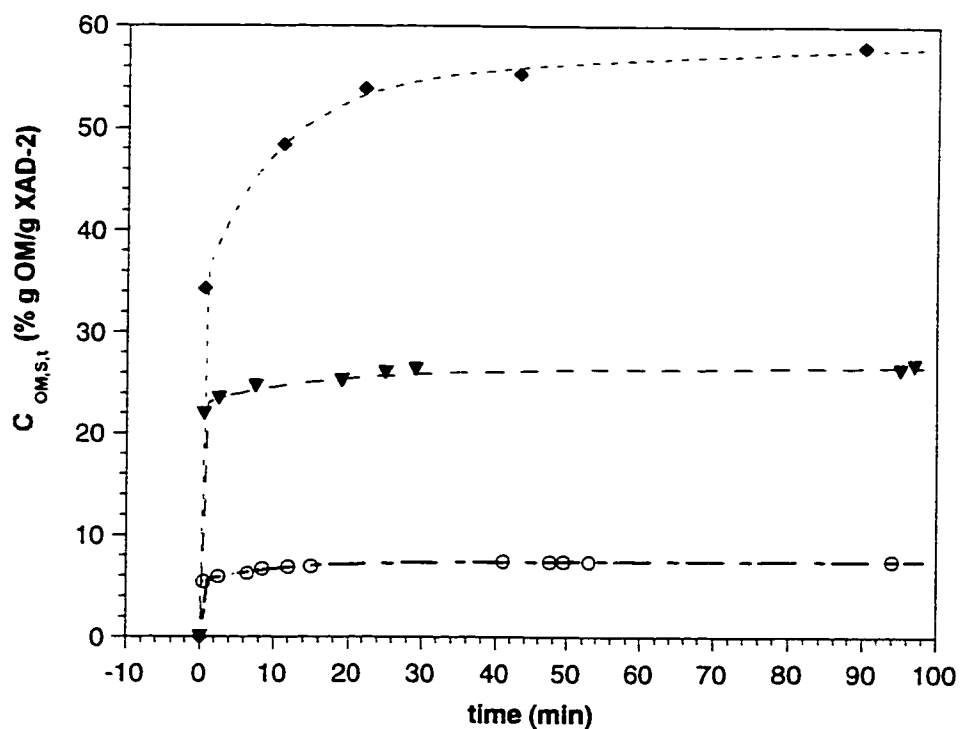
$$C_{MeOH,S,t} = 7.98 - 5.42e^{-8.1605t} - 1.99e^{-0.1042t} - 0.58e^{-0.0005t} \quad (4.15)$$

TABLE 4.2 summarizes all the constants involved in equations 4.13, 4.14, and 4.15. The sorption rate experiments were not performed at infinite bath conditions. These equations will be used in section 4.3.3.

**TABLE 4.2.** Summary of the parameters of the fitted triexponential equation to the experimental sorption data for THF, AN, and MeOH. C and k units are (% gOM/gXAD-2) and (min)<sup>-1</sup> respectively.

	<b>C<sub>∞</sub></b>	<b>C<sub>1</sub></b>	<b>k<sub>1</sub></b>	<b>C<sub>2</sub></b>	<b>k<sub>2</sub></b>	<b>C<sub>3</sub></b>	<b>k<sub>3</sub></b>
<b>THF</b>	62.35	34.38	6.34	19.98	0.1017	7.998	0.005852
<b>AN</b>	27.09	22.97	5.96	3.17	0.0702	0.9399	0.005961
<b>MeOH</b>	7.98	5.42	8.16	1.99	0.1042	0.5752	0.000529





**Figure 4.8** Comparative triexponential fitting (overall) of experimental data for THF, AN, and MeOH up to 100 min. Symbols represent: (◆) THF sorption rate curve fitting to eqn. 4.13, (▼) AN sorption rate curve fitting to eqn. 4.14, and (○) MeOH sorption rate curve fitting to eqn. 4.15. Data Found in Appendix C, TABLE C.14, C.15, and C.16.

(close to infinite bath conditions). The constants gotten from the fittings (i.e.  $C_\infty$ ,  $C_1$ ,  $C_2$ ,  $C_3$ ,  $k_1$ ,  $k_2$ ,  $k_3$  and) have no physical meaning due to the empirical nature of the triexponential fittings. However, a good fitting for the experimental data is needed in order to get accurate interpolation of the sorption data at different times. These rate curves will be used latter in section 4.3.3 together with the swelling rate curves in order to compare rate of swelling to rate of sorption for each organic modifier at a given liquid phase concentration. Figure 4.8 shows the three OM's overall sorption rate curves for THF, AN, and MeOH up to 100 min.

#### 4.3.2 Rate of Swelling of XAD-2 in Different Aqueous Solutions of OM's.

Figures 4.9-4.26 show the fractional swelling of XAD-2 versus time in aqueous solutions of THF (Figures 4.9-4.14), AN (Figures 4.15-4.20), and MeOH (Figures 4.21-4.26) respectively at several concentrations of OM. The first five figures in each group show individual swelling rate curves for different concentrations of the OM in the liquid phase. The sixth figure for each solvent shows the five curves in order to compare different levels of swelling and their corresponding fittings (CurveExpert 1.34, Daniel Hyams, Microsoft Corporation, 1997). Fitting parameters for the three groups of experiments are shown in TABLE 4.3 through TABLE 4.5.

Three main features are observed for all of the curves shown in the plots. a) The rate of swelling increases as the concentration of the organic modifier is increased for the

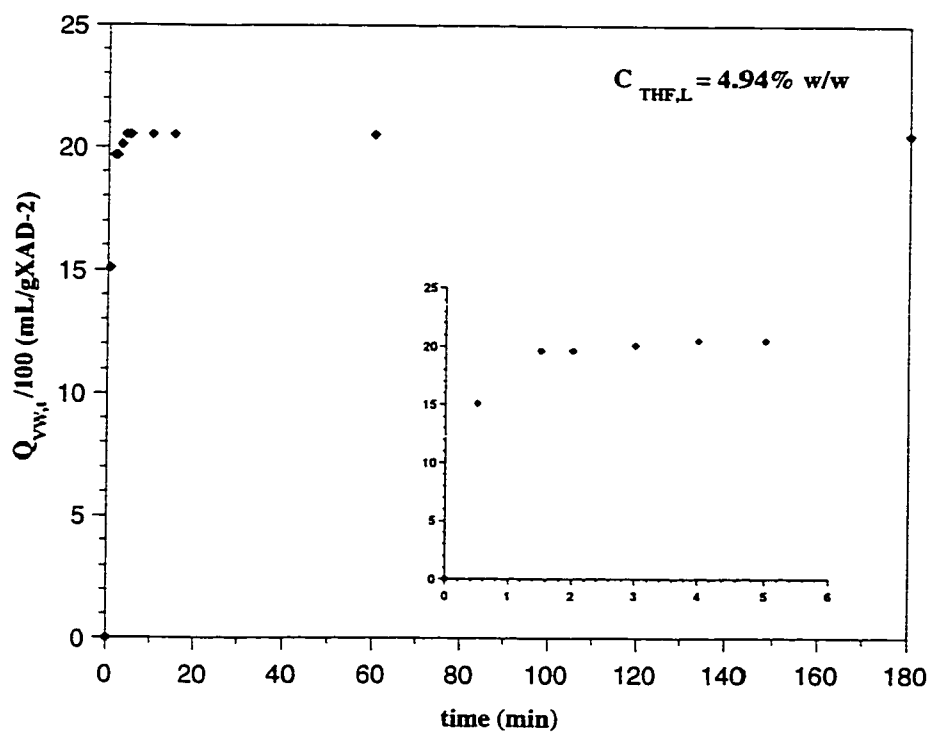


**Figure 4.9** Swelling rate of a particle of XAD-2 in 4.94% THF aqueous solution. Small figure shows early stages of the swelling rate. Data found in Appendix C, TABLE C.17.

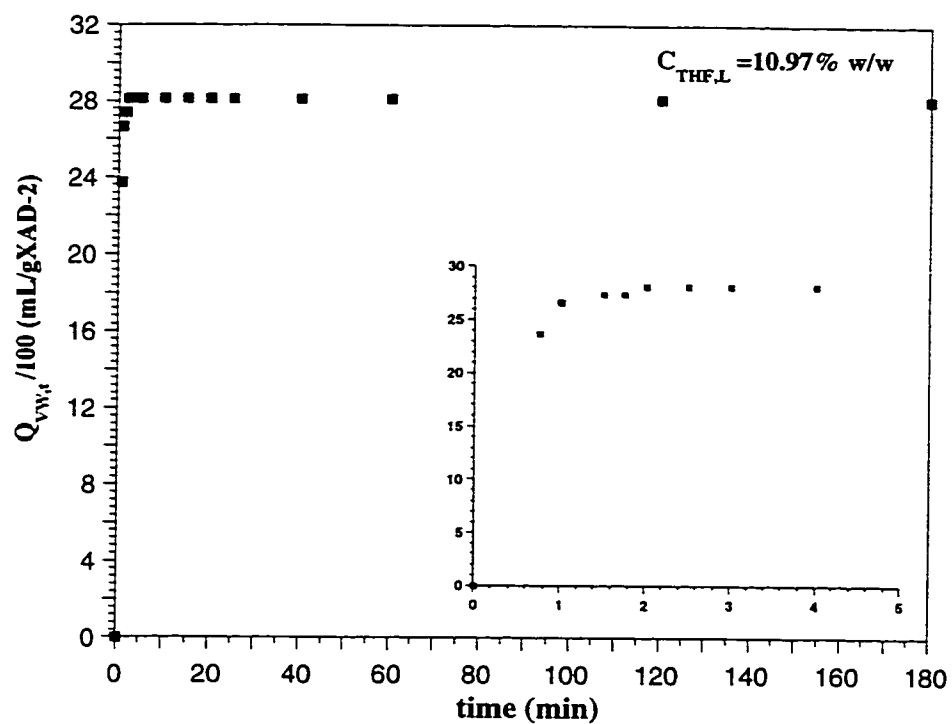


**Figure 4.10** Swelling rate of a particle of XAD-2 in 10.97% THF aqueous solution. Small figure shows early stages of the swelling rate. Data found in Appendix C, TABLE C.18.

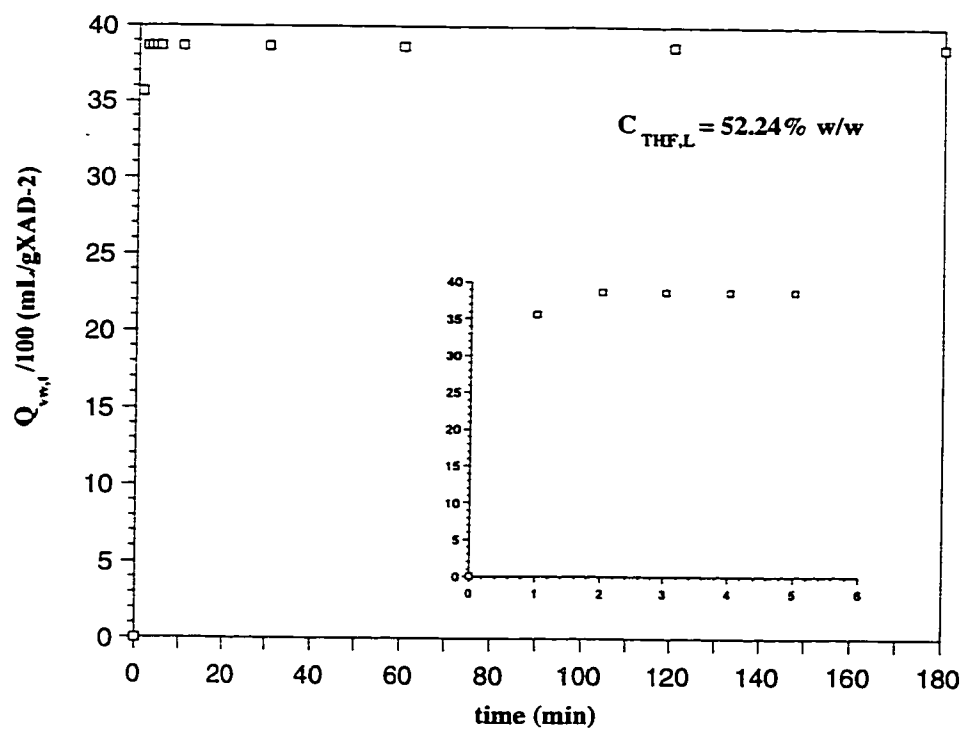


**Figure 4.11** Swelling rate of a particle of XAD-2 in 52.24% THF aqueous solution. Small figure shows early stages of the swelling rate. Data found in Appendix C, TABLE C.19.

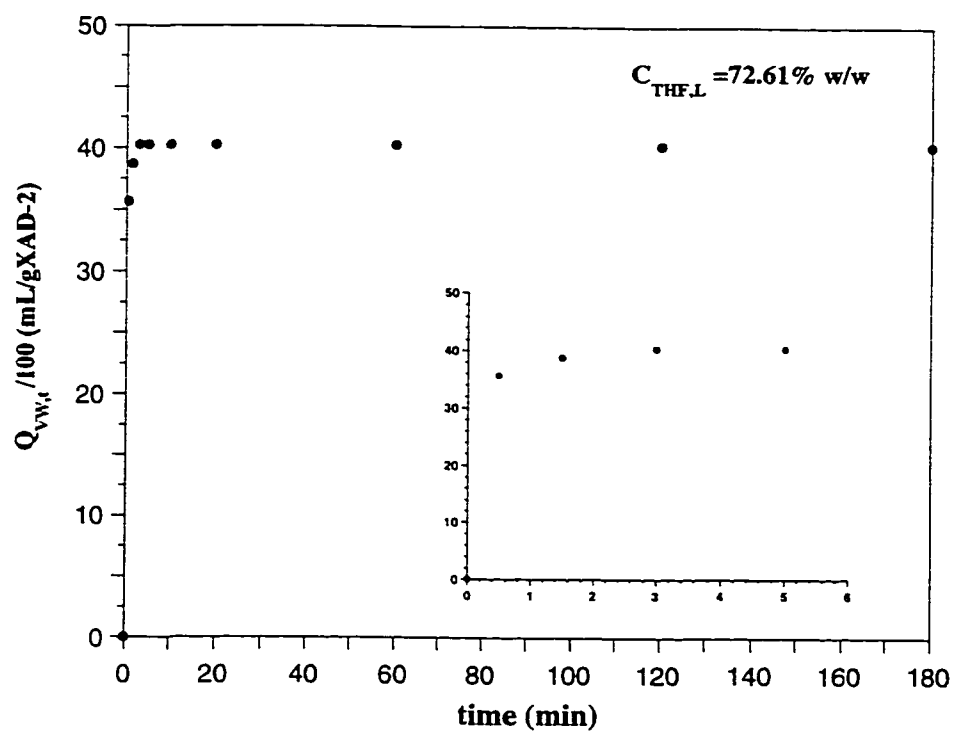


**Figure 4.12** Swelling rate of a particle of XAD-2 in 72.61% THF aqueous solution. Small figure shows early stages of the swelling rate. Data found in Appendix C, TABLE C.20.

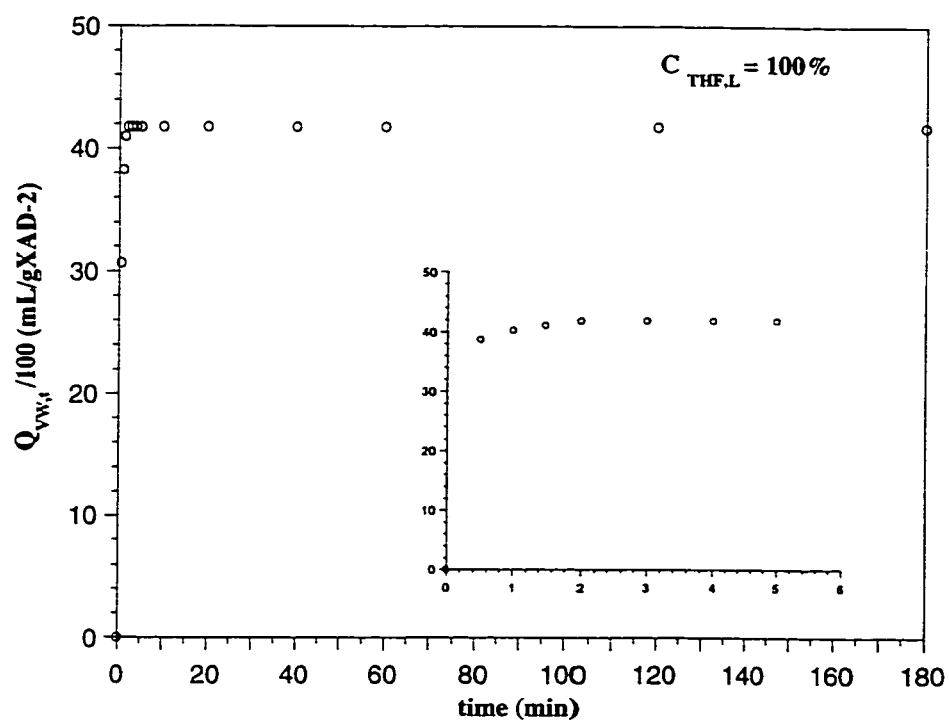


**Figure 4.13** Swelling rate of a particle of XAD-2 in 100% THF aqueous solution. Small figure shows early stages of the swelling rate. Data found in Appendix C, TABLE C.21.

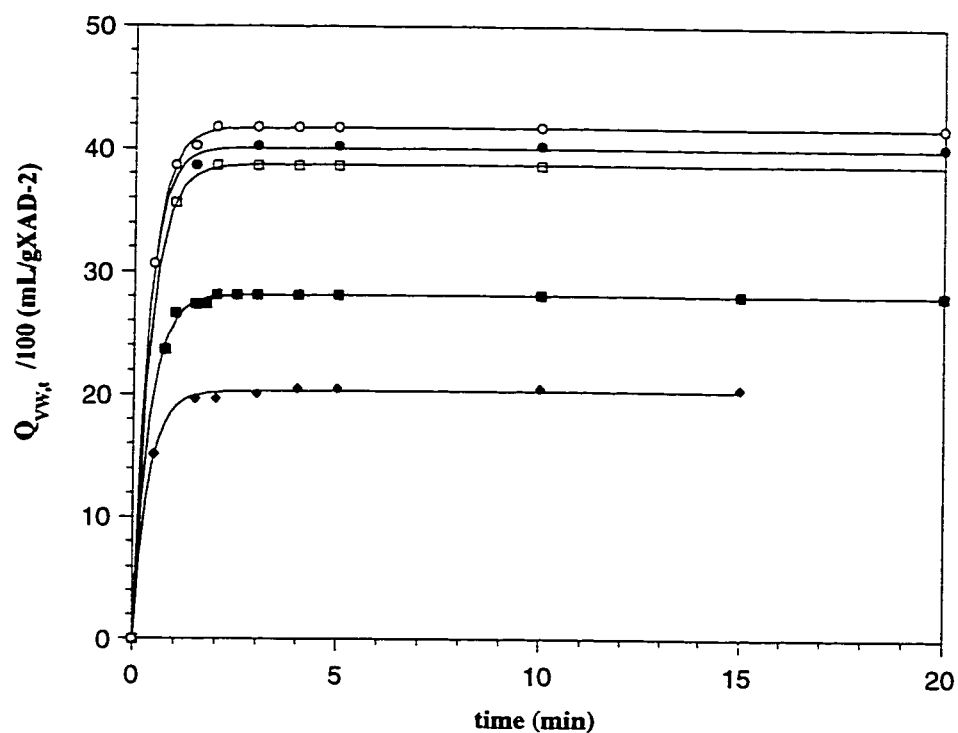


**Figure 4.14** Swelling rate of a particle of XAD-2 in different THF aqueous solutions. These plots are a compilation of the previous shown. Concentrations of THF in the liquid phase are given in % w/w as follows: (♦) 4.94%, (■) 10.97%, (□) 52.24%, (●) 72.61%, and (○) 100%. Solid line represents the fitting to equation 4.16. Data found in appendix C, TABLES C.17. to C.21.



**TABLE 4.3** Curve fittings for the swelling kinetics of XAD-2 using THF as the organic modifier in the liquid phase. Experimental data fits the following equation:  $Q_{VW,t} = Q_{VW,\infty} [1 - e^{(-k.t)}]$ .

<b>C<sub>THF,L</sub></b> <b>(w/w)</b>	<b>Q<sub>VW,∞</sub>/100</b> <b>(mL/gXAD-2)</b>	<b>k</b> <b>(min<sup>-1</sup>)</b>	<b>R</b>
100	41.72 ± 0.10	2.64 ± 0.05	0.9998
72.61	40.06 ± 0.19	2.86 ± 0.09	0.9997
52.24	38.73 ± 0.04	2.53 ± 0.03	1.0000
10.97	28.12 ± 0.10	2.58 ± 0.08	0.9995
4.94	20.29 ± 0.12	2.69 ± 0.12	0.9991

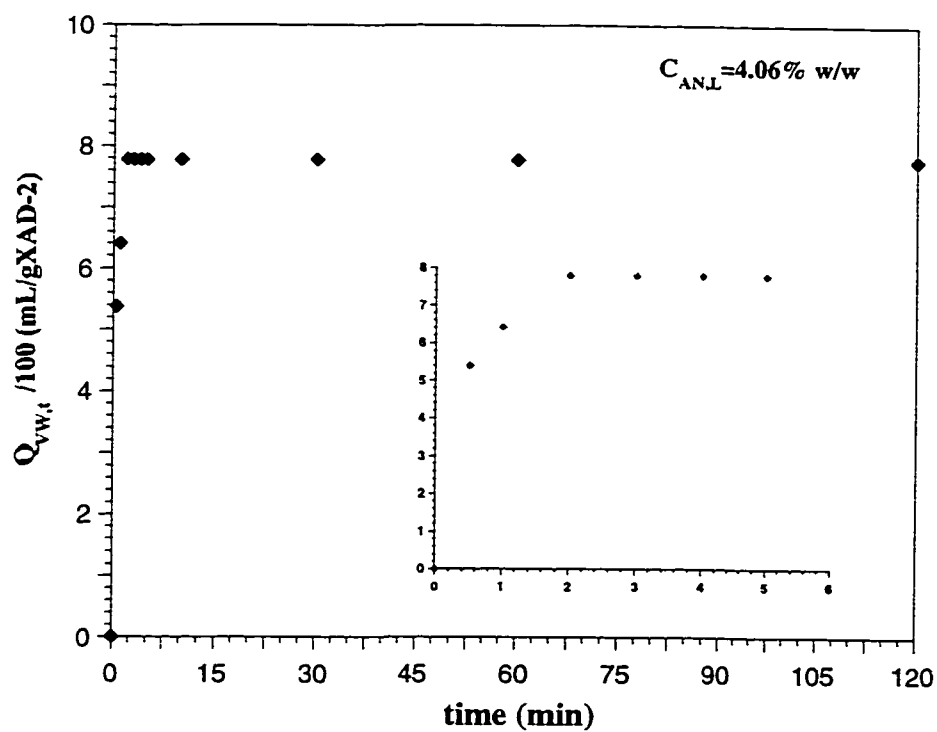


**Figure 4.15** Swelling rate of a particle of XAD-2 in 4.06% AN aqueous solution. Small figure shows early stages of the swelling rate. Data found in Appendix C, TABLE C.22.

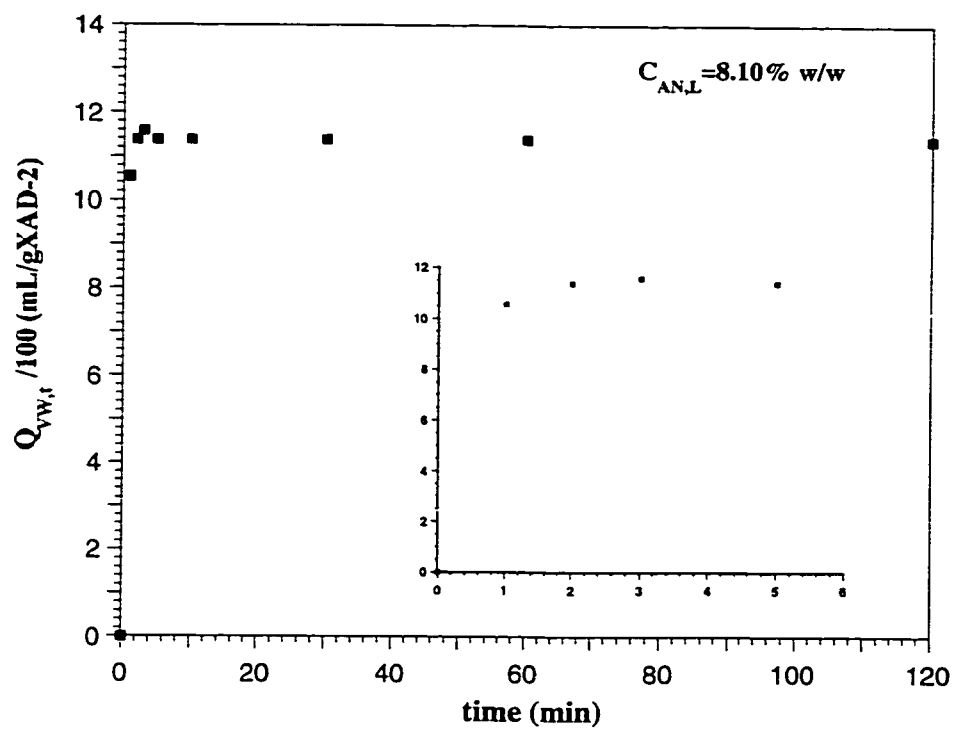


**Figure 4.16** Swelling rate of a particle of XAD-2 in 8.10% AN aqueous solution. Small figure shows early stages of the swelling rate. Data found in Appendix C, TABLE C.23.

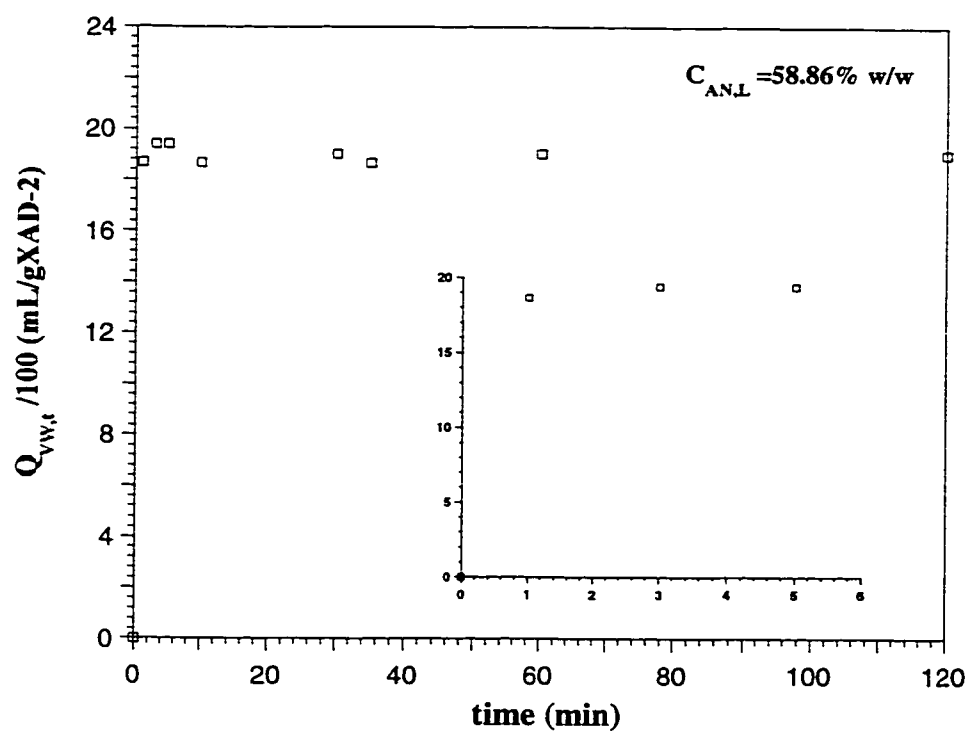


**Figure 4.17** Swelling rate of a particle of XAD-2 in 58.86% AN aqueous solution. Small figure shows early stages of the swelling rate. Data found in Appendix C, TABLE C.24.

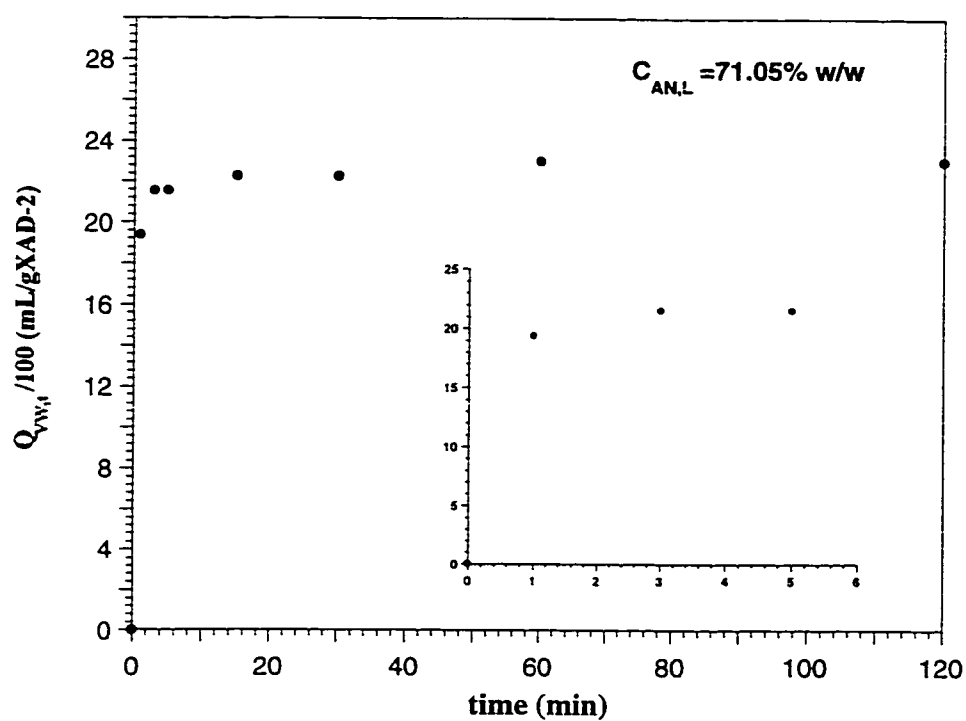


**Figure 4.18** Swelling rate of a particle of XAD-2 in 71.05% AN aqueous solution. Small figure shows early stages of the swelling rate. Data found in Appendix C, TABLE C.25.

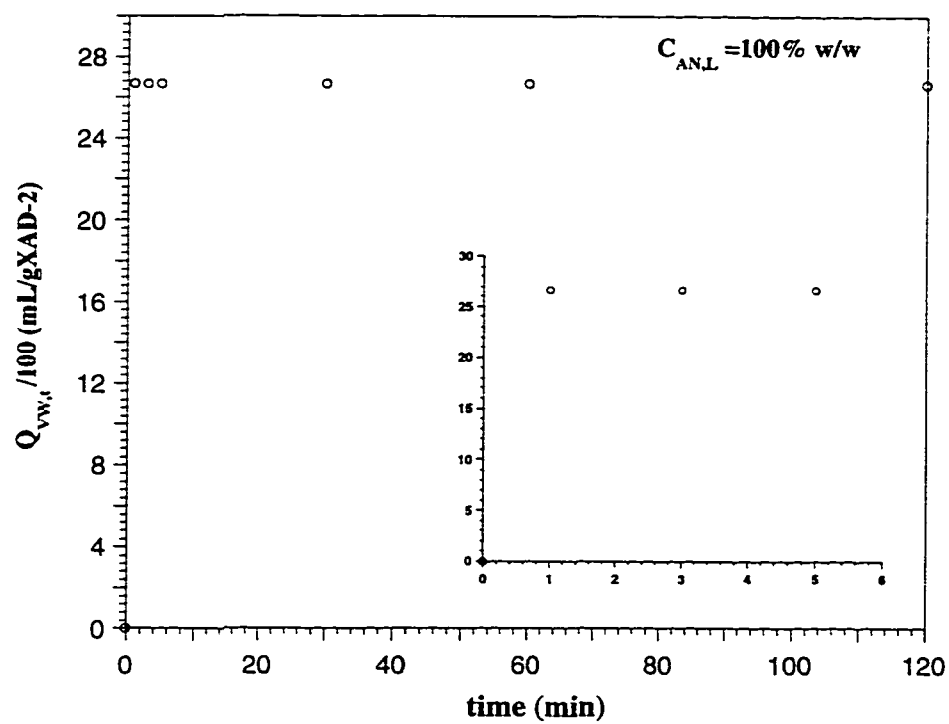


**Figure 4.19** Swelling rate of a particle of XAD-2 in 100% AN aqueous solution. Small figure shows early stages of the swelling rate. Data found in Appendix C, TABLE C.26.

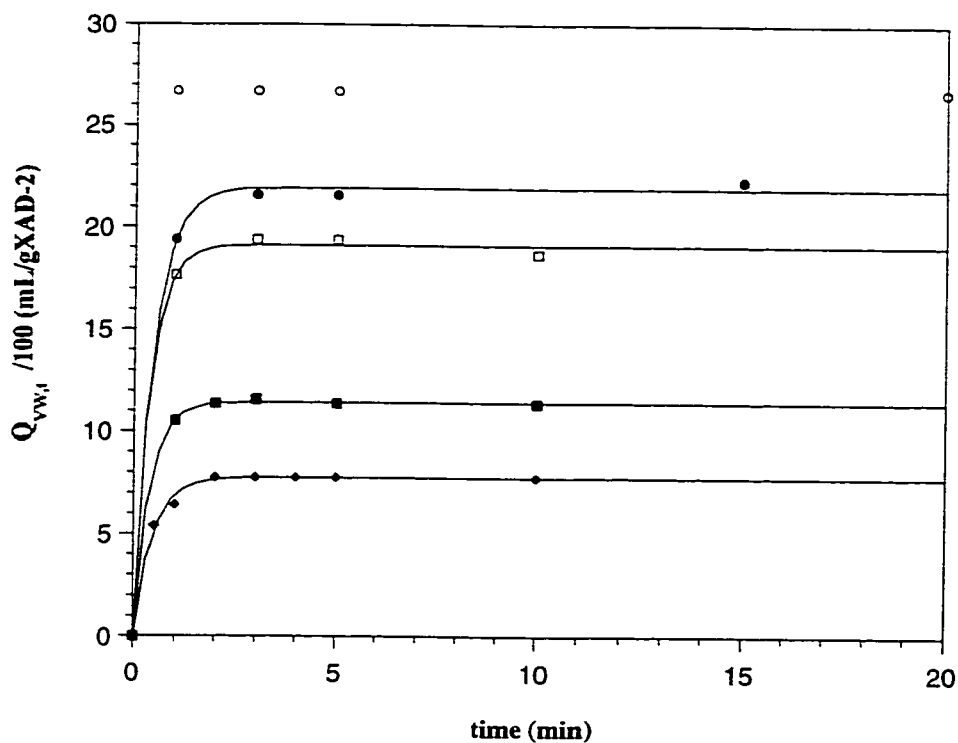


**Figure 4.20** Swelling rate of a particle of XAD-2 in different AN aqueous solutions. These plots are a compilation of the previous shown. Concentrations of AN are given in %w/w as follows: (♦) 4.06%, (■) 8.10%, (□) 58.86%, (●) 71.05%, and (○) 100%. Solid line represents the fitting to equation 4.16. Data found in appendix C, TABLES C.22 to C.26.

**TABLE 4.4** Curve fittings for the swelling kinetics of XAD-2 using AN as the organic modifier in the liquid phase. Experimental data fits the following equation:  $Q_{VW,t} = Q_{VW,\infty} [1 - e^{(-k.t)}]$ .

<b>C<sub>AN,L</sub></b> <b>(w/w)</b>	<b>Q<sub>VW,∞</sub>/100</b> <b>(mL/gXAD-2)</b>	<b>k</b> <b>(min<sup>-1</sup>)</b>	<b>R</b>
100	No fit	No fit	No fit
71.05	21.91 ± 0.18	2.15 ± 0.15	0.9994
58.86	19.11 ± 0.15	2.58 ± 0.23	0.9994
8.10	11.44 ± 0.04	2.56 ± 0.10	0.9998
4.06	7.77 ± 0.09	2.14 ± 0.14	0.9973



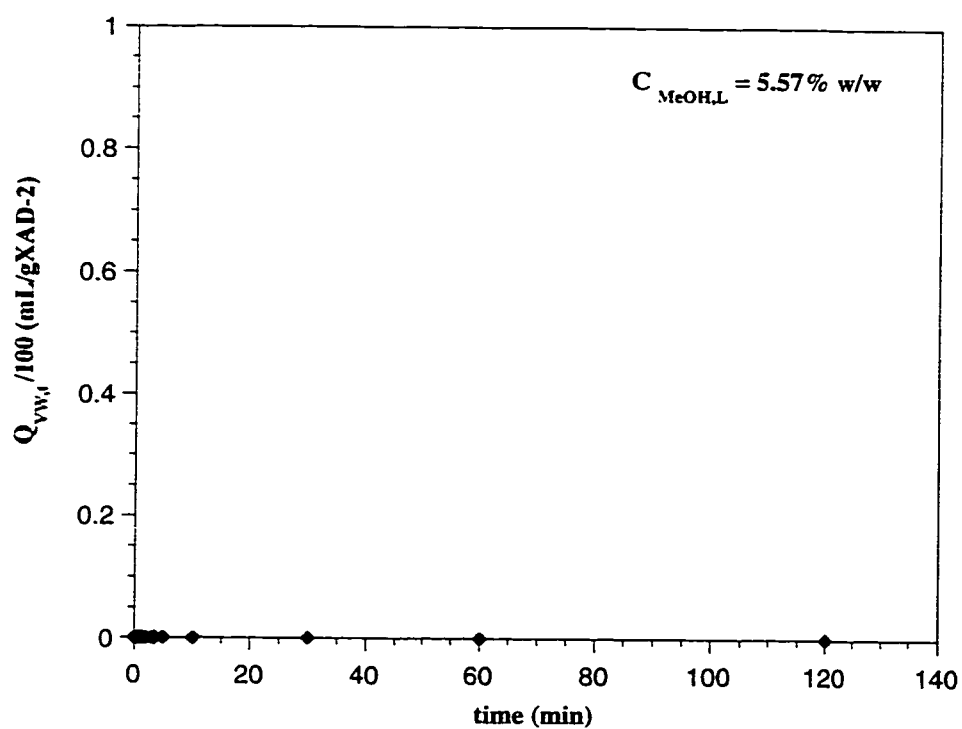


**Figure 4.21** Swelling rate of a particle of XAD-2 in 5.57% MeOH aqueous solution. Data found in Appendix C, TABLE C.27.

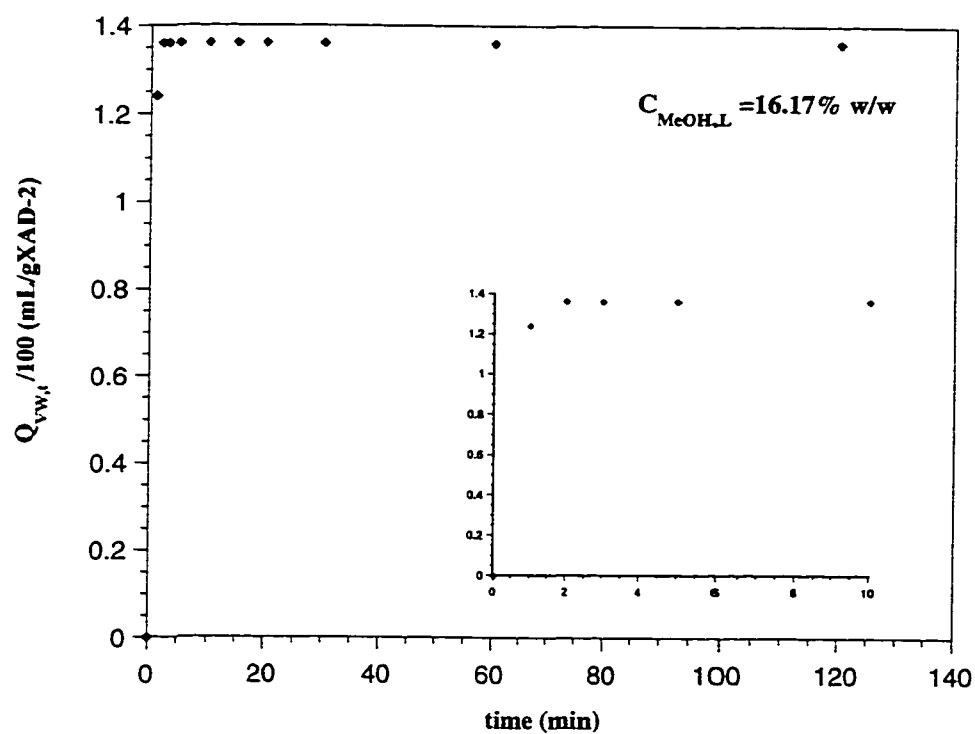


**Figure 4.22** Swelling rate of a particle of XAD-2 in 16.17% MeOH aqueous solution. Small figure shows early stages of the swelling rate. Data found in Appendix C, TABLE C.28.

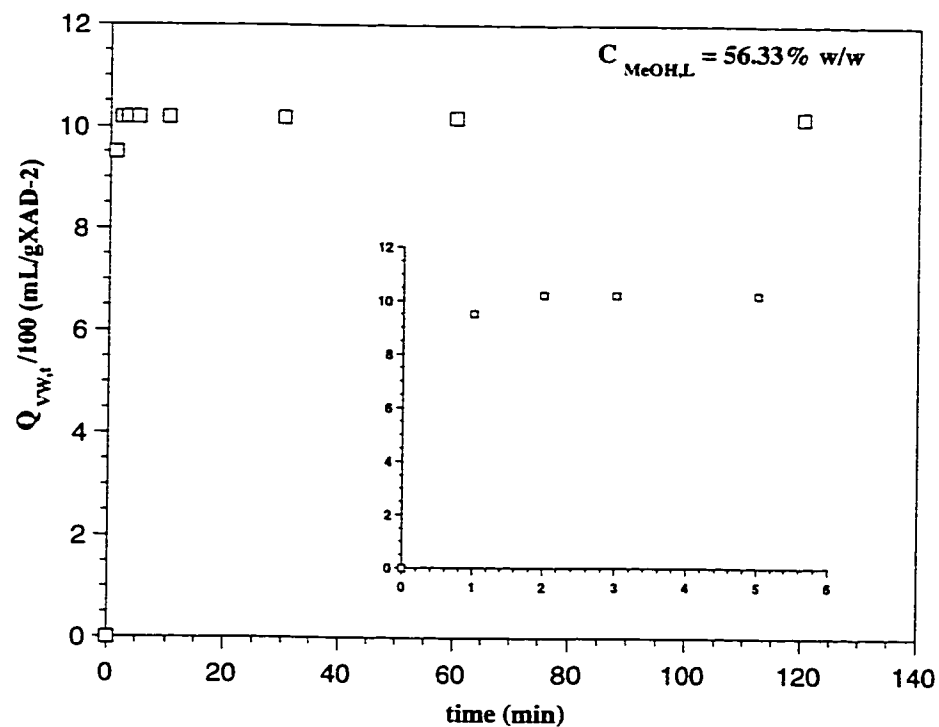


**Figure 4.23** Swelling rate of a particle of XAD-2 in 56.33% MeOH aqueous solution. Small figure shows early stages of the swelling rate. Data found in Appendix C, TABLE C.29.

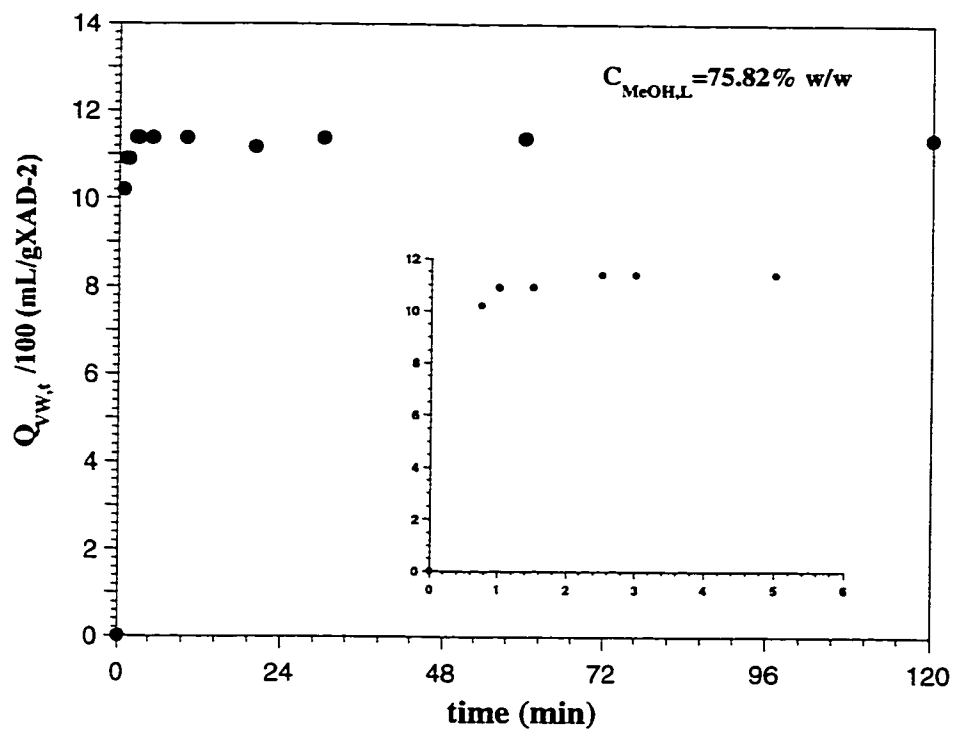


**Figure 4.24** Swelling rate of a particle of XAD-2 in 75.82% MeOH aqueous solution. Small figure shows early stages of the swelling rate. Data found in Appendix C, TABLE C.30.

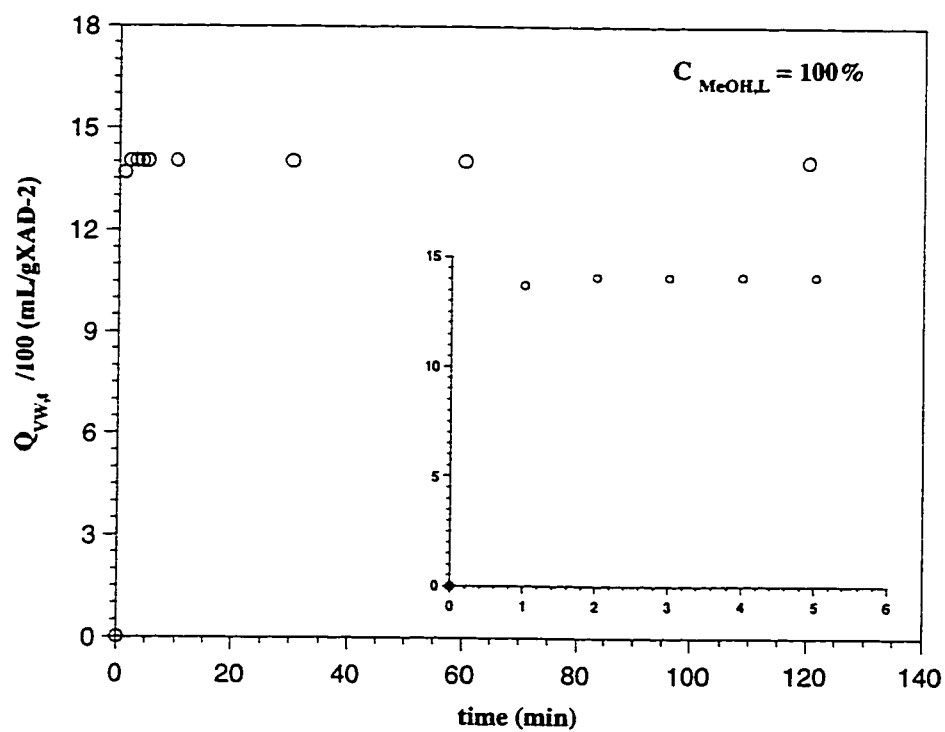


**Figure 4.25** Swelling rate of a particle of XAD-2 in 100% MeOH aqueous solution. Small figure shows early stages of the swelling rate. Data found in Appendix C, TABLE C.31.

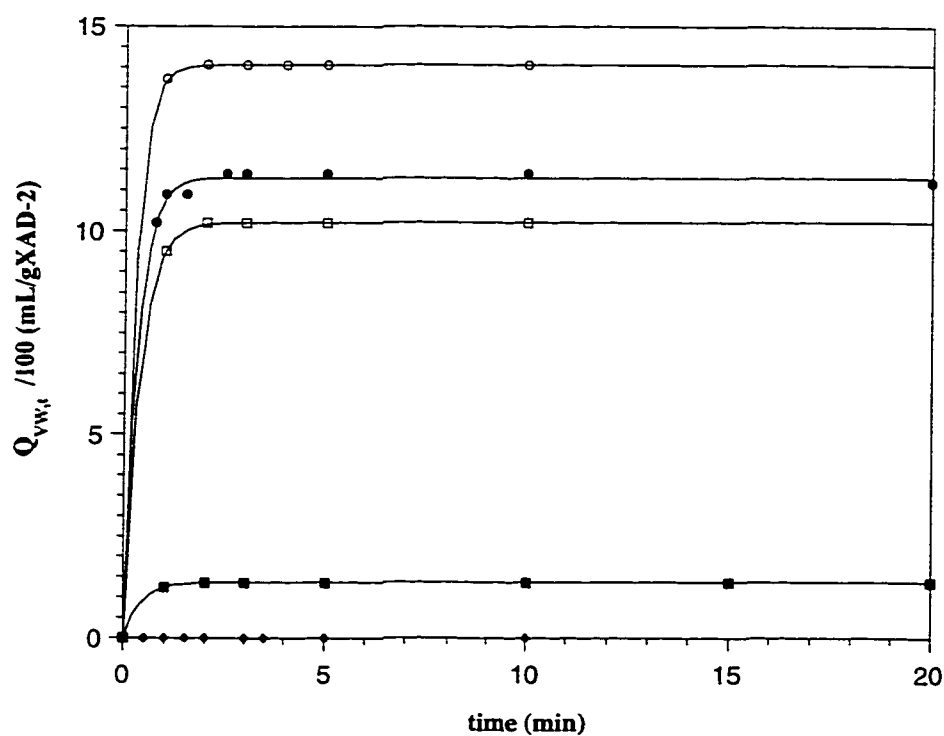


**Figure 4.26** Swelling rate of a particle of XAD-2 in different MeOH aqueous solutions. These plots are a compilation of the previous shown. Concentrations of AN are given in % w/w as follows: (♦) 5.57%, (■) 16.17%, (□) 56.33%, (●) 75.82%, and (○) 100%. Solid line represents the fitting to equation 4.16. Data found in appendix C, TABLES C.27 to C.31.

**TABLE 4.5** Curve fittings for the swelling kinetics of XAD-2 using MeOH as the organic modifier in the liquid phase. Experimental data fits the following equation:  $Q_{VW,t} = Q_{VW,\infty} [1 - \exp(-kt)]$ .

<b>C<sub>MeOH,L</sub></b> <b>(w/w)</b>	<b>Q<sub>VW,∞</sub>/100</b> <b>(mL/gXAD-2)</b>	<b>k</b> <b>(min<sup>-1</sup>)</b>	<b>R</b>
100	14.142 ± 0.001	3.68 ± 0.01	1.0000
75.82	11.30 ± 0.06	3.11 ± 0.17	0.9994
56.33	10.206 ± 0.009	2.68 ± 0.03	1.0000
16.17	1.362 ± 0.001	2.43 ± 0.04	1.0000
5.57	No fit	No fit	No fit

three aqueous-solvent solutions, b) 90% of the way to equilibrium is reached in  $\approx 2$  min, and c) the equilibrium value is reached in less than 5 min.

These rate curves were fit using the equation proposed by others [152, 201] and described in section 4.2.2.2 (equation 4.8).

$$Q_{vw,t} = Q_{vw,\infty} [1 - \exp(-k.t)] \quad (4.16)$$

The rate constant of swelling,  $k$ , has approximately the same value regardless of the organic modifier used (TABLES 4.3, 4.4, and 4.5). This feature suggests that the rate of swelling does not depend on the nature of the OM employed, whereas the extent of swelling does depend on both the nature of the OM and its concentration, as can be observed in the behavior of the XAD-2 under the effect of the three OMs at the same concentration (Figure 4.27).

Similar results have been previously observed in the swelling behavior of ion-exchange resins [140]. When the concentration of the organic modifier is increased, the surrounding liquid phase is more polymer compatible, which causes swelling to occur. This observation is evident for each series in Figures 4.14, 4.20 and 4.26.

Figure 4.27 compares the effect of different OMs at a given concentration in the liquid phase. Concentrations of 52.24% for THF, 58.86% for AN, and 56.33% for MeOH have been chosen. The fitting equations were given in TABLES 4.3, 4.4, and 4.5.



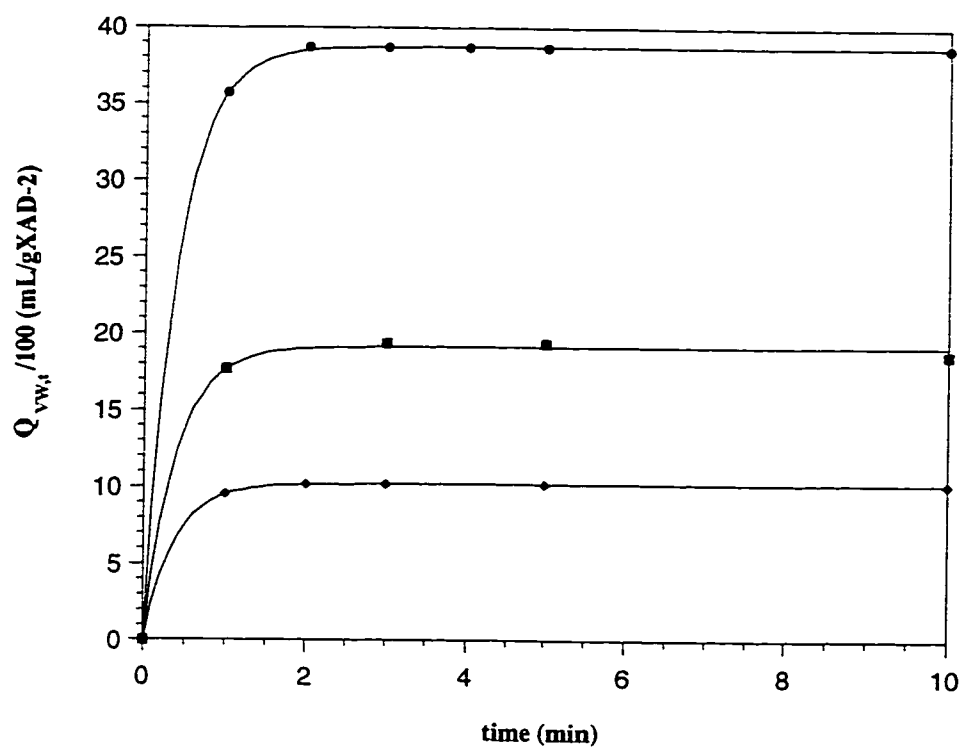


**Figure 4.27** Effect of the organic modifier on fractional swelling of XAD-2. Symbols represent experimental data taken for: (●) THF at 52.24%, (■) AN at 58.86%, and (○) MeOH at 56.33%. Solid lines represent fitting to equation 4.16. Data found in Appendix C, TABLE C.32.

The maximum fractional swelling found for these curves (38.73%, 19.11%, and 10.21% for THF, AN, and MeOH, respectively) agree with those found in the equilibrium swelling of XAD-2 in the OM studied and discussed in section 3.3.4. The  $k$  values for the three experiments are  $2.53 \pm 0.03$ ,  $2.58 \pm 0.23$ , and  $2.68 \pm 0.03 \text{ min}^{-1}$  for THF, AN, and MeOH, respectively. The rate constant has the same value regardless of the OM used. This feature could be discussed in terms of the XAD-2 structure.

The activities of the liquid phase used in the swelling kinetic studies calculated from equations 3.13, 3.14 and 3.15 are close to 0.3 for MeOH and 0.7 (region where capillary condensation starts in the sorption isotherms) for THF and AN. At these activities, each of the OM's penetrates all of the regions in the polymer matrix as seen in the sorption isotherms (Figure 3.12). Activities are high enough to cause the OM to be present throughout the whole bead and cause swelling (Figure 3.17) except in those regions where the cross-linking is very high, i.e. permanent micropores in the nuclei (Figures 3.3 and 3.4).

The XAD-2 polymer chains are capable of swelling under the effect of the different OM's without permanently changing their chain conformation. This was observed as the resin initial stage was consecutively reproduced in terms of particle diameter as the solvent was changed from poor to strong and vice versa. The low cross-linked region of the polymer is capable of swelling, by disentanglement of the polymer coils when exposed to a solvent, and then reversibly returning to the collapsed conformation as the solvent is removed [105, 148, 149]. These studies have shown that

the rate at which coil disentanglement occurs is independent of the solubility parameter of the solvent employed.

### 4.3.3 Rate of Sorption versus Rate of Swelling.

Figures 4.28, 4.29 and 4.30 show the comparative swelling and sorption (overall) rate curves for THF, AN, and MeOH, respectively. The concentrations in the liquid phase were chosen so that they are very close for both the swelling and the sorption experiments. TABLE 4.6 summarizes these concentrations for the two experiments using different OM.

Sorption data fits were shown in section 4.3.1. For swelling data, there were not enough points for AN, at early times, to fit an exponential equation. Instead, it was fit by two linear equations. The best fit to the MeOH swelling data was with a triexponential equation, having a regression coefficient of  $R=0.9800$ . The THF swelling data was fit with an exponential equation giving a regression coefficient of  $R = 0.9957$ . These equations were used empirically and no significance has been assigned to the constants. The equations for the swelling rate for the three OMs are:

For MeOH swelling rate:

$$Q_{vw,t} = 7.98 - 5.42 * \exp(-8.16t) - 1.99 * \exp(-0.1042t) - 0.58 * \exp(-0.0005t) \quad (4.17)$$

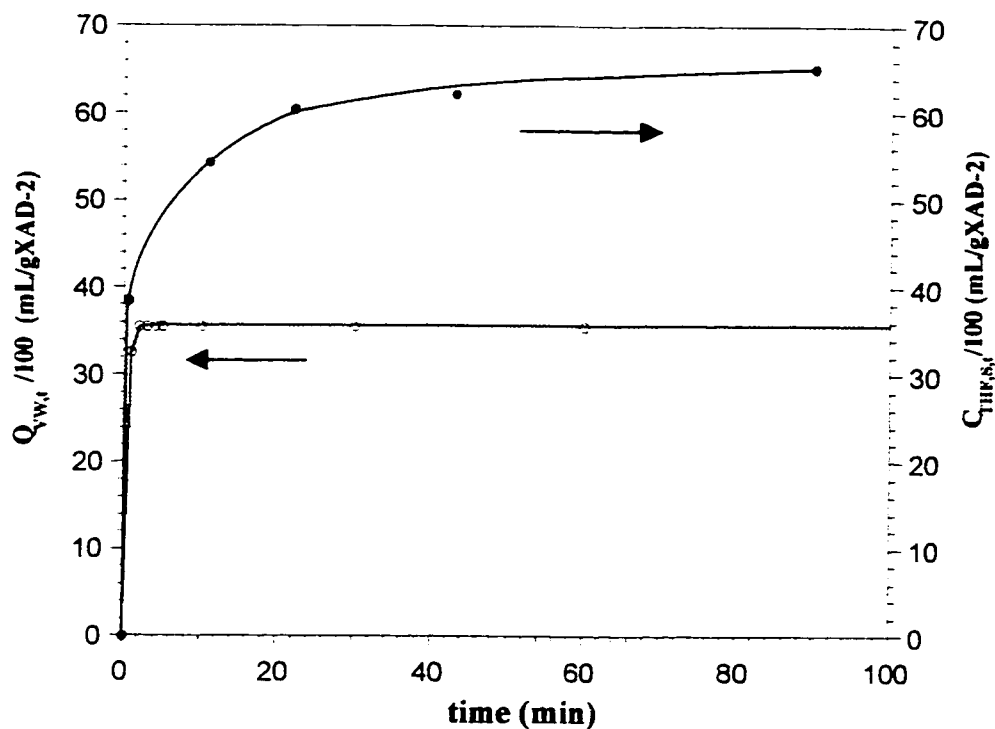


**Figure 4.28** Relative sorption rate of THF onto XAD-2 and the swelling rate of the polymer. Initial and final concentrations of the liquid phases are given in TABLE 4.7. Symbols represent experimental data. (○) Swelling data. (●) Sorption data. Data found in appendix C, TABLES C.33.

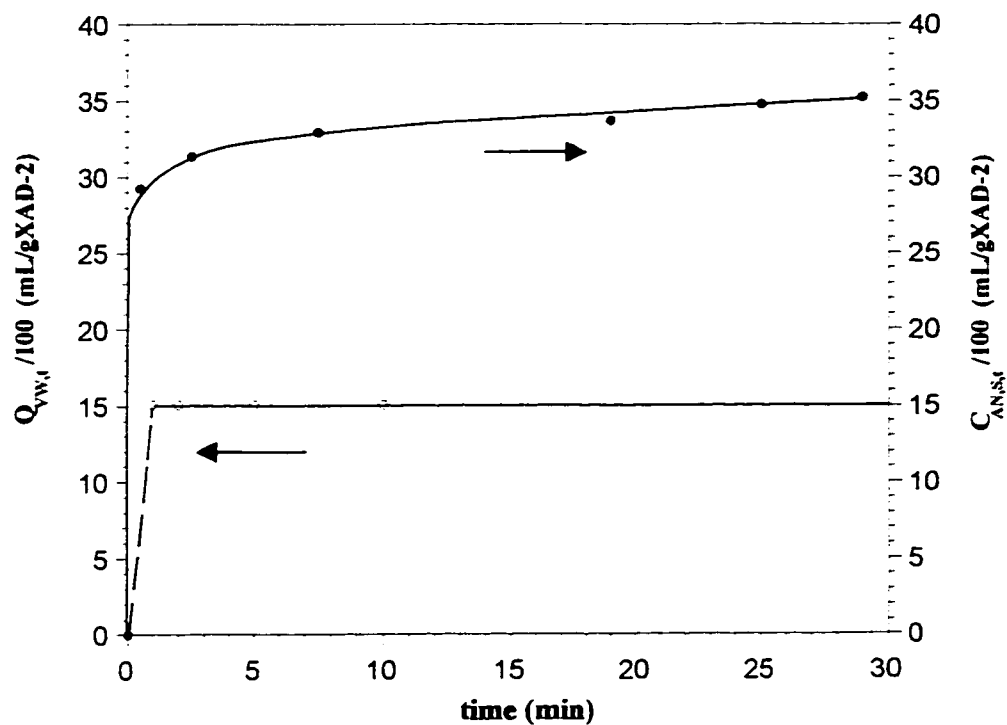


**Figure 4.29** Relative sorption rate of AN onto XAD-2 and the swelling rate of the polymer. Initial and final concentrations of the liquid phases are given in TABLE 4.6. Symbols represent experimental data. (○) Swelling data. (●) Sorption data. Data found in appendix C, TABLES C.34.

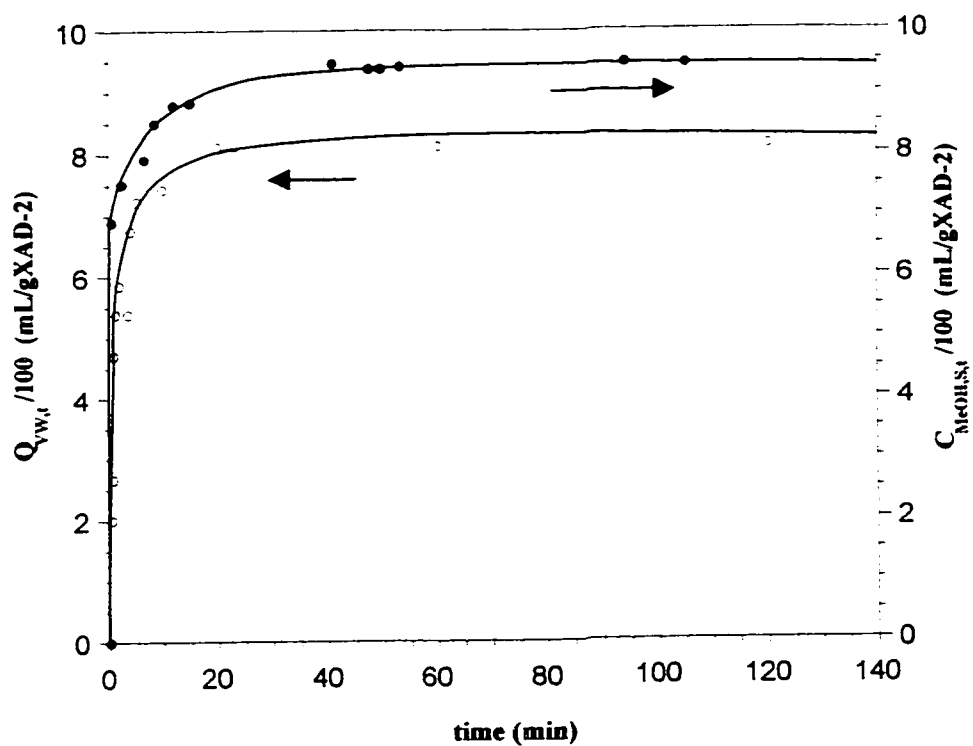


**Figure 4.30** Relative sorption rate of MeOH onto XAD-2 and the swelling rate of the polymer. Initial and final concentrations of the liquid phases are given in TABLE 4.6. Symbols represent experimental data. (○) Swelling data. (●) Sorption data. Data found in appendix C, TABLES C.35.

**TABLE 4.6** Initial and equilibrium concentrations of organic modifier in the supernatant solutions used in the experiments of sorption and swelling rate and  $C_{OM,L,\infty}$  and  $Q_{vw,\infty}$  for the curves presented in Figures 4.28, 4.29, and 4.30

	THF	AN	MeOH
$C_{OM,L,0}$ and $C_{OM,L,\infty}$ % w/w swelling	32.19	30.99	38.59
$C_{OM,L,0}$ % w/w sorption	35.83	35.46	34.07
$C_{OM,L,\infty}$ % w/w sorption	29.44	31.99	33.14
$C_{OM,S,\infty}$ (% gOM/gXAD-2)	62.35	27.09	7.98
$Q_{vw,\infty}$ (% mL/gXAD-2)	35.6	15.1	7.8

For AN swelling rate:

$$Q_{vw,t} = 15.099 * t \quad \text{for times between 0 and 1 minute.} \quad (4.18a)$$

$$Q_{vw,t} = 15.099 \quad \text{for times greater than 1 minute.} \quad (4.18b)$$

For THF swelling rate:

$$Q_{vw,t} = 35.675[1 - \exp(-2.467t)] \quad (4.19)$$

When the rate of sorption is slower than that of swelling the system is considered a normal Fickian diffusion process (Case I). It has been found that MeOH/PSDVB systems follow case I diffusion [190]. The sorption kinetic curves exhibit a slow approach to equilibrium that could be interpreted as sorption onto micropores in the nuclei, which do not swell considerably (highly cross-linked regions of the polymer).

Swelling equilibrium is reached sooner than sorption equilibrium, and the difference is more pronounced in the order THF>AN>MeOH. Also, as the solvent solubility parameter is closer to that of the PSDVB the swelling effect of the organic modifier is more noticeable [211] (larger extent of swelling, more difference between the equilibrium sorption and swelling values).



Initially, after diffusion into the macropores has occurred (a process that does not produce swelling and is very fast due to the size of the macropores), adsorption on the polymer surface and diffusion into the polymer matrix takes place. As the polymer chains become solvated, swelling starts in the latent porosity [107] or gel phase, where the cross-linking density is low. This expansion of the latent porosity takes only a few minutes. As the polymer chains swell, the solvent reaches permanent microporosity. Although diffusion and sorption continue in the micropores, no more swelling occurs in the permanent micropores in the highly cross-linked polymer network. This diffusion in the micropores is slow because it is hindered due to the small size of these micropores.

Overall, the slow swelling process is much faster than the slow sorption process regardless of the solvent employed. After swelling has reached its maximum value there is still a considerable sorption of the organic modifier taking place that lasts days before equilibrium sorption is reached. That effect is observed in the sorption rate curves, where equilibrium is approached very slowly. Once the micropores have been filled (very long times in the sorption rate curve), sorption equilibrium is reached and a plateau is observed.

Normalized composite plots of swelling rate versus sorption rate have been made and are shown in Figure 4.31. From the plot, it is observed that the maximum swelling is reached when sorption is still going on regardless the OM being considered. The maximum swelling is reached at approximately 60%, 85%, and 90% sorption, for THF, AN, and MeOH, respectively. These values are consistent with the discussion given above.

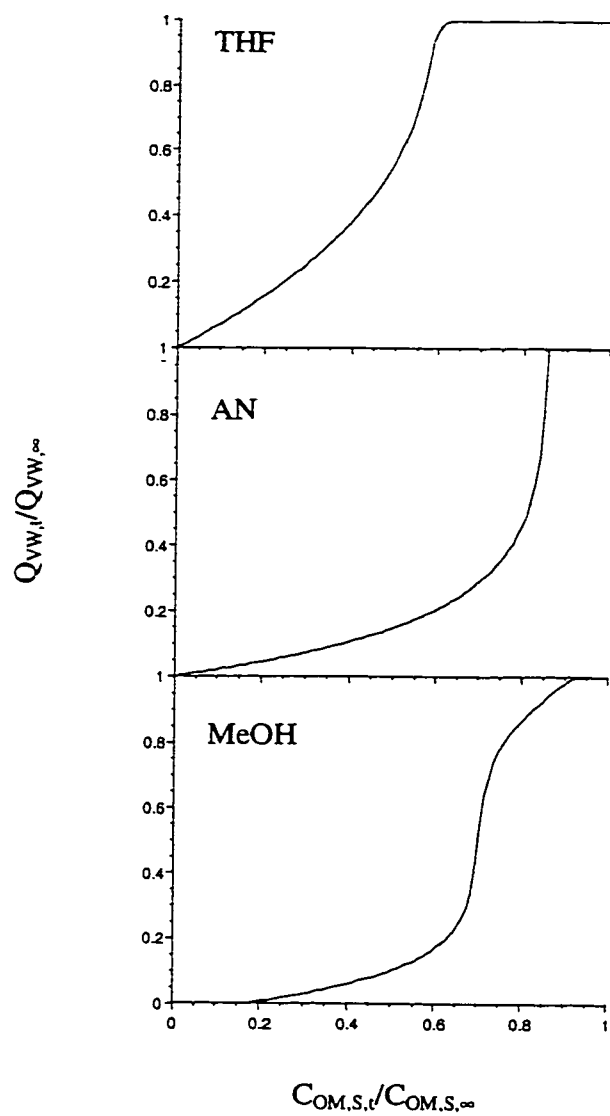


**Figure 4.31.** Normalized composite plots (swelling rate versus sorption rate) for the three OM's studied. Data has been calculated from fits to swelling and sorption rate curves. Curve fits to equations 4.14, 4.15, 4.16 for sorption and to 4.17, 4.18a, 4.18b, and 4.19 for swelling.

#### **4.3.4 Proposed Mechanism for Solvent Sorption and Swelling by XAD-2.**

Diffusion through the liquid in the macropores is quite fast because its viscosity is low and there are no restrictions [140]. Previous studies [22] showed that the measured diffusion coefficient in the large pores of Hamilton PRP-1, another macroporous PSDVB co-polymer, was close to the free-solution diffusion coefficient. Also, the process of adsorption onto the surface of the macropores is expected to be a very fast, non swelling process [22, 212] that does not contribute to the general sorption rate.

Once the molecules are adsorbed onto the macroporous surface, diffusion into the low cross-linked regions of the polymer occurs, producing swelling (opening of latent porosity). This step occurs during the early stages in which the particles are in contact with the solution. These processes (sorption + swelling) occur simultaneously [120] and are fast, even for a poor solvent such as MeOH.

After the resin has swollen to its maximum value (a process that takes only a few minutes), more sorption occurs in the more hindered [22, 106, 113, 213] regions in the polymer (i.e. microporous region, containing the permanent porosity). Sorption into micropores is a very slow process during which no more swelling can occur due to the rigidity of the matrix [214]. Hence the micropores are about the same size as OM molecules and they exist among highly cross-linked polymer chains which have very little flexibility thus sorption of OM onto micropores essentially blocks them from being accessed by other solute molecules.

## Chapter 5

### Conclusions and Future Work

#### 5.1 Conclusions and Significance for Chromatography.

The effect of organic modifiers on polystyrene divinylbenzene copolymers is shown to be related to the solvation of the polymer chains by the OM. The solvating power of the organic modifiers, reflected in their solubility parameters, decreases in the order: THF>AN>MeOH. This result is consistent with the Flory-Rehner model [218]. The swelling behavior of XAD-2 under the influence of these solvents allows for some conclusions. MeOH is a poor solvent for XAD-2, and swelling in this solvent is not enough to completely open up the collapsed porous structure of the gel regions in the polymer matrix. THF not only can access the low cross-linked region of the polymer matrix but also the rigid highly cross-linked region, composed of permanent micropores. AN, a medium strength solvent, can penetrate both regions to an extent intermediate between MeOH and THF.

The idea of a gradient of cross-linking of polystyrene divinylbenzene copolymers helps in explaining the behavior of similar stationary phases used in liquid chromatography. Studies on the porous structure of PSDVB co-polymers have proved the heterogeneous nature of the polymer based packings [99, 104, 107, 139, 142, 148, 149]. The selection of stationary and mobile phases can be made so that the mobile phase that

produces the most swelling is the one expected to have better performance in terms of peak shape and efficiency [215]. The associated improvement in peak shape has been related to the swelling of the low cross-linked gel structure, reducing hindrance there (increased pore diameter) and by filling up (blocking) of micropores (making them inaccessible to the sample [95, 107, 158]) and avoiding hindered diffusion of sample molecules there [72, 216]. Only small amounts of a good organic modifier [99-101] are required to fill the highly energetic sites in the micropores in the polystyrene matrix (slow mass transfer sites). Even if the polymer is not fully swollen, this process will occur. When the sample molecule to be sorbed diffuses into a polymer matrix that has been pretreated with a solution of organic modifier of low activity, the micropores fill with essentially pure solvent (activity close to unity) due to low interaction between the matrix and water.

Both swelling of the gel and blocking of micropores explain the improved efficiency [11, 99, 103, 107, 142, 159, 184, 215] and peak shape of the sample compounds observed by others and in this laboratory [158, 217] in liquid chromatography systems.

The kinetics of swelling of XAD-2 by sorption of THF, AN, and MeOH as organic modifiers in the liquid phase have been studied, and experimental data fit an empirical exponential equation [140, 152, 156, 201, 202]. For THF, the sorption rate constant is 3 times larger than that of swelling. This indicates that the relaxation or disentanglement of the polymer chains occurs after the fast sorption process. It is well known that several forces contribute to the swelling of a polymer network, i.e. polymer-

solvent interactions (depending on the polymer-solvent solubility parameter closeness) and the elastic deformation of the polymer chains (depending on the degree of cross-linking). When the gel is swelling it takes time for the network to swell, from the surface to the highly cross-linked core. Swelling starts after the polymer has been in interaction with the solvent, which induces a polymer density gradient and the appearance of stress [202]. For MeOH and AN, the rate of swelling is much faster than that of sorption (20-30 times), which is in accordance with a diffusion controlled process [190].

## 5.2 Recommended Future Work.

Amberlite XAD-2 does not show a large volume change during swelling, and certainly  $\Omega$  is smaller than 2.5 (the value below which a sigmoidal curve of fractional approach to equilibrium swelling versus  $\sqrt{t}$  is predicted). It would be interesting to develop experimentally a way to determine swelling at the very early stages, in the steep part of the swelling rate curve. This way, the construction of a plot of fractional approach to equilibrium swelling versus  $\sqrt{t}$  would be possible. This would give realistic evidence for Fickian behavior.

In order to get kinetic data at the early swelling stages, a video camera could be attached to the optical microscope and on line recording be achieved. The volume of the shallow bed cell used in the swelling rate experiments presented in this work would have to be reduced in order to get a smaller viewing area so that the particle under study is on screen at all times. After equilibrium is reached, the tape can be played by frames and

measurements of the diameter of the swollen particle in any direction can be done. By knowing the rate of tape recording, the time for swelling can be estimated.

Sorption in finite bath conditions has some drawbacks. Firstly, the sorbed amount of sample (solvent in this case), is calculated from a difference. It is clear that at early times when not much solvent has been sorbed, the uncertainty in the determination is big. Also, the experiment is not performed at constant concentration. This (could) have a retardation effect in the sorption rate curve. A more precise method for the sorption rate determinations in big spheres should be sought, such as column determinations.

PRP- $\infty$  is a non-porous PSDVB co-polymer. The matrix of this packing resembles that of the XAD-2. This material is commercially available in small particles. The kinetic effects of the solvents could also be studied in this packing. For example, determination of diffusion coefficients for the slow diffusion processes in the permanent microporosity. This will provide evidence for the diffusion of solutes and swelling characteristics of the permanent microstructure of this family of polymers.

## Bibliography

- (1) Meyer, V. R. *Practical high-performance liquid chromatography*, second ed.; John Wiley & Sons: New York, **1996**, pp 4-6
- (2) Horvath, C. *High performance liquid chromatography advances and perspectives*; Academic Press.: NY, **1980**, pp 50-63
- (3) Majors, R. E. *Journal of Chromatographic Science* **1980**, *18*, 488-511.
- (4) Ohkuma, T.; Hara, S. *Journal of Chromatography*. **1987**, *400*, 47-63.
- (5) Bien-Vogelsang, B.; Deege, A.; Figge, H.; Kohler, J.; Schombourg, G. *Journal of Chromatography* **1984**, *19*, 170.
- (6) Jedrzejewski, P. T.; Taylor, L. T. *Journal of Chromatographic Science* **1995**, *33*, 438-445.
- (7) Rigney, M. P.; Weber, T. P.; Carr, P. W. *Journal of Chromatography* **1989**, *484*, 273.
- (8) Meyer, V. R. *Practical high performance liquid chromatography*; John Wiley & Sons: NY, **1996**, pp 98
- (9) Pecsok, R. L.; Shields, L. D.; Cairns, T.; McWilliams, I. G. *Modern methods of chemical analysis*, second ed.; John Wiley and Sons: NY, **1976**, pp 42-44
- (10) Robinson, J. L.; Robinson, W. J.; Marshall, M. A.; Barnes, A. D.; Johnson, K. J.; Salas, D. S. . *Journal of Chromatography* **1980**, *189*, 145-167.
- (11) Tanaka, N.; Ebata, T.; Hashizume, K.; Hosoya, K.; Araki, M. . *Journal of Chromatography* **1989**, *475*, 195-209.
- (12) Sanders, L. C.; Wise, S. A. *CRC Critical Reviews in Analytical Chemistry*. **1987**, *18*, 299-415.
- (13) Snyder, L. R.; Kirkland, J. J. *Introduction to Modern Liquid Chromatography*, 2nd ed.; John Wiley & Sons, Inc.: Toronto, **1979**, pp Chapter 10
- (14) Pietrzyk, D. J. *Talanta* **1969**, *16*, 169-179.
- (15) Bauman, W. C.; Eichhorn, J. *JACS* **1947**, *69*, 2830-2836.
- (16) Higuchi, T.; Michaelis, A.; Tan, T.; Hurwitz, A. *Analytical Chemistry* **1967**, *8*, 974-979.



- (17) Hosoya, K.; Kimata, K.; Tanaka, N.; Araky, T.; Terashima, M.; Frechet, J. M. J. *Journal of Liquid Chromatography* **1993**, *16*, 3059-3071.
- (18) Meyer, V. R. *Practical high-performance liquid chromatography*, second ed.; John Wiley & Sons: NY, **1996**, pp 4-5
- (19) Meyer, V. R. *Practical high-performance liquid chromatography*, second ed.; John Wiley & Sons: NY, **1996**, pp 17
- (20) Horvath, C. *High performance liquid chromatography advances and perspectives*; Academic Press: NY, **1980**,
- (21) Snyder, L. R.; Kirkland, J. J. *Introduction to modern liquid chromatography*, second ed.; John Wiley & Sons: NY, **1979**, pp 23-25, Chapter 2.
- (22) Li, J.; Cantwell, F. F. *Journal of Chromatography* **1996**, *726*, 37-44.
- (23) Olive, J.; Grimalt, J. O. *Journal of Chromatographic science* **1995**, *33*, 194-204.
- (24) Meyer, V. R. *Practical high-performance liquid chromatography*, second ed.; John Wiley & Sons: NY, **1996**, pp 24-26, 39
- (25) Snyder, L. R.; Kirkland, J. J. *Introduction to modern liquid chromatography*, second ed.; John Wiley & Sons: NY, **1979**, pp 22-26
- (26) Giddings, J. C. *Dynamics of Chromatography. Part I, Principles and Theory*; Marcel Dekker: New York, **1965**, pp 52-58
- (27) Giddings, J. C. *Dynamics of Chromatography, Part I, Principles and Theory*; Marcel Dekker: New York, **1965**,
- (28) Horvath, C.; Lin, H.-J. . *Journal of Chromatography* **1978**, *149*, 43-70.
- (29) Snyder, L. R.; Kirkland, J. J. *Introducton to modern liquid chromatography*; John Wiley & Sons: Toronto, **1979**, pp 34, Chapter 7
- (30) Meyer, V. R. *Practical high performance liquid chromatography*, second ed.; John Wiley & Sons: NY, **1996**, pp 29-32
- (31) Meyer, V. R. *Practical high-performance liquid chromatography*, second ed.; John Wiley & Sons, **1996**, pp 19-22
- (32) Giddings, J. C. *Dynamics of Chromatography. Part I, Principles and Theory*; Marcel Dekker: NY, **1965**, pp 40-47
- (33) Giddings, J. C. *Dynamics of Chromatography. Part I, Principles and Theory*; Marcel Dekker: NY, **1965**, pp 36-39

- (34) Giddings, J. C. *Dynamics of chromatography. Part 1, Principles and theory*; Marcel Dekker: NY, **1965**,
- (35) Snyder, L. R.; Kirkland, J. J. *Introduction to modern liquid chromatography*, second ed.; John Wiley & Sons: NY, **1979**, pp 16-21
- (36) Hawkes, S. J. . *Journal of Chromatography* **1972**, 68, 1-8.
- (37) Giddings, J. C. *Dynamics of Chromatography. Part I, Principles and Theory*; Marcel Dekker: NY, **1965**, pp 35-36
- (38) Dubetz, T. Ph.D. Thesis, University of Alberta, Edmonton, **1988**.
- (39) Giddings, J. C. *Dynamics of Chromatography. Part I, Principles and Theory*; Marcel Dekker: NY, **1965**, pp 52-61
- (40) Snyder, L. R.; Kirkland, J. J. *Introduction to modern liquid chromatography*, second ed.; John Wiley & Sons: NY, **1979**, pp Chapter 5
- (41) Giddings, C. *Analytical Chemistry* **1963**, 35, 1999-2002.
- (42) Melin, A. T.; Ljungcrantz, M.; Schill, G. *Journal of Chromatography* **1979**, 185, 225-239.
- (43) Helfferich, F. *Ion Exchange*; McGraw-Hill: New York, **1995**,
- (44) Weber, W. I. , Schloss Elmau, Bavaria, Germany **1983**; *Engineering Foundation*; 679-692.
- (45) Frey, D. D.; Schweinheim, E.; Horvath, C. *Biotechnology Progress* **1993**, 9, 273-284.
- (46) Suzuki, M. *Adsorption Engineering*; Elsevier: New York, **1990**,
- (47) Ruthven, D. M. *Principles of Adsorption and Adsorption Processes*; Wiley: New York, **1984**,
- (48) Peel, R. G.; Benedek, A. *Environmental Science and Technology* **1980**, 14, 66-71.
- (49) Dorsey, J. G.; Dill, K. A. *Chemical Reviews*. **1989**, 89, 331.
- (50) Tanaka, N.; Kimata, K.; Hosoya, K.; Miyanishi, H.; Araki, T. *Journal of Chromatography* **1993**, 656, 265-287.
- (51) Tanaka, N.; Goodell, H.; Karger, B. L. . *Journal of Chromatography* **1978**, 158, 233.

- (52) Barton, A. F. M. *Handbook of Solubility Parameters and Other Cohesion Parameters*, 2nd ed.; CRC Press, **1991**,
- (53) Garden, J. Z. In *Encyclopedia of Polymer Science and Technology*, **1965**; Vol. 3, pp 833-862.
- (54) Krstulovic, A. M.; Brown, P. R. *Reversed-phase high performance liquid chromatography: theory, practice and biomedical applications*; Wiley: Toronto, **1982**,
- (55) Grieser, M.; Pietrzyk, D. J. *Analytical Chemistry* **1973**, *45*, 1348-1353.
- (56) Benson, J. R.; Woo, D. J. *Journal of Chromatographic Science* **1984**, *22*, 386-399.
- (57) Stevenson, R. *American Laboratory* **1998**, *30*, 16F-16BB.
- (58) Halasz, I.; Sebastian, I. *Chromatographia* **1974**, *7*, 371.
- (59) Dorsey, J. G.; Cooper, W. T. *Analytical Chemistry*. **1994**, *66*, 857A-866A.
- (60) Pietrzyk, D. J.; Kroeff, E. P.; Rotsch, T. D. *Analytical Chemistry*. **1978**, *50*, 497-502.
- (61) Kirkland, J. J.; Straten, M. A. V.; Claessens, H. A. . *Journal of Chromatography A* **1995**, *691*, 3-19.
- (62) Fairbank, R. W. P.; Xiang, Y.; Wirth, M. J. *Analytical Chemistry*. **1995**, *67*, 3879-3885.
- (63) LabAlliance ; [www.laballiance.com](http://www.laballiance.com): Lemont, PA, USA, **1998**.
- (64) Sokolowski, A.; Wahlund, K. G. . *Journal of Chromatography* **1980**, *189*, 299-316.
- (65) Reeuwijk, H. J. E. M.; Tjaden, U. R. . *Journal of Chromatography* **1986**, *353*, 339-350.
- (66) Sadek, P. C.; Carr, P. W. *Journal of Chromatographic Science*. **1983**, 314.
- (67) Grobe-Rhode, C.; Kicinski, H. G.; Kettrup, A. *Chromatographia* **1988**, *26*, 209-214.
- (68) Cole, L. A.; Dorsey, J. G. *Analytical Chemistry*. **1990**, 16.
- (69) IUPAC *Pure Applied Chemistry*. **1972**, *31*, 578.
- (70) Arshady, R. *Makromolecular Chemistry*. **1988**, *189*, 1295-1303.
- (71) Li-Ru, D. *Journal of Chromatography* **1979**, *186*, 317-338.

- (72) Lloyd, L. L. . *Journal of Chromatography* **1991**, 544, 201-217.
- (73) Mackey, D. J.; Higgins, H. W. *Journal of Chromatography* **1988**, 436, 243-257.
- (74) Alvoch-Orwa, J.; Quintens, I.; Roetz, E.; Hoogmartens, J. *European Journal of Pharmaceutical Sciences* **1995**, 3, 301-308.
- (75) Cantwell, F. F. *Analytical Chemistry*. **1976**, 48, 1854-1859.
- (76) Pankow, J. F.; Luo, W.; Isabelle, L. M.; Hart, K. M.; Hagen, D. F. *Journal of Chromatography A* **1996**, 732, 317-326.
- (77) Paesen, J.; Roets, E.; Hoogmartens, J. *Chromatographia* **1991**, 32, 162-166.
- (78) Liu, L.; Roetz, E.; Hoogmartens, J. *Journal of Chromatography A* **1997**, 764, 45-53.
- (79) Weiner, M. P.; Thannhauser, T. W.; Laity, J. H.; Benning, M. E.; Lee, D. P.; Scheraga, H. A. *Nucleic Acids Research* **1988**, 16, 8185.
- (80) Huber, C.; Oefner, P. J.; Bonn, G. K. *Analytical Biochemistry* **1993**, 212, 351-358.
- (81) Huber, C. G.; Oefner, P. J.; Bonn, G. K. *Chromatographia* **1993**, 37, 653-658.
- (82) Rozing, G. P.; Goetz, H. . *Journal of Chromatography* **1989**, 476, 3-19.
- (83) Albright, R. L. *Reactive Polymers* **1986**, 4, 155-174.
- (84) Lloyd, L. L.; Warner, F. P. . *Journal of Chromatography* **1990**, 512, 365-376.
- (85) Nash, D. C.; McCreath, G. E.; Chase, H. A. *Journal of Chromatography A* **1997**, 758, 53-64.
- (86) Tanaka, N.; Araki, M. *Polymer-based packing materials for reversed-phase liquid chromatography*; Marcel Dekker: New York, **1989**, pp 81-122
- (87) Reh, E.; Kapfer, U. *Chromatographia* **1990**, 30.
- (88) Tweeten, K. A.; Tweeten, T. N. . *Journal of Chromatography* **1986**, 359, 111-119.
- (89) Dawkins, J. V.; Lloyd, L. L.; Warner, F. P. . *Journal of Chromatography* **1986**, 352, 157-167.
- (90) Klampfl, C. W.; Spanos, E. . *Journal of Chromatography A* **1995**, 715, 213-218.
- (91) Ordemann, D. M.; Walton, H. F. *Analytical Chemistry*. **1976**, 48, 1728.
- (92) Lee, D. P.; Kindsvater, J. H. *Analytical Chemistry*. **1980**, 52, 2425-2428.

- (93) Pocurull, E.; Marce, R. M.; Borrull, F. . *Journal of Chromatography A* **1996**, 738, 1-9.
- (94) Smith, R. M. . *Journal of Chromatography* **1984**, 291, 372-376.
- (95) Lee, D. P. . *Journal of Chromatography* **1988**, 443, 143-153.
- (96) Yang, Y. B.; Verzele, M. *Journal of Chromatography* **1987**, 387, 197-205.
- (97) Janssen, H.; Shoenmakers, P. J.; Cramers, C. A. *Mikrochimica. Acta [Wien]* **1991**, II, 337-351.
- (98) Rudzinski, W. E.; Aminaphavi, T. M. *Journal of Macromolecular Science - Chemistry* **1983**, A19, 1247-1253.
- (99) Bowers, L. D.; Pedigo, S. . *Journal of Chromatography* **1986**, 371, 243-251.
- (100) Coppi, S.; Betti, A.; Bigli, C.; Cartoni, G. P.; Coccioli, F. . *Journal of Chromatography* **1988**, 442, 97-103.
- (101) Smith, R. M.; Garside, D. R. . *Journal of Chromatography* **1987**, 407, 19-35.
- (102) Cornel, P.; Sontheimer, H. *Chemical Engineering Science* **1986**, 41, 1791-1800.
- (103) Stuurman, H. W.; Kohler, J.; Jansson, S. O.; Litzen, A. *Chromatographia* **1987**, 23, 341-349.
- (104) Shea, K. J.; Stoddard, G. J. *Macromolecules* **1991**, 24.
- (105) O'Kane, J. M.; Sherrington, D. C. *Macromolecules* **1990**, 23, 5286-5291.
- (106) Li, J.; Litwinson, L. M.; Cantwell, F. F. *Journal of Chromatography* **1996**, 726, 25-36.
- (107) Nevejans, F.; Verzele, M. *Journal of Chromatography* **1987**, 406, 325-342.
- (108) Deng, L. R.; Hu, X.; Wu, Q.; Meng, Q.; Li, Y.; Zhang, Y. *Scientia Sinica (Series B)* **1982**, 25, 905.
- (109) Jerabek, K. *Analytical Chemistry* **1985**, 57, 1598-1602.
- (110) Heitz, W. In *Advances in Polymer Science Reactivities*; Springer-Verlag: New York, **1977**; Vol. 23, pp 1-23.
- (111) Pietrzyk, D. J.; Chu, C.-H. *Analytical Chemistry* **1977**, 49, 757-764.
- (112) Rohm and Haas Co., P., PA 19105 *Technical Bulletin* .
- (113) Gowanlock, D.; Bailey, R.; Cantwell, F. F. *Journal of Chromatography* **1996**, 726, 1-24.
- (114) Jandera, P.; Komers, D. *Journal of Chromatography A* **1997**, 762, 3-13.

- (115) Jandera, P.; Posvec, Z.; Vraspir, P. *Journal of Chromatography A* **1996**, 734, 125.
- (116) Wilks, A. D.; Pietrzyk, D. J. *Analytical Chemistry* **1972**, 44, 676-681.
- (117) Conder, J.; Young, C. L. *Physicochemical measurements by gas chromatography*; John Wiley and sons.: Toronto, **1979**,
- (118) Miller, J. M. *Separation methods in chemical analysis*; Interscience: N.Y., **1975**,
- (119) May, S.; Hux, R. A.; Cantwell, F. F. *Analytical Chemistry* **1982**, 54, 1279-1282.
- (120) Cornel, P.; Sontheimer, H.; Summers, R. S.; Roberts, P. V. *Chemical Engineering Science* **1986**, 41, 1801-1810.
- (121) Lundgren, J. L.; Schilt, A. A. *Analytical Chemistry* **1977**, 49, 974-980.
- (122) Sarzanini, C.; Porta, V.; Mentasti, E. *New Journal of Chemistry* **1989**, 13, 463-471.
- (123) Simpson, E. J.; Abukhadra, R. K.; Koros, W. J.; Schechter, R. S. *Industrial Engineering and Chemical Research* **1993**, 32, 2269-2276.
- (124) Colton, C. K.; Satterfield, C. N.; Lai, C.-J. *AJChE Journal* **1975**, 21, 289-298.
- (125) Edeskuty, F. J.; Amundson, N. R. *Industrial and Engineering Chemistry* **1952**, 44, 1698-1703.
- (126) Lowell, S.; Shields, J. E. *Powder surface and porosity*, third ed.; Chapman & Hall: NY, **1991**,
- (127) Snyder, L. R. *Principles of Adsorption Chromatography*; Marcel Dekker: New York, **1968**,
- (128) Kipling, J. J. *Adsorption from Solutions of Non-Electrolytes*; Academic Press: New York, **1965**,
- (129) Shaw, D. J. *Introduction to colloid and surface chemistry*, fourth ed.; Butterworth Heinemann: Oxford, **1994**,
- (130) Shaw, D. J. *Introduction to colloid and surface chemistry*, fourth ed.; Butterworth Heinemann: Great Britain, **1992**,
- (131) Fornstedt, T.; Zhong, G.; Bensetiti, Z.; Guichon, G. *Analytical Chemistry* **1996**, 68, 2370-2378.
- (132) Quinones, I.; Guiochon, G. *Journal of Colloids and Interface science* **1996**, 183, 57-67.

- (133) Jandera, P.; Guichon, G. *Journal of Chromatography* **1992**, *605*, 1-17.
- (134) Giona, M.; Giustiniani, M. *Industrial Engineering and Chemical Research* **1995**, *34*, 3848-3855.
- (135) Graham, D. *Journal of Physical Chemistry* **1953**, *57*, 665.
- (136) Gustafson, R. L.; Albright, R. L.; Heisler, J.; Lirio, J. A.; O. T. Reid, J. *I & EC product research and development* **1968**, *7*, 107-115.
- (137) Esposito, F.; Nobile, M. A. D.; Monsitieri, G.; Astarita, G. . *Industrial Engineering and Chemical Research* **1996**, *35*, 2939-2945.
- (138) Vliet, B. M. v.; J.r, W. J. W.; Hozumi, H. *Water Research* **1980**, *14*, 1719-1728.
- (139) Ohino, K.; Sato, H. *Journal of Applied Polymer Science* **1995**, *58*, 1015-1020.
- (140) Ikkai, F.; Shibayama, M. *Journal of Polymer Science. Part B.* **1996**, *34*, 1637-1645.
- (141) Sederel, W. L.; DeJong, G. J. *Journal of Applied Polymer Science* **1973**, *17*, 2835-2846.
- (142) Nevejans, F.; Verzele, M. *Chromatographia* **1985**, *20*, 173-178.
- (143) Parrish, J. R. *Journal of Applied Chemistry* **1965**, *15*, 280-288.
- (144) Gregor, H. P.; Held, K. M.; Bellin, J. *Analytical Chemistry* **1951**, *23*, 620-622.
- (145) Pepper, K. W.; Reichenberg, D.; Hale, D. K. *Journal of American Chemical Society* **1952**, 3129-3136.
- (146) Errede, L. A.; Newmark, R. A.; Hill, J. R. *Macromolecules* **1986**, *19*, 651-654.
- (147) Errede, L. A.; Stoesz, J. D.; Sirvio, L. M. *Journal of Applied Polymer Science.* **1986**, *31*, 2721-2737.
- (148) Errede, L. A. *Journal of Applied Polymer Science.* **1986**, *31*, 1749-1761.
- (149) Errede, L. A. *Journal of Physical Chemistry* **1989**, *93*, 2668-2671.
- (150) Bell, C. L.; Peppas, N. A. *Polymer Engineering and Science* **1996**, *36*, 1856-1861.
- (151) Kim, J.; Suh, K. *Polymer Bulletin* **1996**, *36*, 737-744.
- (152) Rathna, G. V. N.; Rao, D. V. M.; Chatterji, P. R. *J. M. S. - Pure Applied Chemistry* **1996**, *A33*, 1199-1207.
- (153) Bajpai, A. K. *Revue Roumaine de Chimie* **1996**, *41*, 219-222.

- (154) Bell, C. L.; Peppas, N. A. *International Journal of Pharmaceutics*. **1996**, *134*, 167-172.
- (155) Turpin, M.; Rand, B.; Ellis, B. *Fuel* **1996**, *75*, 107-113.
- (156) Wironen, J.; Shen, C.; Yan, J.; Batich, C. *Journal of Applied Polymer Science* **1996**, *59*, 825-830.
- (157) English, A. E.; Mafe, S.; Manzanares, J. A.; Yu, X.; Grosberg, A. Y. *Journal of Chemical Physics*. **1996**, *104*, 8713-8718.
- (158) Ells, B.; Wang, Y.; Cantwell, F. F. *Journal of Chromatography* **1999**, *in press*.
- (159) Nevejans, F.; Verzele, M. *Journal of Chromatography* **1985**, *350*, 145-150.
- (160) Bosch, E.; Bou, P.; Allemann, H.; Roses, M. *Analytical Chemistry* **1996**, *68*, 3651-3657.
- (161) Katz, E. D.; Ogan, K.; Scott, R. P. W. *Journal of Chromatography* **1986**, *352*, 67-90.
- (162) Katz, E. D.; Lochmuller, C. H.; Scott, R. P. W. *Analytical Chemistry*. **1989**, *61*, 349-355.
- (163) Levine, I. N. *Physical Chemistry*, third ed.; Mc Graw Hill, **1988**,
- (164) Castellan, G. W. *Physical Chemistry*; Addison-Wesley Publishing Company, Inc., **1983**,
- (165) Alberty, R. A.; Daniels, F. *Physical Chemistry*, fifth ed.; Wiley, **1980**,
- (166) Gmehling, J.; Onken, U. In *Chemistry data series*; Dechema, **1981**; Vol. 1.
- (167) Signer, R.; Arm, H.; Daeniker, H. *Helvetica Chimica Acta* **1969**, *52*, 2347.
- (168) Renon, H.; Prausnitz, J. M. *AIChE J* **1968**, *14*, 135-143/.
- (169) Wilson, S. R.; Patel, R. B.; Abbott, M. M.; Ness, H. C. V. *Journal of Chemical Engineering Data* **1979**, *24*, 130.
- (170) Gmehling, J.; Onken, U.; Arlt, W. In *Chemistry data series*; Dechema, **1981**; Vol. 1.
- (171) Keatch, C. J.; Dollimore, D. *An introduction to thermogravimetry*; Heyden: Great Britain, **1975**,
- (172) Wang, Q. C.; Svec, F.; Frechet, J. M. J. *Journal of Chromatography A* **1994**, *669*, 230-235.



- (173) Stamatialis, D. F.; Wessling, W.; Sanopoulou, M.; Strathmann, H.; Petropoulos, J. H. *Journal of Membrane Science* **1997**, *130*, 75-83.
- (174) Bolton, B. A.; Kint, S.; Bailey, G. F.; Scherer, J. R. *Journal of Physical Chemistry*. **1986**, *90*, 1207-1211.
- (175) Weast, R. C. *Handbook of chemistry and physics*, 53rd ed.; CRC Press, **1972-1973**,
- (176) Jansson, S. O.; Andersson, I.; Person, B. A. *Journal of Chromatography* **1981**, *203*, 93-105.
- (177) Riddick, J. A.; Bunger, N. B. *Organic Solvents Physical Properties and Methods of Purification*.; Wiley-Interscience: New York, **1970**,
- (178) Jeffery, G. H. *Journal of the Chemical Society* **1948**, 674.
- (179) Timmermans, J. *Physico-chemical constants of pure organic compounds*; Elsevier Publishing Co. Inc., **1950**,
- (180) Sherrington, D. C.; Hodge, P.; Eds, P. J. *Solubility parameters: functional polymers*; John Wiley & sons: Chichester, **1988**, pp Chapter 11, 387
- (181) Brandrup, J.; Immergut, E. H. *Polymer Handbook*, second ed.; John Wiley & sons: NY, **1975**,
- (182) Frahn, S.; Borchard, W. *Makromolecules Rapid Communications* **1996**, *17*, 455-459.
- (183) Poinescu, I. C.; Beldie, C.; Vlad, C. *Journal of Applied Polymer Science* **1984**, *29*, 23-34.
- (184) Poole, S. K.; Poole, C. F. *Analyst* **1995**, *120*, 1733-1738.
- (185) Helfferich, F. In *Ion Exchange*, **1966**, pp 65-100.
- (186) Horvath, C.; Lin, H. J. *Journal of Chromatography* **1976**, *126*, 401.
- (187) Lydersen, A. L. *Mass Transfer in Engineering Practice*; John Wiley and Sons: Norwich, **1983**, pp Chapter 1
- (188) Lenhoff, A. M. *Journal of Chromatography*. **1987**, *384*, 285-299.
- (189) Crank, J. *The Mathematics of Diffusion*, 2nd ed.; Oxford University Press: London, **1975**,
- (190) Alfrey, T.; Gurnee, E. F.; Lloyd, W. G. *Journal of Polymer Science*. **1966**, *C12*, 249.

- (191) Astarita, G.; Sarti, G. C. *Polymer Engineering and Science* **1978**, *18*, 388-395.
- (192) Kuipers, N. J. M.; Beenackers, A. A. C. *Polymer Engineering and Science* **1996**, *36*, 2108-2118.
- (193) Cussler, E. L. *Diffusion: Mass Transfer in Fluid Systems*, 1 ed.; Cambridge University Press: Cambridge, **1984**,
- (194) Cussler, E. L. *Multicomponent Diffusion*; Elsevier Scientific Publishing Co.: Amsterdam, **1976**,
- (195) Crank, J.; Park, G. S. *Transactions of the Faraday Society*. **1949**, *45*, 240.
- (196) Mandelkern, L.; Long, F. A. *Journal of Polymer Science*. **1951**, *6*, 457.
- (197) Singh, J.; Weber, M. E. *Chemical Engineering Science* **1996**, *51*, 4499-4508.
- (198) Thomas, N. L.; Windle, A. H. *Polymer* **1982**, *23*, 529-542.
- (199) Hui, C. Y.; Wu, K. C. *Journal of Applied Physics* **1987**, *61*, 5129-5136.
- (200) Hui, C. Y.; Wu, K. C. *Journal of Applied Physics* **1987**, *61*, 5137-5149.
- (201) Sedev, R. V.; Ptrov, J. G.; Newmann, A. W. *Journal of Colloid and Interface Science* **1996**, *180*, 36-42.
- (202) Budtova, T. S., Ibragim. *Polymer* **1997**, *38*, 5947-5960.
- (203) Errede, L. A.; Bogart, J. W. C. V. *Journal of Polymer Science: Part A: Polymer Chemistry* **1989**, *27*, 2015-2049.
- (204) Bell, C. L.; Peppas, N. A. *Polymer Engineering and Science* **1996**, *36*, 1856-1861.
- (205) Chen, C. J.; Parcher, J. F. *Analytical Chemistry* **1971**, *43*, 1738-1744.
- (206) Marshall, D. B.; Burns, J. W.; Connolly, D. E. *Journal of Chromatography* **1986**, *360*, 13-24.
- (207) Waite, S. W.; Marshall, D. B.; Harris, J. M. *Analytical Chemistry* **1994**, *66*, 2052.
- (208) Costa, C.; Rodriguez, A. *Engineering Foundations* **1983**, 163.
- (209) Jun, Y.; Rongnan, X.; Juntan, Y. *Journal of Applied Polymer Science* **1989**, *38*, 45-54.
- (210) Ruckenstein, E.; Vaidyanathan, A. S.; Youngquist, G. R. *Chemical Engineering Science* **1971**, *26*, 1305-1318.
- (211) Mori, S. *Analytical Chemistry* **1978**, *50*, 745-748.

- (212) Smith, J. M. In *ACS Symposium Series*; W. J. Weber, J., Matijevic, E., Eds.; Amer. Chem. Soc., **1968**; Vol. 79, pp 8-22.
- (213) Dryden, C. E.; Kay, W. B. *Industrial and Engineering Chemistry* **1954**, 46, 2294-2300.
- (214) Kim, D.; Caruthers, J. M.; Peppas, N. A. *Macromolecules* **1993**, 26, 1841-1847.
- (215) Stwart, R.; Brouwer, S.; Kraak, J. C.; Poppe, H. . *Journal of Chromatography* **1996**, 732, 201-207.
- (216) Lloyd, L. L.; Kennedy, J. F. In *Process scale liquid chromatography*; Subramanian, G., Ed.; VCH Publishers: New York, **1995**, pp 99-130.
- (217) Ells, B. D. PhD Thesis., The University of Alberta, Edmonton, **1998**.
- (218) Flory, P. J., *Principles of Polymer Chemistry*, Cornell University Press, NY, **1953**, pp 576-581.

## Appendix A

### Procedure to Pack a Gas-Chromatography Column.

#### Materials:

1. Stainless Steel Tubing: 10'x0.0865"(internal diameter), 1/8" (external diameter).
2. Packing: Porapak QS, Gas Chromatography column packing material, batch #35, mesh 50-80, Chromatographic Specialties Inc.

#### Cleaning of the column:

A soft vacuum is applied to one end of the column while the other end is consecutively immersed into each of the following solutions.

- a. 250 mL Acetone.
- b. 250 mL concentrated  $\text{HNO}_3$ .
- c. 250 mL  $\text{H}_2\text{O}$ .
- d. 250 mL concentrated  $\text{NH}_4\text{OH}$ .
- e. 250 mL  $\text{H}_2\text{O}$ .
- f. 100 mL Acetone.

After finishing the cleaning procedure, the free end is covered with a filter and left under vacuum for 3 hours.

#### Filling the column:

One end of the SS tubing is stoppered using a small plug of silanized glass wool. After estimating the column volume and the mass of packing to be used, the column is filled

with a known amount of Porapak QS. Small amounts are added to the top. The column is tapped very gently, using a piece of rubber hose, to avoid breakage of the particles. When the column has been completely filled, another plug of glass wool is used to keep the particles from spilling. The column is then coiled to the desired diameter and fitted with the appropriated ferrules and ends. A tag is added for identification.

**Conditioning:**

Optimum results are obtained by conditioning the column using the following procedure:

- a. The column is connected to the injector at room temperature.
- b. A carrier gas flow is set at 30 mL/min for 15 min.
- c. The column is warmed up at 100°C for 30 min.
- d. Programmed temperature up to 230°C (20°C below the maximum allowed) at a rate of 4°C/min, and hold the column at this temperature for 4 hours or longer.
- e. Cool down and connect to the detector.

## Appendix B

### Calculation of Distribution Coefficients in the Batch Method.

Each distribution coefficient was determined by the batch equilibration technique. In these experiments, the goal is to determine the sorption isotherm of the organic modifier from aqueous solution on the stationary phase, Amberlite XAD-2. The distribution coefficient is for the distribution of organic modifier between the polymer matrix and the bulk solution. The bulk solution is present both outside the particles and inside the large (macro- and meso-) pores.

Known:

$W_{OM,i}$  = Initial mass of organic modifier

$W_{XAD-2}$  = Mass of dry resin

$W_{H_2O,i}$  = Initial mass of water

When equilibrium has been reached, the concentration of the supernatant liquid is obtained from a GC-calibration curve obtained using the internal standard method. The composition of liquid filling the large (macro- and meso-) pores is taken to be identical to the composition of the equilibrium bulk liquid outside the particles.

$C_{OM,L}$  = Concentration of organic modifier in the liquid after equilibrium has been reached, in g/g

$$C_{OM,L} = \frac{W_{OM,f}}{W_{H_2O,i} + W_{OM,f}} \quad (B.1)$$

$W_{OM,f}$  = Mass of organic modifier at equilibrium in the liquid

Assuming that the mass of water remains constant throughout the experiment:

$$W_{H_2O.f} = W_{H_2O.i} = W_{H_2O} \quad (B.2)$$

$W_{H_2O.f}$  = Mass of water in the liquid phase at equilibrium

Solving for  $W_{OM.f}$  from equation (B.1):

$$W_{OM.f} = \frac{W_{H_2O} \cdot C_{lp.f}}{1 - C_{lp.f}} \quad (B.3)$$

$C_{lp.f}$  = Concentration of liquid phase after equilibrium has been reached, in g/g.

The mass balance on the mass of organic modifier is given by:

$$W_{OM.i} = W_{OM.s} + W_{OM.f} \quad (B.4)$$

$W_{OM.s}$  = sorbed mass of organic modifier at equilibrium

solving for  $W_{OM.s}$  :

$$W_{OM.s} = W_{OM.i} - W_{OM.f} \quad (B.5)$$

and dividing by  $W_{XAD-2}$  :

$$C_{OM,S} = \frac{W_{OM,s}}{W_{XAD-2}} \quad (B.6)$$

$C_{OM,S}$  = Concentration of the sorbed organic modifier at equilibrium, in g/g.

The sorption isotherm can be obtained by plotting [(B.1),(B.6)] values.



## Appendix C

This appendix contains tabulated data for the plots shown in chapters 3 and 4.

**Table C.1: Data for Figure 3.5a.**

$x_{THF}$	$\gamma_{THF}$	$x_{AN}$	$\gamma_{AN}$	$x_{MeOH}$	$\gamma_{MeOH}$
0	20.19	0	15.79	0	1.878
0.01297	17.18	0.02256	12.55	0.02872	1.792
0.02699	14.62	0.04646	10.09	0.05875	1.711
0.04220	12.45	0.07182	8.210	0.09028	1.634
0.05875	10.60	0.09879	6.753	0.1232	1.561
0.07683	9.036	0.1275	5.613	0.1577	1.493
0.09665	7.704	0.1582	4.713	0.1941	1.430
0.1185	6.578	0.1910	3.996	0.2323	1.370
0.1427	5.625	0.2262	3.420	0.2725	1.315
0.1696	4.818	0.2640	2.952	0.3149	1.265
0.1998	4.134	0.3048	2.570	0.3597	1.218
0.2338	3.555	0.3489	2.254	0.4071	1.176
0.2725	3.064	0.3970	1.992	0.4573	1.139
0.3168	2.647	0.4488	1.772	0.5106	1.106
0.3681	2.290	0.5057	1.586	0.5673	1.077
0.4282	1.983	0.5681	1.429	0.6276	1.053
0.4997	1.717	0.6369	1.296	0.6920	1.033
0.5859	1.484	0.7130	1.184	0.7610	1.018
0.6920	1.277	0.7978	1.093	0.8349	1.008
0.8259	1.100	0.8928	1.028	0.9143	1.002
1	1	1	1	1	1

**Table C.2: Data for Figure 3.5b.**

$x_{THF}$	$a_{THF}$	$x_{AN}$	$a_{AN}$	$x_{MeOH}$	$a_{MeOH}$
0	0	0	0	0	0
0.01297	0.223	0.02257	0.2831	0.02872	0.0287
0.02699	0.395	0.04646	0.4689	0.05875	0.0588
0.04220	0.525	0.07182	0.5900	0.09020	0.0902
0.05875	0.623	0.09879	0.667	0.1232	0.123
0.07683	0.694	0.1275	0.716	0.1577	0.158
0.09665	0.745	0.1582	0.746	0.1941	0.194
0.1185	0.780	0.1910	0.763	0.2323	0.232
0.1427	0.803	0.2262	0.774	0.2725	0.272
0.1696	0.817	0.2640	0.779	0.3149	0.315
0.1998	0.826	0.3048	0.783	0.3597	0.360
0.2338	0.831	0.3489	0.787	0.4071	0.407
0.2725	0.835	0.3968	0.790	0.4573	0.457
0.3168	0.838	0.4488	0.795	0.5110	0.511
0.3681	0.843	0.5057	0.802	0.5673	0.567
0.4282	0.849	0.5681	0.812	0.6276	0.628
0.4997	0.858	0.6369	0.825	0.6920	0.692
0.5859	0.869	0.7130	0.844	0.7610	0.761
0.6920	0.884	0.7978	0.872	0.8349	0.835
0.8259	0.908	0.8928	0.918	0.9143	0.914
1	1	1	1	1	1

**Table C.3: Data for Figure 3.11.**

$C_{THF,L}$ (%w/w)	$C_{THF,S}$ (%g/g XAD)	$C_{AN,L}$ (%w/w)	$C_{AN,S}$ (%g/g XAD)	$C_{MeOH,L}$ (%w/w)	$C_{MeOH,S}$ (%g/g XAD)
0	0	0	0	0	0
0.547±0.005	6.8±2.0	0.947±0.005	4.4±1.5	4.22±0.02	1.4±0.3
0.551±0.006	6.9±1.6	1.58±0.04	10.5±0.9	6.23±0.04	2.3±0.2
0.599±0.005	7.2±1.0	1.89±0.03	11.3±0.8	10.32±0.05	3.8±0.2
0.831±0.004	8.9±1.0	3.41±0.05	14.0±0.6	11.22±0.08	4.1±0.4
0.846±0.005	9.7±0.9	5.78±0.07	15.9±0.5	13.77±0.09	4.9±0.3
0.984±0.002	10.8±0.9	10.24±0.08	18.4±0.5	14.33±0.05	5.1±0.3
0.996±0.005	10.9±0.8	16.3±0.1	19.5±0.4	18.2±0.5	5.6±0.3
1.03±0.03	11.0±0.8	18.54±0.09	21.2±0.4	21.2±0.2	6.4±0.4
1.04±0.03	11.0±0.8	23.9±0.5	23.1±0.4	28.5±0.5	7.3±0.5
1.77±0.04	14.3±0.7	27.35±0.09	25.7±0.3	31.7±0.5	7.8±0.4
1.79±0.04	15.2±0.7	31.0±0.5	26.0±0.3	42.2±0.5	8.4±0.5
1.83±0.04	15.5±0.7	32.1±0.5	26.7±0.3	62±2	9.0±0.8
1.89±0.04	16.0±0.7	38.0±0.6	29.5±0.3	84±2	9.0±0.8
2.74±0.04	17.8±0.6	40.1±0.3	29.9±0.2		
2.86±0.03	17.9±0.6	44.7±0.7	31.5±0.3		
2.91±0.03	18.0±0.6	52.1±0.9	33.6±0.2		
3.44±0.05	19.0±0.5				
3.49±0.02	19.0±0.5				
3.51±0.02	19.1±0.5				
3.52±0.02	19.9±0.5				
4.14±0.04	20.4±0.4				
4.14±0.02	20.8±0.4				
4.20±0.03	21.1±0.4				
4.98±0.05	22.2±0.3				
4.99±0.05	22.6±0.3				
5.33±0.05	24.0±0.3				
5.35±0.04	24.3±0.3				
5.82±0.02	25.5±0.3				
6.11±0.05	25.5±0.2				
11.62±0.08	37.5±0.2				
27.9±0.5	61.1±0.2				
31.7±0.5	69.9±0.3				
59.7±0.7	112.5±0.9				

**Table C.4: Data for Figure 3.12.**

Activity ( $a_{\text{THF},M}$ )	$C_{\text{THF},S}$ (% g/gXAD)	Activity ( $a_{\text{AN},M}$ )	$C_{\text{AN},S}$ (% g/gXAD)	Activity ( $a_{\text{MeOH},M}$ )	$C_{\text{MeOH},S}$ (% g/gXAD)
0	0	0	0	0	0
0.0272±0.0001	6.8±2.0	0.0630±0.0003	4.4±1.5	0.0436±0.0002	1.4±0.3
0.0274±0.0001	6.9±1.6	0.103±0.001	10.5±0.9	0.0638±0.0003	2.3±0.2
0.0298±0.0001	7.2±1.0	0.121±0.001	11.3±0.8	0.104±0.001	3.8±0.2
0.0410±0.0002	8.9±1.0	0.206±0.001	14.0±0.6	0.112±0.001	4.1±0.4
0.0418±0.0002	9.7±0.9	0.317±0.002	15.9±0.5	0.136±0.001	4.9±0.3
0.0484±0.0002	10.8±0.9	0.476±0.002	18.4±0.5	0.141±0.001	5.1±0.3
0.0490±0.0002	10.9±0.8	0.614±0.003	19.5±0.4	0.177±0.001	5.6±0.3
0.0506±0.0003	11.0±0.8	0.648±0.003	21.2±0.4	0.203±0.001	6.4±0.4
0.0509±0.0003	11.0±0.8	0.707±0.004	23.1±0.4	0.265±0.001	7.3±0.5
0.0855±0.0004	14.3±0.7	0.732±0.004	25.7±0.3	0.292±0.001	7.8±0.4
0.0862±0.0004	15.2±0.7	0.750±0.004	26.0±0.3	0.376±0.002	8.4±0.5
0.0884±0.0004	15.5±0.7	0.754±0.004	26.7±0.3	0.539±0.003	9.0±0.8
0.0907±0.0004	16.0±0.7	0.770±0.004	29.5±0.3	0.763±0.004	9.0±0.8
0.129±0.001	17.8±0.6	0.774±0.004	29.9±0.2		
0.134±0.001	17.9±0.6	0.779±0.004	31.5±0.3		
0.137±0.001	18.0±0.6	0.787±0.004	33.6±0.2		
0.159±0.001	19.0±0.5				
0.161±0.001	19.0±0.5				
0.162±0.001	19.1±0.5				
0.163±0.001	19.9±0.5				
0.188±0.001	20.4±0.4				
0.189±0.001	20.8±0.4				
0.191±0.001	21.1±0.4				
0.222±0.001	22.2±0.3				
0.223±0.001	22.6±0.3				
0.236±0.001	24.0±0.3				
0.237±0.001	24.3±0.3				
0.254±0.001	25.5±0.3				
0.265±0.001	25.5±0.2				
0.441±0.002	37.5±0.2				
0.725±0.004	61.1±0.2				
0.758±0.004	69.9±0.3				
0.835±0.004	112.5±0.9				

**Table C.5: Data for Figures 3.13, 3.14, and 3.15 (X versus Y1).**

Activity ( $a_{\text{THF},M}$ )	$C_{\text{THF},S}$ (% mL/gXAD)	Activity ( $a_{\text{AN},M}$ )	$C_{\text{AN},S}$ (% mL/gXAD)	Activity ( $a_{\text{MeOH},M}$ )	$C_{\text{MeOH},S}$ (% mL/gXAD)
0	0	0	0	0	0
0.0272±0.0001	4.2±1.2	0.0630±0.0003	3.056±0.3	0.0436±0.0002	0.9±0.2
0.0274±0.0001	4.2±0.9	0.103±0.001	7.3±0.6	0.0638±0.0003	1.5±0.1
0.0298±0.0001	4.4±1.6	0.121±0.001	7.8±0.6	0.104±0.001	2.6±0.1
0.0410±0.0002	5.5±0.6	0.206±0.001	9.7±0.4	0.112±0.001	2.8±0.3
0.0418±0.0002	6.0±0.6	0.317±0.002	11.0±0.3	0.136±0.001	3.3±0.2
0.0484±0.0002	6.7±0.6	0.476±0.002	12.7±0.3	0.141±0.001	3.5±0.2
0.0490±0.0002	6.8±0.5	0.614±0.003	13.5±0.3	0.177±0.001	3.8±0.2
0.0506±0.0003	6.8±0.5	0.648±0.003	14.7±0.3	0.203±0.001	4.3±0.3
0.0509±0.0003	6.8±0.5	0.707±0.004	16.0±0.3	0.265±0.001	5.0±0.3
0.0855±0.0004	8.9±0.4	0.732±0.004	17.8±0.2	0.292±0.001	5.3±0.3
0.0862±0.0004	9.5±0.4	0.750±0.004	18.0±0.2	0.376±0.002	5.7±0.3
0.0884±0.0004	9.7±0.4	0.754±0.004	18.5±0.2	0.539±0.003	6.1±0.5
0.0907±0.0004	10.0±0.4	0.770±0.004	20.4±0.2	0.763±0.004	6.1±0.5
0.129±0.001	11.1±0.4	0.774±0.004	20.7±0.2		
0.134±0.001	11.2±0.4	0.779±0.004	21.8±0.1		
0.137±0.001	11.2±0.4	0.787±0.004	23.3±0.1		
0.159±0.001	11.8±0.3				
0.161±0.001	11.9±0.3				
0.162±0.001	11.9±0.3				
0.163±0.001	12.4±0.3				
0.188±0.001	12.7±0.3				
0.189±0.001	13.0±0.2				
0.191±0.001	13.1±0.2				
0.222±0.001	13.8±0.2				
0.223±0.001	14.1±0.2				
0.236±0.001	14.9±0.2				
0.237±0.001	15.2±0.2				
0.254±0.001	15.9±0.2				
0.265±0.001	15.9±0.1				
0.441±0.002	23.3±0.1				
0.725±0.004	38.1±0.1				
0.758±0.004	43.6±0.2				
0.835±0.004	70.1±0.6				

**Table C.6: Data for Figures 3.13, 3.14, and 3.15 (X versus Y2).**

Activity ( $a_{\text{THF},M}$ )	$C_{\text{THF},S}$ (% mL/gXAD)	Activity ( $a_{\text{AN},M}$ )	$C_{\text{AN},S}$ (% mL/gXAD)	Activity ( $a_{\text{MeOH},M}$ )	$C_{\text{MeOH},S}$ (% mL/gXAD)
0	0	0	0	0	0
0.0272±0.0001	7.6±2.2	0.0630±0.0003	5.9±0.7	0.0436±0.0002	1.7±0.4
0.0274±0.0001	7.7±1.8	0.103±0.001	14.0±1.2	0.0638±0.0003	2.9±0.3
0.0298±0.0001	8.0±1.1	0.121±0.001	15.1±1.1	0.104±0.001	4.8±0.3
0.0410±0.0002	10.0±1.1	0.206±0.001	18.6±0.8	0.112±0.001	5.2±0.5
0.0418±0.0002	10.9±1.0	0.317±0.002	21.3±0.7	0.136±0.001	6.2±0.4
0.0484±0.0002	12.2±1.0	0.476±0.002	24.5±0.7	0.141±0.001	6.5±0.4
0.0490±0.0002	12.3±0.9	0.614±0.003	26.0±0.5	0.177±0.001	7.1±0.4
0.0506±0.0003	12.3±0.9	0.648±0.003	28.3±0.5	0.203±0.001	8.1±0.5
0.0509±0.0003	12.3±0.9	0.707±0.004	30.8±0.5	0.265±0.001	9.3±0.6
0.0855±0.0004	16.1±0.8	0.732±0.004	34.4±0.4	0.292±0.001	9.9±0.5
0.0862±0.0004	17.1±0.8	0.750±0.004	34.7±0.4	0.376±0.002	10.7±0.6
0.0884±0.0004	17.4±0.8	0.754±0.004	35.7±0.4	0.539±0.003	11±1
0.0907±0.0004	17.1±0.7	0.770±0.004	39.4±0.4	0.763±0.004	11±1
0.129±0.001	19.1±0.6	0.774±0.004	39.9±0.3		
0.134±0.001	20.2±0.7	0.779±0.004	42.0±0.4		
0.137±0.001	20.2±0.7	0.787±0.004	44.9±0.3		
0.159±0.001	21.3±0.6				
0.161±0.001	21.4±0.6				
0.162±0.001	21.5±0.6				
0.163±0.001	22.4±0.6				
0.188±0.001	23.0±0.4				
0.189±0.001	23.4±0.4				
0.191±0.001	23.7±0.4				
0.222±0.001	24.9±0.3				
0.223±0.001	25.4±0.3				
0.236±0.001	27.0±0.3				
0.237±0.001	27.4±0.3				
0.254±0.001	28.7±0.3				
0.265±0.001	28.7±0.2				
0.441±0.002	42.2±0.2				
0.725±0.004	68.7±0.2				
0.758±0.004	78.7±0.3				
0.835±0.004	126±1				

**Table C.7: Data for Figure 3.16.**

$C_{THF,L}$ (% w/w)	$Q_{VW}$ (% mL /gXAD-2)	$C_{AN,L}$ (% w/w)	$Q_{VW}$ (%mL /gXAD-2)	$C_{MeOH,L}$ (% w/w)	$Q_{VW}$ (% mL/gXAD-2)
0.0000	0.00	0.0000	0.00	0.0000	0.00
0.6712±0.0002	5.39±0.01	1.390±0.001	0.00	5.572±0.001	0.00
1.571±0.001	8.12±0.02	1.390±0.001	0.00	5.572±0.001	0.00
1.920±0.001	12.28±0.02	2.632±0.001	0.83±0.01	16.17±0.01	2.01±0.01
4.351±0.001	19.83±0.04	2.632±0.001	0.83±0.01	16.17±0.01	2.01±0.01
5.643±0.001	22.23±0.04	4.061±0.001	4.59±0.01	21.87±0.01	3.35±0.01
8.441±0.001	25.23±0.05	4.061±0.001	5.01±0.01	21.87±0.01	3.35±0.01
10.40±0.01	27.38±0.05	8.100±0.001	9.48±0.01	32.30±0.01	5.38±0.01
16.96±0.01	31.07±0.06	8.100±0.001	9.74±0.02	32.30±0.01	6.06±0.01
21.05±0.01	32.57±0.07	11.04±0.01	12.56±0.02	38.59±0.01	7.42±0.01
32.19±0.01	35.59±0.07	11.04±0.01	12.56±0.02	38.59±0.01	8.12±0.02
42.31±0.01	37.11±0.07	21.77±0.01	13.68±0.03	51.77±0.01	9.50±0.02
52.24±0.01	38.64±0.08	21.77±0.01	14.38±0.03	51.77±0.01	10.19±0.02
72.61±0.01	40.18±0.08	30.99±0.01	15.09±0.03	56.33±0.01	10.19±0.02
86.78±0.01	40.18±0.08	30.99±0.01	15.09±0.03	75.82±0.01	11.17±0.02
100.0±0.01	41.72±0.08	46.07±0.01	16.50±0.03	75.82±0.01	11.57±0.02
		46.07±0.01	16.50±0.03	90.22±0.01	12.28±0.02
		58.86±0.01	18.64±0.04	90.22±0.01	12.97±0.03
		58.86±0.01	19.35±0.04	100.0±0.01	13.66±0.03
		71.05±0.01	22.24±0.04	100.0±0.01	14.38±0.03
		71.05±0.01	22.24±0.04		
		100.0±0.01	28.09±0.05		
		100.0±0.01	28.09±0.05		

Table C.8: Data for Figure 3.17.

$a_{THF,L}$	$Q_{VW}$ (% mL /gXAD-2)	$a_{AN,L}$	$Q_{VW}$ (% mL /gXAD-2)	$a_{MeOH,L}$	$Q_{VW}$ (% mL /gXAD-2)
0.000	0.00	0.0000	0.00	0.000	0.00
0.0332±0.0002	5.39±0.01	0.0677±0.0004	0.00	0.245±0.001	0.00
0.0761±0.0003	8.12±0.02	0.0677±0.0004	0.00	0.245±0.001	0.00
0.0923±0.0005	12.28±0.02	0.124±0.001	0.83±0.01	0.551±0.003	2.01±0.01
0.197±0.001	19.83±0.04	0.124±0.001	0.83±0.01	0.551±0.003	2.01±0.01
0.248±0.001	22.23±0.04	0.185±0.001	4.59±0.01	0.652±0.003	3.35±0.01
0.346±0.002	25.23±0.05	0.185±0.001	5.01±0.01	0.652±0.003	3.35±0.01
0.407±0.002	27.38±0.05	0.335±0.002	9.48±0.01	0.762±0.004	5.38±0.01
0.567±0.003	31.07±0.06	0.335±0.002	9.74±0.02	0.762±0.004	6.06±0.01
0.640±0.003	32.57±0.07	0.425±0.002	12.56±0.02	0.797±0.004	7.42±0.01
0.762±0.004	35.59±0.07	0.425±0.002	12.56±0.02	0.797±0.004	8.12±0.02
0.810±0.004	37.11±0.07	0.651±0.003	13.68±0.03	0.828±0.004	9.50±0.02
0.829±0.004	38.64±0.08	0.651±0.003	14.38±0.03	0.828±0.004	10.19±0.02
0.846±0.004	40.18±0.08	0.753±0.004	15.09±0.03	0.832±0.004	10.19±0.02
0.874±0.004	40.18±0.08	0.753±0.004	15.09±0.03	0.851±0.004	11.17±0.02
1.000±0.005	41.72±0.08	0.819±0.004	16.50±0.03	0.851±0.004	11.57±0.02
		0.819±0.004	16.50±0.03	0.885±0.004	12.28±0.02
		0.834±0.004	18.64±0.04	0.885±0.004	12.97±0.03
		0.834±0.004	19.35±0.04	1.000±0.005	13.66±0.03
		0.844±0.004	22.24±0.04	1.000±0.005	14.38±0.03
		0.844±0.004	22.24±0.04		
		1.000±0.005	28.09±0.05		



**Table C.9:** Data for Figures 3.18, 3.19, 3.20, and 3.21. Interpolated data from Figures 3.11 and 3.16 by using mathematical fittings.

$C_{THF,S}$ (% mL/gXAD)	$Q_{VW}$ (% mL /gXAD-2)	$C_{AN,S}$ (% mL/gXAD)	$Q_{VW}$ (% mL /gXAD-2)	$C_{MeOH,S}$ (% mL/gXAD)	$Q_{VW}$ (% mL/gXAD-2)
0.00	0.00	0.00	0.00	0.00	0.00
7.5±0.6	3.90±0.01	9.4±0.4	0.00	0.24±0.05	0.00
11.9±0.4	7.08±0.01	13.5±0.3	0.49±0.01	0.7±0.1	0.00
17.2±0.1	11.98±0.02	15.9±0.3	5.14±0.01	1.2±0.2	0.00
20.7±0.1	15.57±0.03	17.5±0.2	7.50±0.01	1.7±0.2	0.00
23.6±0.1	18.32±0.04	18.8±0.2	9.17±0.02	2.2±0.2	0.04±0.01
26.1±0.1	20.50±0.04	19.8±0.2	10.14±0.02	2.7±0.2	0.12±0.01
28.4±0.1	22.28±0.04	20.7±0.2	10.83±0.02	3.2±0.2	0.23±0.01
30.6±0.1	23.75±0.05	21.5±0.2	11.39±0.02	3.7±0.2	0.39±0.01
32.7±0.1	25.00±0.05	22.2±0.2	11.81±0.02	4.2±0.2	0.40±0.01
34.7±0.1	26.07±0.05	22.9±0.2	12.08±0.02	4.7±0.3	0.66±0.01
36.7±0.1	27.00±0.05	25.8±0.1	13.26±0.03	6.5±0.3	1.63±0.01
46.3±0.2	30.33±0.06	28.4±0.1	14.03±0.03	7.9±0.3	2.83±0.01
55.5±0.4	32.43±0.06	30.8±0.2	14.65±0.03	8.8±0.5	4.15±0.01
64.7±0.5	33.93±0.07	33.1±0.2	15.28±0.03	9.5±0.5	5.47±0.01
73.7±0.6	35.10±0.07	35.4±0.2	15.97±0.03	10.1±0.5	6.75±0.01
82.8±0.6	36.05±0.07	37.7±0.2	16.67±0.03	10.5±0.6	7.91±0.02
91.8±0.7	36.86±0.07	39.9±0.2	17.36±0.03	10.6±0.5	8.33±0.02
100.7±0.7	37.58±0.07	42.1±0.2	17.92±0.04	10.8±0.5	8.91±0.02
109.7±0.8	38.23±0.08	44.3±0.2	18.54±0.04	11.1±0.6	9.74±0.02
118.7±0.9	38.83±0.08	46.5±0.3	19.03±0.04	11.3±0.6	10.40±0.02
128±1	39.38±0.08			11.5±0.6	10.91±0.02
				11.6±0.6	11.15±0.02

**Table C.10: Data for Figure 4.4.**

time (min)	$C_{THF,S,t}$ (% g THF/gXAD-2)	$C_{THF,S,t} / C_{THF,S,\infty}$
0	0	0
0.5	34.3±0.2	0.539±0.004
11	48.4±0.2	0.762±0.005
22	53.9±0.2	0.847±0.005
43	55.3±0.2	0.870±0.005
90	58.0±0.2	0.912±0.005
215	58.7±0.2	0.923±0.005
520	60.6±0.3	0.954±0.007
1620	61.6±0.3	0.970±0.007
1175	61.6±0.3	0.969±0.007
2522	63.5±0.3	0.999±0.007
2856	64.2±0.3	1.011±0.007
4112	63.1±0.3	0.992±0.007
7358	63.6±0.3	1.000±0.007

**Table C.11: Data for Figure 4.5.**

time (min)	$C_{AN,S,t}$ (% g AN/gXAD-2)	$C_{AN,S,t} / C_{AN,S,\infty}$
0	0	0
0.5	21.9±0.3	0.822±0.015
2.5	23.5±0.3	0.881±0.015
7.5	24.7±0.3	0.925±0.015
19	25.3±0.3	0.947±0.015
25	26.1±0.3	0.977±0.016
29	26.4±0.3	0.990 ±0.016
95	26.3±0.3	0.985 ±0.016
97	26.8±0.3	1.004 ±0.016
263	26.2±0.3	0.982 ±0.016
270	26.6±0.3	0.998 ±0.016
563	27.4±0.3	1.026 ±0.016
569	27.4±0.3	1.026 ±0.016
1409	27.0±0.3	1.013 ±0.016
4525	26.7±0.3	1.000 ±0.016

**Table C.12: Data for Figure 4.6.**

time (min)	$C_{MeOH,S,t}$ (%g MeOH/gXAD-2)	$C_{MeOH,S,t} / C_{MeOH,S,\infty}$
0	0	0
0.5	5.4±0.3	0.714±0.054
2.5	5.9±0.3	0.779±0.057
6.5	6.2±0.3	0.820±0.068
8.5	6.7±0.3	0.881±0.070
12	6.9±0.3	0.910±0.071
15	7.0±0.3	0.915±0.071
41	7.5±0.3	0.980±0.074
47.5	7.4±0.3	0.971±0.073
49.5	7.4±0.3	0.971±0.073
53	7.4±0.3	0.975±0.074
94	7.5±0.3	0.980±0.074
105	7.4±0.3	0.979±0.074
180	7.4±0.3	0.971±0.074
420	7.5±0.3	0.990±0.074
726	7.6±0.3	1.000±0.074

**Table C.13: Data for Figure 4.7. Hypothetical data for monodisperse model.**

$t$ (sec)	$C_{THF,S,t}$ (% gTHF/gXAD-2)
0.01	8.106579
0.05	17.32417
0.1	23.64948
0.15	28.16519
0.2	31.7442
0.25	34.7246
0.3	37.27978
0.35	39.51277
0.4	41.49066
0.6	47.61804
0.8	51.87395
1	54.9434
1.5	59.50723
2.45	62.58998
3.5	63.36145
5	63.54096
8	63.56177
10	63.56199
15	63.562
20	63.562
25	63.562
35	63.562
45	63.562
55	63.562
65	63.562
75	63.562
85	63.562
100	63.562

**Table C.14: Data for THF fitting. Figure 4.8.**

<b>Time (min)</b>	<b>Overall (experimental) (% gTHF/gXAD-2)</b>
0	0
0.5	34.3±0.2
11	48.4±0.2
22	53.8±0.2
43	55.3±0.2
90	58.0±0.2
215	58.7±0.2
520	60.6±0.2
1620	61.6±0.2
2175	61.6±0.2
2522	63.5±0.2
2856	64.2±0.2
4112	63.1±0.2
7358	63.6±0.2

**Table C.15: Data for AN fitting. Figure 4.8.**

<b>Time (min)</b>	<b>Overall (experimental) (% gAN/gXAD-2)</b>
0	0
0.5	21.9±0.4
2.5	23.5±0.4
7.5	24.7±0.4
19	25.3±0.3
25	26.1±0.3
29	26.4±0.3
95	26.3±0.3
97	26.8±0.3
263	26.2±0.3
270	26.6±0.3
563	27.4±0.3
569	27.4±0.3
1409	27.0±0.3
4525	26.7±0.3

**Table C.16: Data for MeOH fitting. Figure 4.8.**

<b>Time (min)</b>	<b>Overall (experimental) (% gMeOH/gXAD-2)</b>
0	0
0.5	5.4±0.3
2.5	5.9±0.3
6.5	6.2±0.3
8.5	6.7±0.4
12	6.9±0.4
15	6.9±0.4
41	7.4±0.5
47.5	7.4±0.5
49.5	7.4±0.5
53	7.4±0.5
94	7.4±0.5
105	7.4±0.5
180	7.4±0.5
420	7.5±0.5
726	7.6±0.5



**Table C.17: Data for Figure 4.9**

<b>Time (min)</b>	<b><math>Q_{VW,t}</math> (%mL/gXAD-2) (4.94% THF in the liquid)</b>
0	0
0.5	15.10±0.03
1.5	19.66±0.04
2	19.66±0.04
3	20.09±0.04
4	20.53±0.04
5	20.53±0.04
10	20.53±0.04
15	20.53±0.04
60	20.53±0.04
180	20.53±0.04

**Table C.18: Data for Figure 4.10.**

<b>Time (min)</b>	<b><math>Q_{VW,t}</math> (%mL/gXAD-2) (10.97% THF in the liquid)</b>
0	0
0.75	23.72±0.05
1	26.65±0.05
1.5	27.39±0.05
1.75	27.39±0.05
2	28.13±0.06
2.5	28.13±0.06
3	28.13±0.06
4	28.13±0.06
5	28.13±0.06
10	28.13±0.06
15	28.13±0.06
20	28.13±0.06
25	28.13±0.06
40	28.13±0.06
60	28.13±0.06
120	28.13±0.06
180	28.13±0.06

**Table C.19: Data for Figure 4.11.**

<b>time (min)</b>	<b><math>Q_{VW,t}</math> (% mL/gXAD-2) (52.24% THF in the liquid)</b>
0	0
1	35.6±0.07
2	38.7±0.08
3	38.7±0.08
4	38.7±0.08
5	38.7±0.08
10	38.7±0.08
30	38.7±0.08
60	38.7±0.08
120	38.7±0.08
180	38.7±0.08

**Table C.20: Data for Figure 4.12.**

<b>time (min)</b>	<b><math>Q_{VW,t}</math> (%mL/gXAD-2) (72.61% THF in the liquid)</b>
0	0
0.5	35.64±0.07
1.5	38.69±0.08
3	40.23±0.08
5	40.23±0.08
10	40.23±0.08
20	40.23±0.08
60	40.23±0.08
120	40.23±0.08
180	40.23±0.08

**Table C.21: Data for Figure 4.13.**

<b>time (min)</b>	<b><math>Q_{VW,t}</math> (% mL/gXAD-2) (100% THF in the liquid)</b>
0	0
0.5	38.69±0.08
1	40.23±0.08
1.5	41.01±0.08
2	41.78±0.08
3	41.78±0.08
4	41.78±0.08
5	41.78±0.08
10	41.78±0.08
20	41.78±0.08
40	41.78±0.08
60	41.78±0.08
120	41.78±0.08
180	41.78±0.08

**Table C.22: Data for Figure 4.14.**

time (min)	$Q_{VW,t}$ (%mL/gXAD-2) (4.06% AN in the liquid)
0	0
0.5	5.39±0.01
1	6.41±0.01
2	7.78±0.02
3	7.78±0.02
4	7.78±0.02
5	7.78±0.02
10	7.78±0.02
30	7.78±0.02
60	7.78±0.02
120	7.78±0.02

**Table C.23: Data for Figure 4.15.**

time (min)	$Q_{VW,t}$ (%mL/gXAD-2) (8.10% AN in the liquid)
0	0
1	7.78±0.02
2	7.78±0.02
3	7.78±0.02
5	7.78±0.02
10	7.78±0.02
30	7.78±0.02
60	7.78±0.02
120	7.78±0.02

**Table C.24: Data for Figure 4.16.**

time (min)	$Q_{VW,t}$ (% mL/gXAD-2) (58.86% AN in the liquid)
0	0
1	7.78±0.04
3	19.37±0.04
5	19.37±0.04
10	18.66±0.04
30	19.02±0.04
35	18.66±0.04
60	19.02±0.04
120	19.02±0.04



**Table C.25: Data for Figure 4.17.**

time (min)	$Q_{VW,t}$ (% mL/gXAD-2) (71.05% AN in the liquid)
0	0
1	19.37±0.04
3	21.54±0.04
5	21.54±0.04
15	22.26±0.04
30	22.26±0.04
60	22.99±0.05
120	22.99±0.05

**Table C.26: Data for Figure 4.18.**

<b>time (min)</b>	<b><math>Q_{VW,t}</math> (%mL/gXAD-2) (100% AN in the liquid)</b>
0	0
1	26.65±0.05
3	26.65±0.05
5	26.65±0.05
30	26.65±0.05
60	26.65±0.05
120	26.65±0.05

**Table C.27: Data for Figure 4.19.**

<b>time (min)</b>	<b><math>Q_{VW,t}</math> (%mL/gXAD-2) (5.57% MeOH in the liquid)</b>
0	0
0.5	0
1	0
1.5	0
2	0
3	0
3.5	0
5	0
10	0
30	0
60	0
120	0

**Table C.28: Data for Figure 4.20.**

<b>time (min)</b>	<b><math>Q_{VW,t}</math> (%mL/gXAD-2) (16.17% MeOH in the liquid)</b>
0	0
1	1.24±0.01
2	1.36±0.01
3	1.36±0.01
5	1.36±0.01
10	1.36±0.01
15	1.36±0.01
20	1.36±0.01
30	1.36±0.01
60	1.36±0.01
120	1.36±0.01

**Table C.29: Data for Figure 4.21.**

time (min)	$Q_{VW,t}$ (%mL/gXAD-2) (56.33% MeOH in the liquid)
0	0
1	9.50±0.02
2	10.20±0.02
3	10.20±0.02
5	10.20±0.02
10	10.20±0.02
30	10.20±0.02
60	10.20±0.02
120	10.20±0.02

**Table C.30: Data for Figure 4.22.**

time (min)	$Q_{VW,t}$ (%mL/gXAD-2) (75.82% MeOH in the liquid)
0	0
0.75	10.20±0.02
1	10.89±0.02
1.5	10.89±0.02
2.5	11.38±0.02
3	11.38±0.02
5	11.38±0.02
10	11.38±0.02
20	11.38±0.02
30	11.38±0.02
60	11.38±0.02
120	11.38±0.02

**Table C.31: Data for Figure 4.23.**

time (min)	$Q_{vw,t}$ (% mL/gXAD-2) (100% MeOH in the liquid)
0	0
1	13.69±0.03
2	14.04±0.03
3	14.04±0.03
4	14.04±0.03
5	14.04±0.03
10	14.04±0.03
30	14.04±0.03
60	14.04±0.03
120	14.04±0.03

**Table C.32: Data for Figure 4.24.**

Time (min)	$Q_{VW,t}$ (%mL/gXAD-2) for THF	$Q_{VW,t}$ (%mL/gXAD-2) for AN	$Q_{VW,t}$ (%mL/gXAD-2) for MeOH
0	0		
1	35.64±0.07		
2	38.69±0.08		
3	38.69±0.08		
4	38.69±0.08		
5	38.69±0.08		
10	38.69±0.08		
0		0	
1		18.66±0.04	
3		19.37±0.04	
5		19.37±0.04	
10		18.66±0.04	
0			0
1			9.50±0.02
2			10.20±0.02
3			10.20±0.02
5			10.20±0.02
10			10.20±0.02



**Table C.33: Data for Figure 4.25.**

Time (min)	$Q_{VW,t}/100$ (mL/gXAD-2)	$C_{THF,S,t}/100$ (mL/gXAD-2)
0	0	
1	32.61±0.07	
2	35.64±0.07	
3	35.64±0.07	
4	35.64±0.07	
5	35.64±0.07	
10	35.64±0.07	
30	35.64±0.07	
60	35.64±0.07	
0		0
0.5		38.5±0.1
11		54.4±0.4
22		60.6±0.5
43		62.2±0.5
90		65.2±0.5

**Table C.34: Data for Figure 4.26.**

Time (min)	$Q_{VW,t}/100$ (mL/gXAD-2)	$C_{AN,S,t}/100$ (mL/gXAD-2)
0	0	
1	15.10±0.03	
2	15.10±0.03	
5	15.10±0.03	
10	15.10±0.03	
0		0
0.5		29.28±0.1
2.5		31.36±0.2
7.5		32.93±0.2
19		33.72±0.2
25		34.78±0.2
29		35.23±0.2

**Table C.35: Data for Figure 4.27.**

Time (min)	$Q_{VW,t}/100$ (mL/gXAD-2)	$C_{MeOH,S,t}/100$ (mL/gXAD-2)
0	0	
0.5	2.01±0.01	
0.75	2.68±0.01	
1	4.71±0.01	
1.25	5.39±0.01	
2	5.86±0.01	
3.5	5.39±0.01	
4	6.75±0.01	
5	7.23±0.01	
10	7.44±0.01	
20	8.12±0.02	
60	8.12±0.02	
120	8.12±0.02	
0		0
0.5		6.90±0.3
2.5		7.52±0.3
6.6		7.92±0.4
8.5		8.51±0.5
12		8.79±0.5
15		8.83±0.5
41		9.47±0.5
47.5		9.38±0.5
49.5		9.38±0.5
53		9.42±0.5
94		9.47±0.5
105		9.46±0.5

## Appendix D

### Differential Scanning Calorimetry (DSC).

DSC experiments were kindly run by Jiang Bai and Waleed Hussein, graduate students under the supervision of Dr. M. Williams in the Department of Chemical Engineering, at The University of Alberta.

Differential Scanning Calorimetry (DSC) is a thermal analysis technique. This method involves monitoring energy changes between a substance and a reference material when exposed to energy input. The analysis is run in a controlled temperature program. Heat flow (mW) versus temperature ( $^{\circ}\text{C}$ ) plots are obtained for the freezing-melting behavior of the sample. An upward peak is obtained for exothermic transitions (i.e., freezing releases heat). For endothermic physical or chemical changes (e.g., melting of crystals absorbs heat) a downward peak would be expected. All of these changes are with respect to the reference cell.

The DSC apparatus is comprised of a *sample holder/measuring system*, which consists of sample and reference cells, thermocouples, and a block to ensure even heat distribution, a *furnace* for warming and heating, a *temperature programmer* that supplies energy to the furnace, and a *recorder*.

DSC experiments were performed on XAD-2 samples equilibrated with different water/OM solutions. A sample of approximately  $(20.0 \pm 0.1)$  mg, previously centrifuged on a screen to eliminate the liquid between particles, was placed in the sample holder. The sample holder was then sealed and placed in the furnace. An empty sample holder was used as the reference cell. The program of analysis used was:

1 min at 25 °C

10°C/min up to -50°C (cooling cycle)

1 min at -50°C

10°C/min up to +50°C (heating cycle)

Representative results from the experiments are shown in Figures D.1 and D.2. The XAD-2 sample used in obtaining Figure D.1 was equilibrated with pure water, while the sample used in obtaining Figure D.2 was equilibrated with a 50% THF aqueous solution.

Figure D.1 shows a peak in the cooling cycle which corresponds to the freezing of pure water. The freezing point of water is lower than expected due to the high temperature ramp used which caused supercooling of the water. Figure D.2 shows a peak in the cooling cycle at a temperature around -30°C. This peak temperature for freezing of water is lower than for pure water because of the depression of the freezing temperature of water in binary solutions [179]. The cooling cycle in both Figures shows a peak around 0°C which corresponds to the melting point of pure water.

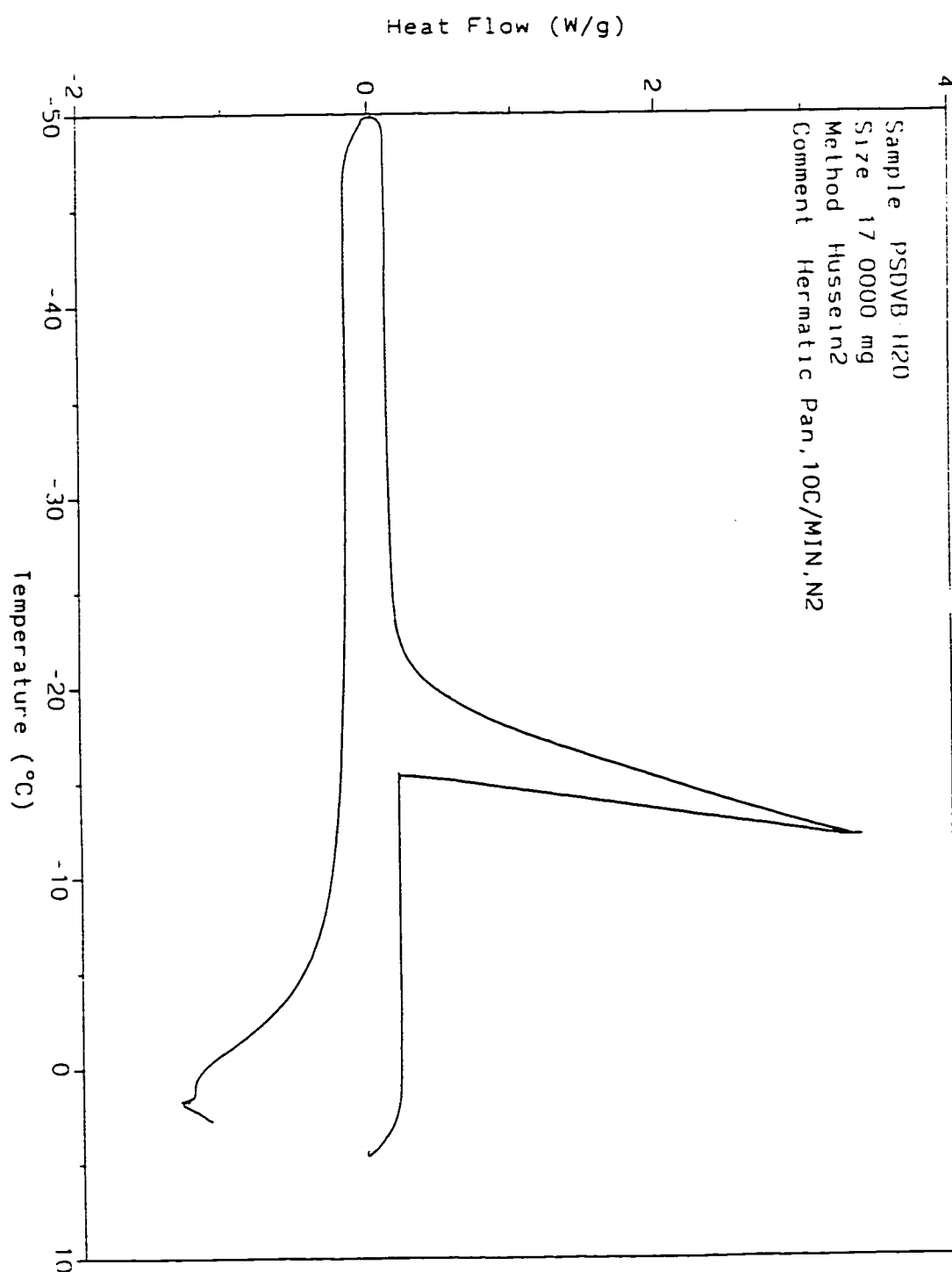


**Figure D.1. Differential Scanning Calorimetry (DSC) analysis. Sample: PSDVB after four-day equilibration with pure water.**

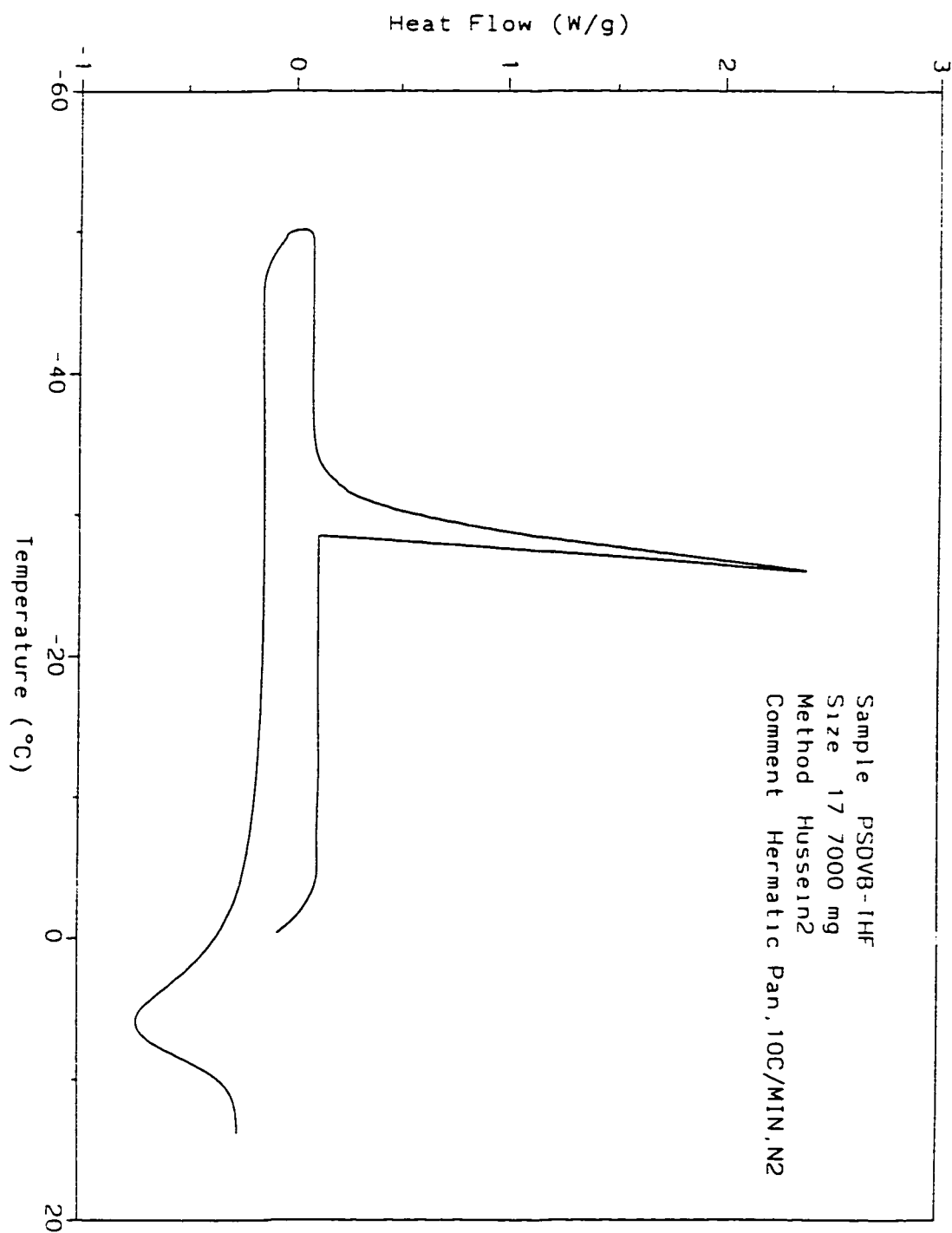


**Figure D.2. Differential Scanning Calorimetry (DSC) analysis. Sample: PSDVB after four-day equilibration with a 1:1 THF:water solution (g/g).**